X-ray Spectroscopy of Massive Star Winds: Shocks, Mass-Loss Rates, and Clumping

David Cohen
Department of Physics & Astronomy
Swarthmore College

Maurice Leutenegger (GSFC), Jon Sundqvist (Madrid), Stan Owocki (Delaware),
Véronique Petit (Florida Institute of Technology), Marc Gagné (West Chester), Asif ud-Doula (Penn St.)

with Zack Li (Swarthmore '16), James MacArthur (Swarthmore '11), Emma Wollman (Swarthmore '09), Erin Martell (Swarthmore '09)

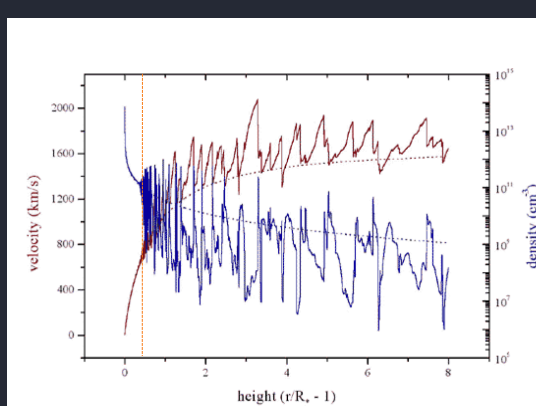

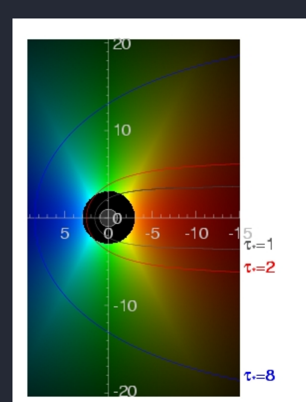

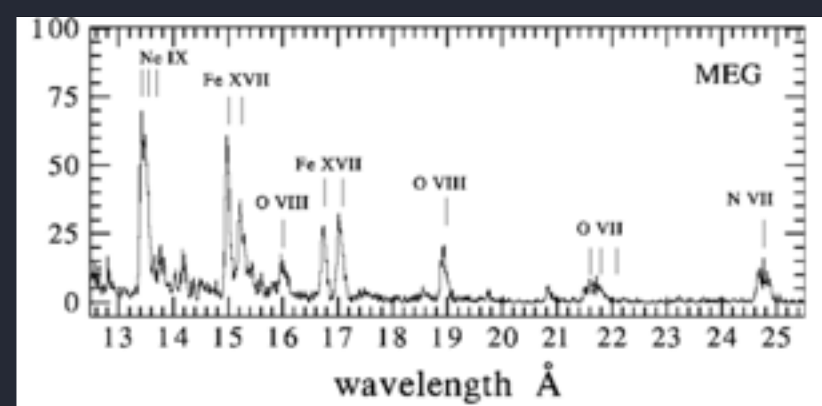

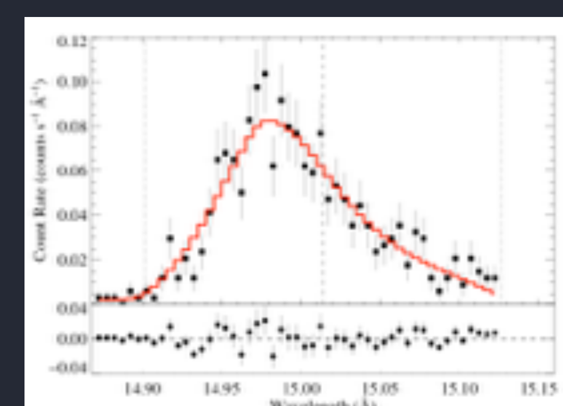

Outline

Chandra resolved X-ray line profile spectroscopy of O star winds

1. Resolved X-ray line profiles can provide diagnostically useful information about:
    A. plasma kinematics
    B. local absorption

2. Applications to massive star X-rays
    A. wind-shock physics
    B. wind absorption: wind mass-loss rate
    C. with H-alpha: wind clumping

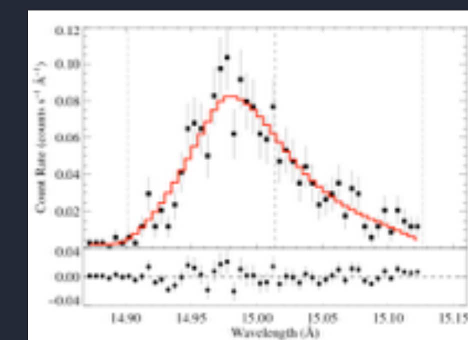

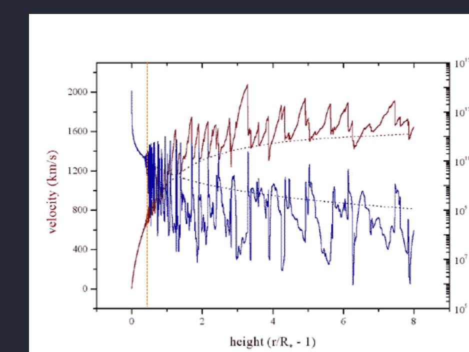

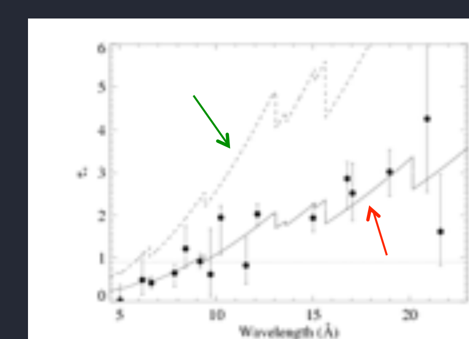

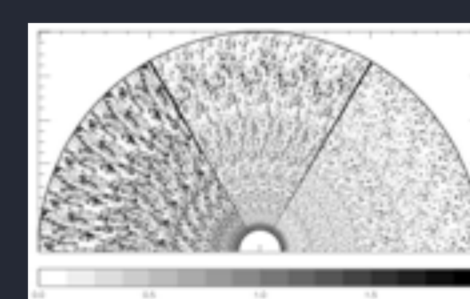

Prior to 2000: only *low*-resolution X-ray data

zeta Pup (O4 If) : runaway, single O supergiant

ROSAT (early 1990s): resolving power, *R* ~ *3*

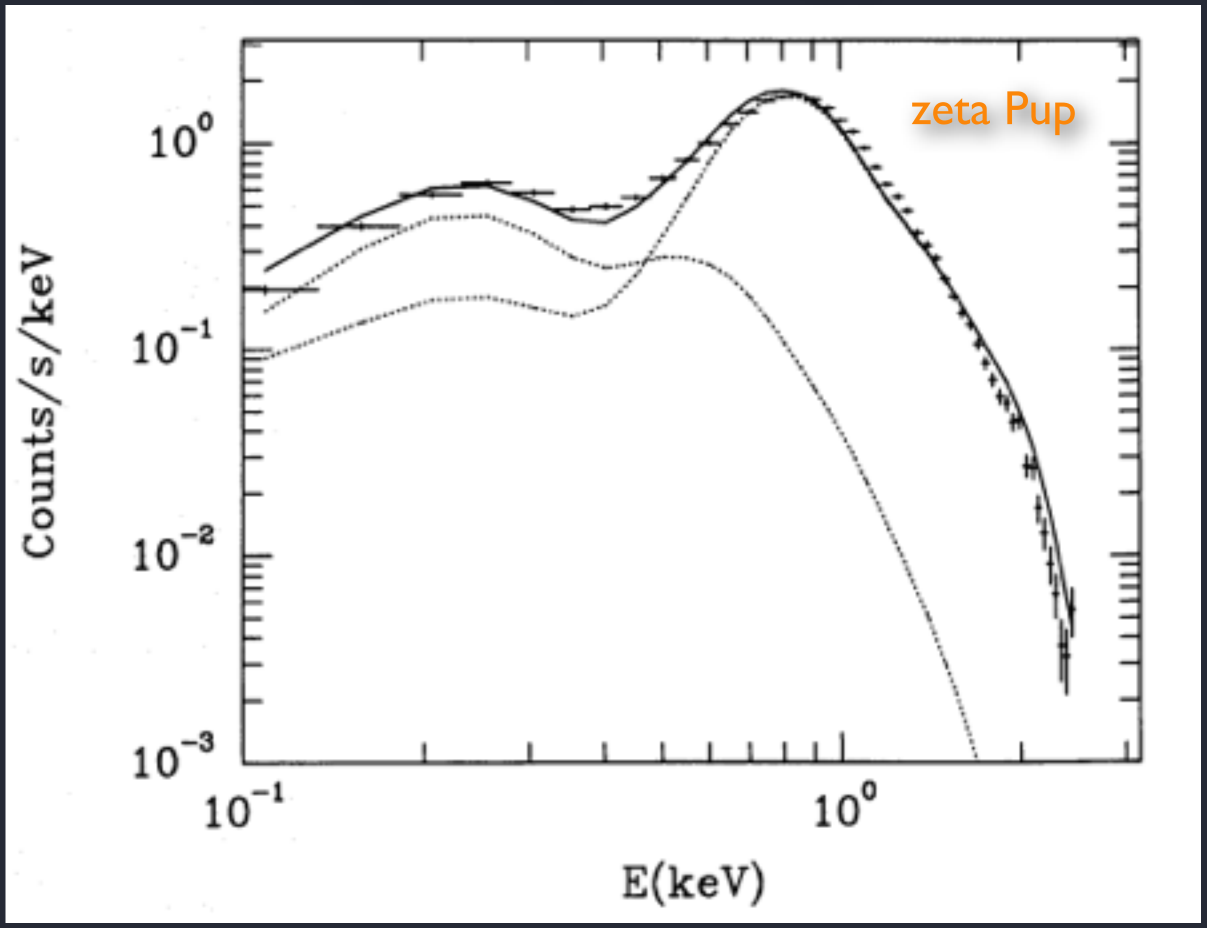

Hillier et al. (1993)

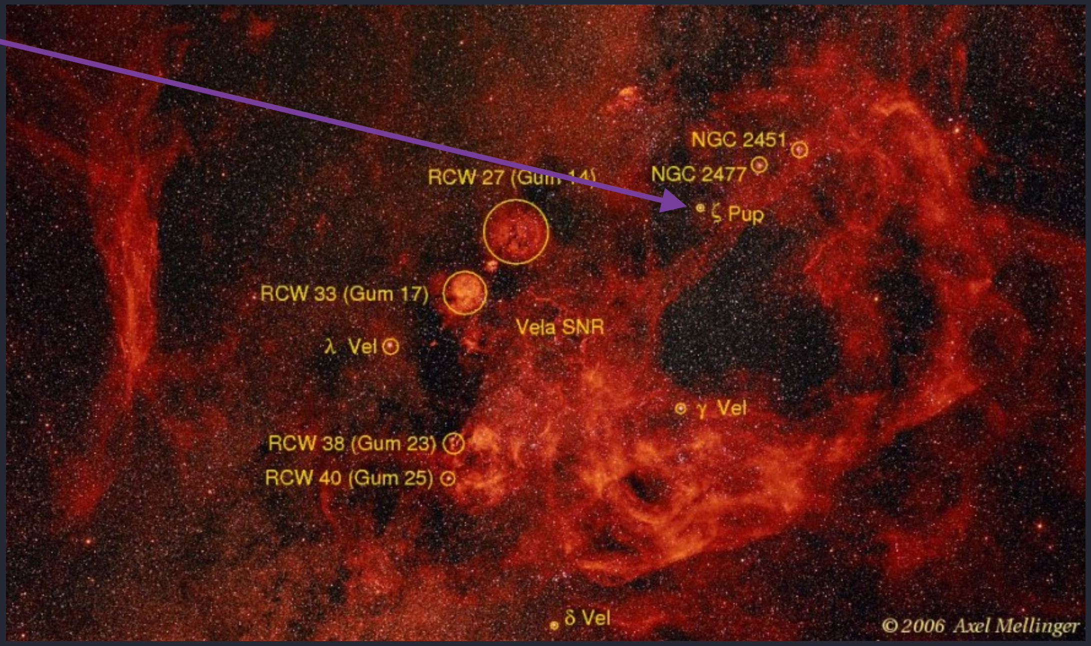

BBXRT (early 1990s): resolving power, *R* ~ *10*

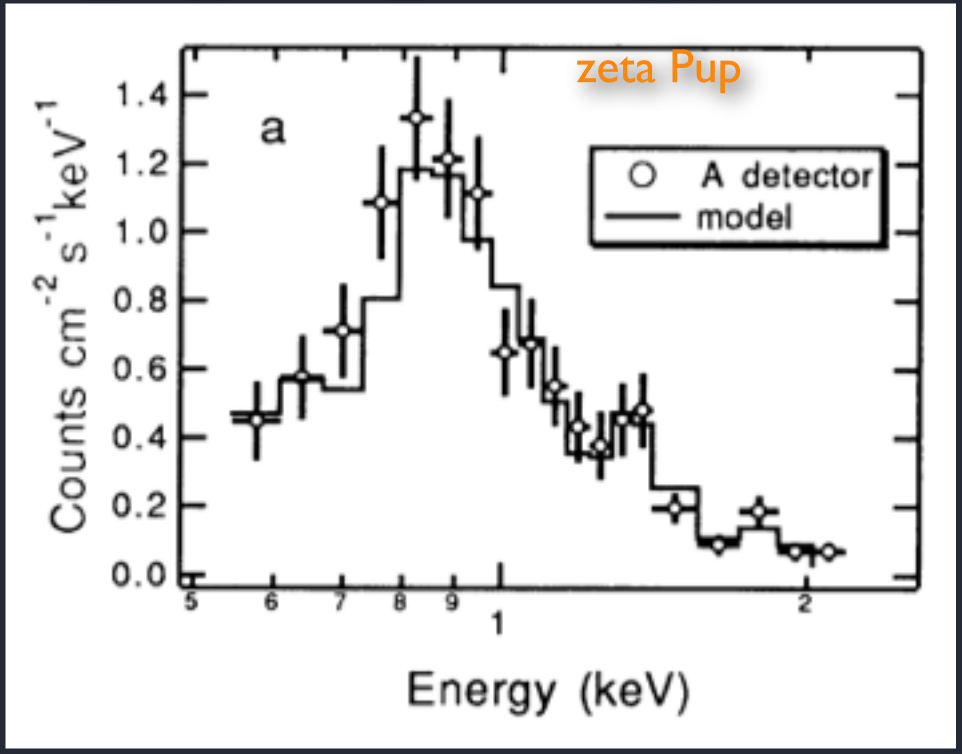

Corcoran et al. (1993)

overall X-ray luminosity; crude, model-dependent plasma temperature information

Chandra and *XXM-Newton* launched ~2000

ROSAT (early 1990s): resolving power, *R ~ 3*

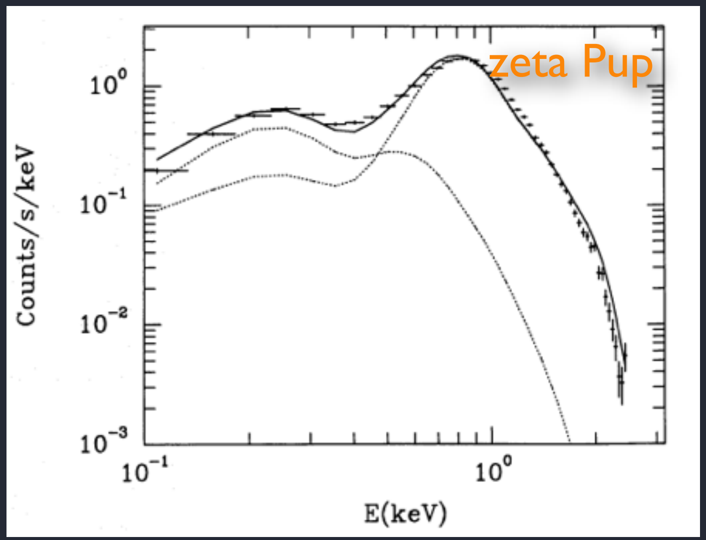

Hillier et al. (1993)

Chandra MEG: resolving power, *R up to 1000*

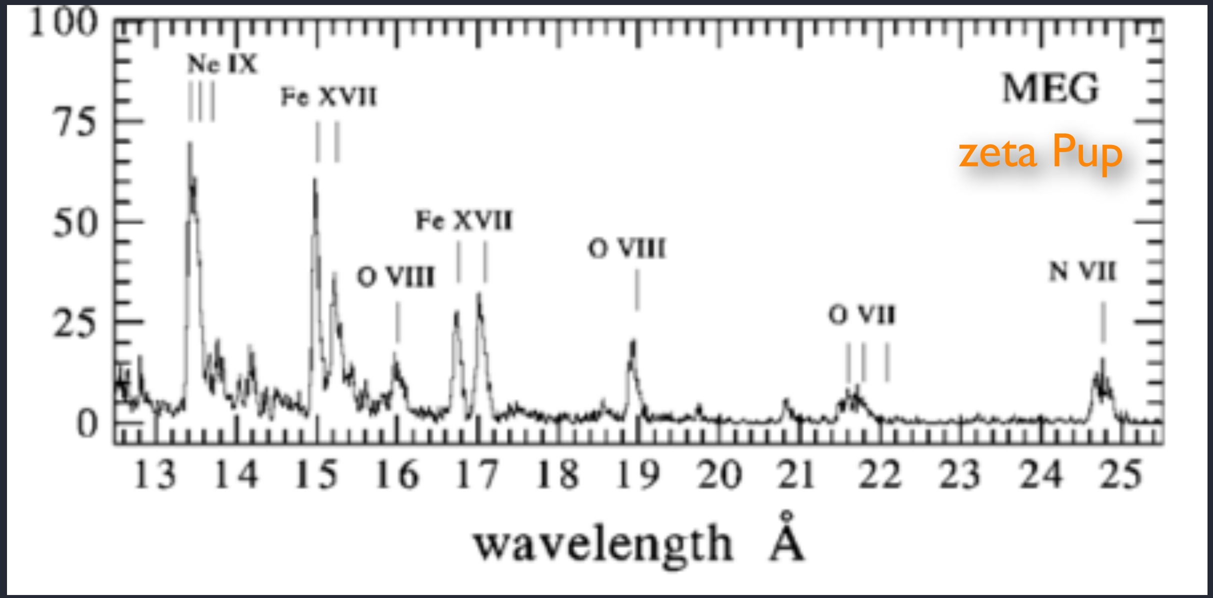

Cassinelli et al. (2001)

BBXRT (early 1990s): resolving power, *R ~ 10*

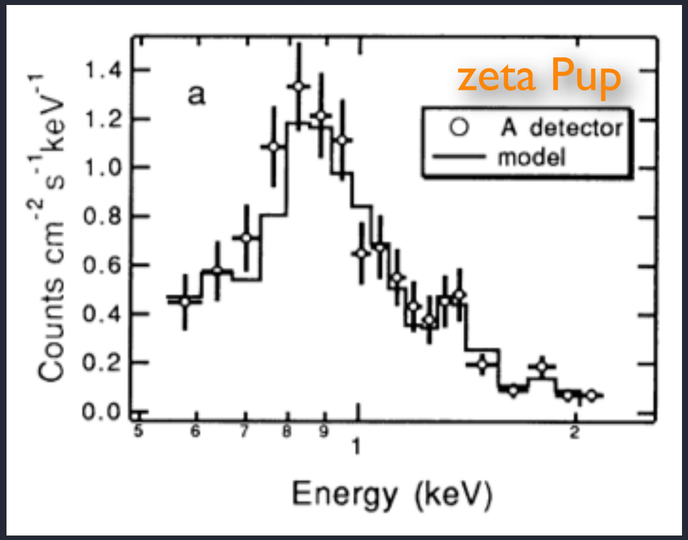

Corcoran et al. (1993)

XMM RGS: resolving power, *R ~ few 100*

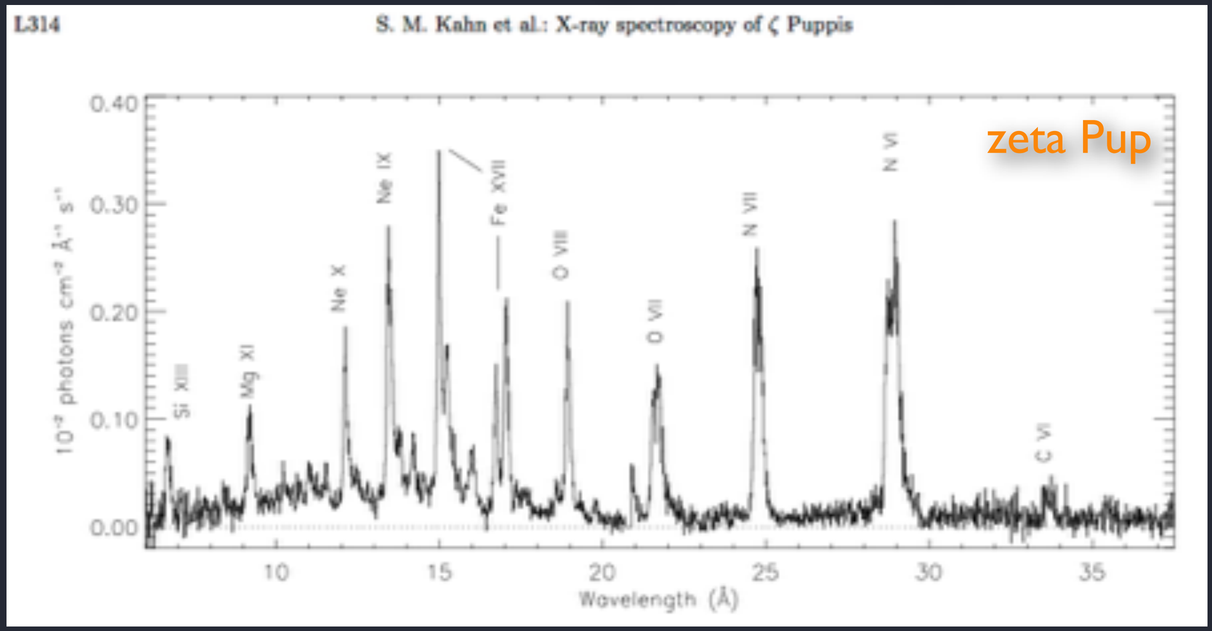

Kahn et al. (2001)

O star X-ray spectra have broad lines

63 ks HETGS zeta Pup (O4 If)

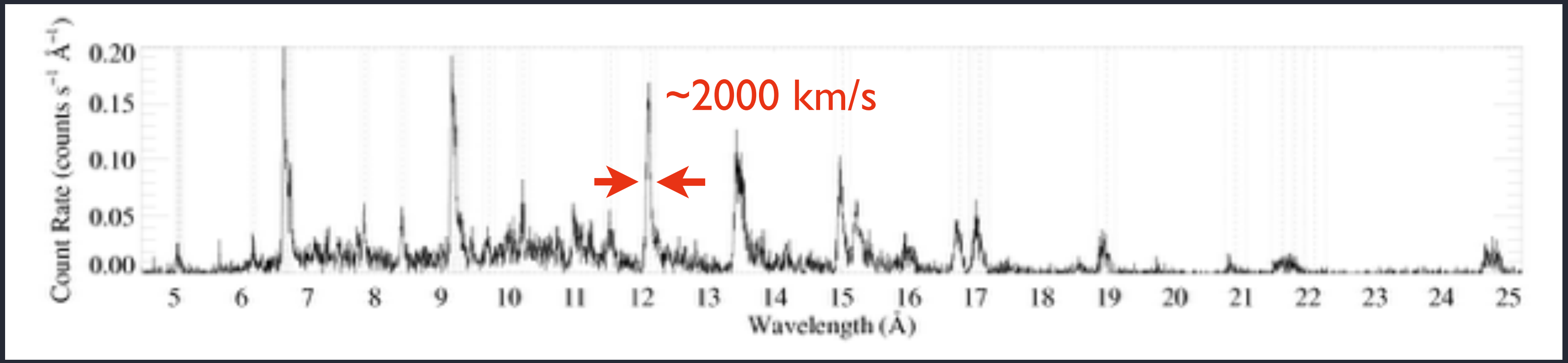

$v_{wind} \sim 10^3$ km/s

$v_{resolution} \sim 10^2$ km/s

$v_{therm} \sim 10^1$ km/s

Chandra resolution

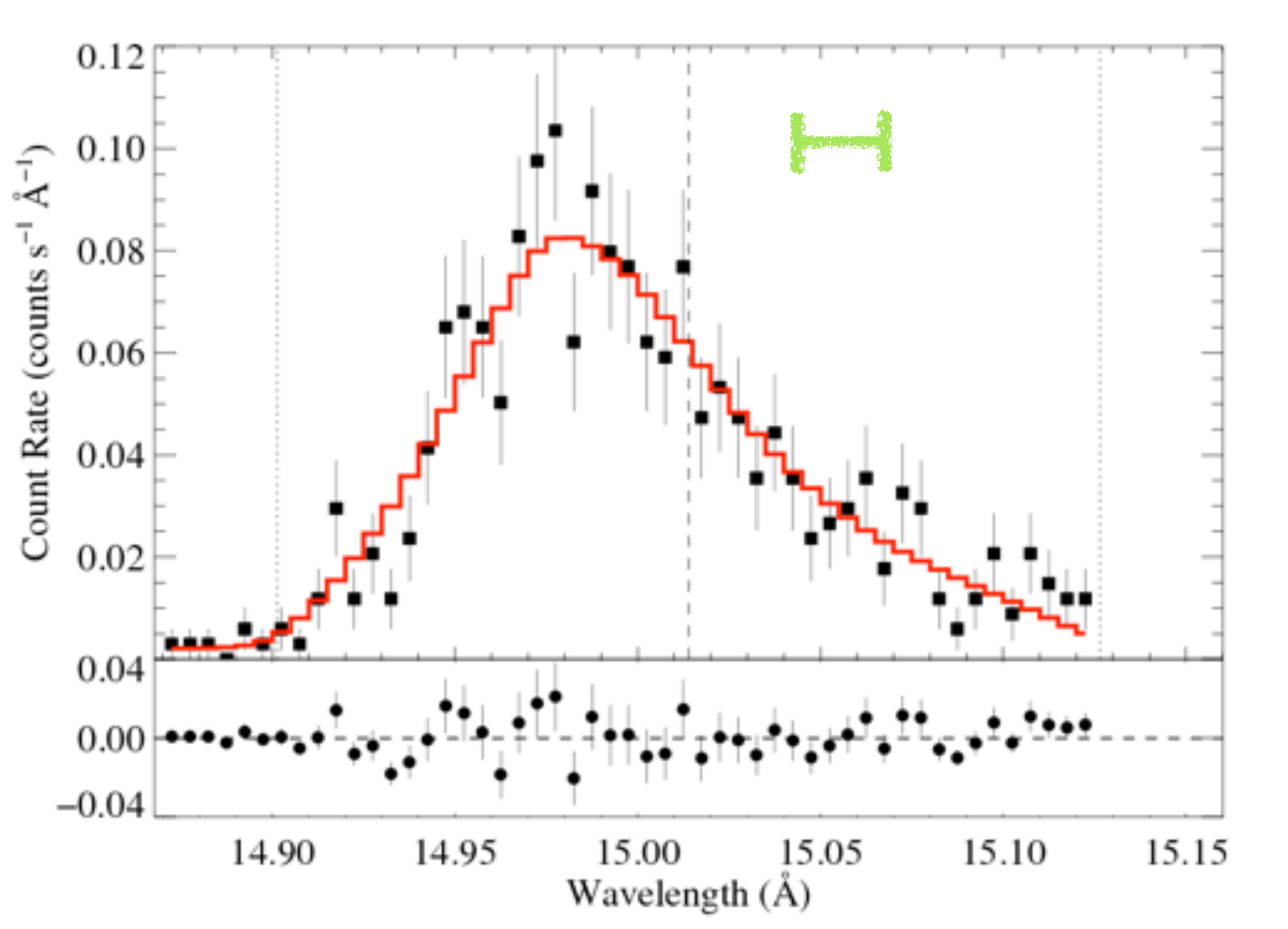

O star X-ray spectra have broad lines

Doppler, $v/c = \Delta\lambda/\lambda$

resolving power, $R = \lambda/\Delta\lambda$

$v_{wind} \sim 10^3$ km/s

$v_{resolution} \sim 10^2$ km/s

$v_{therm} \sim 10^1$ km/s

Chandra resolution

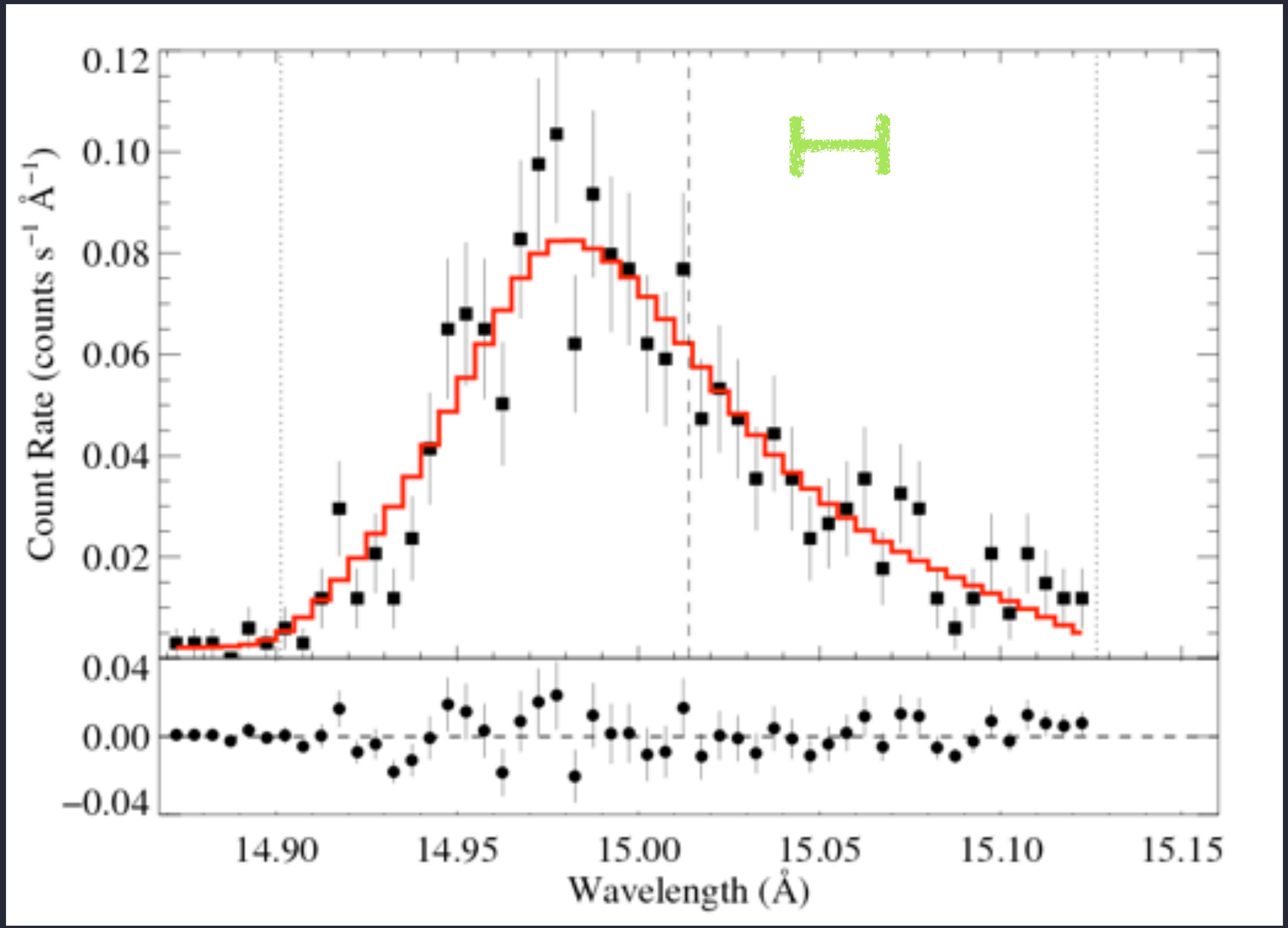

X-ray emission lines are well resolved

Typical O star line profile; here Fe XVII

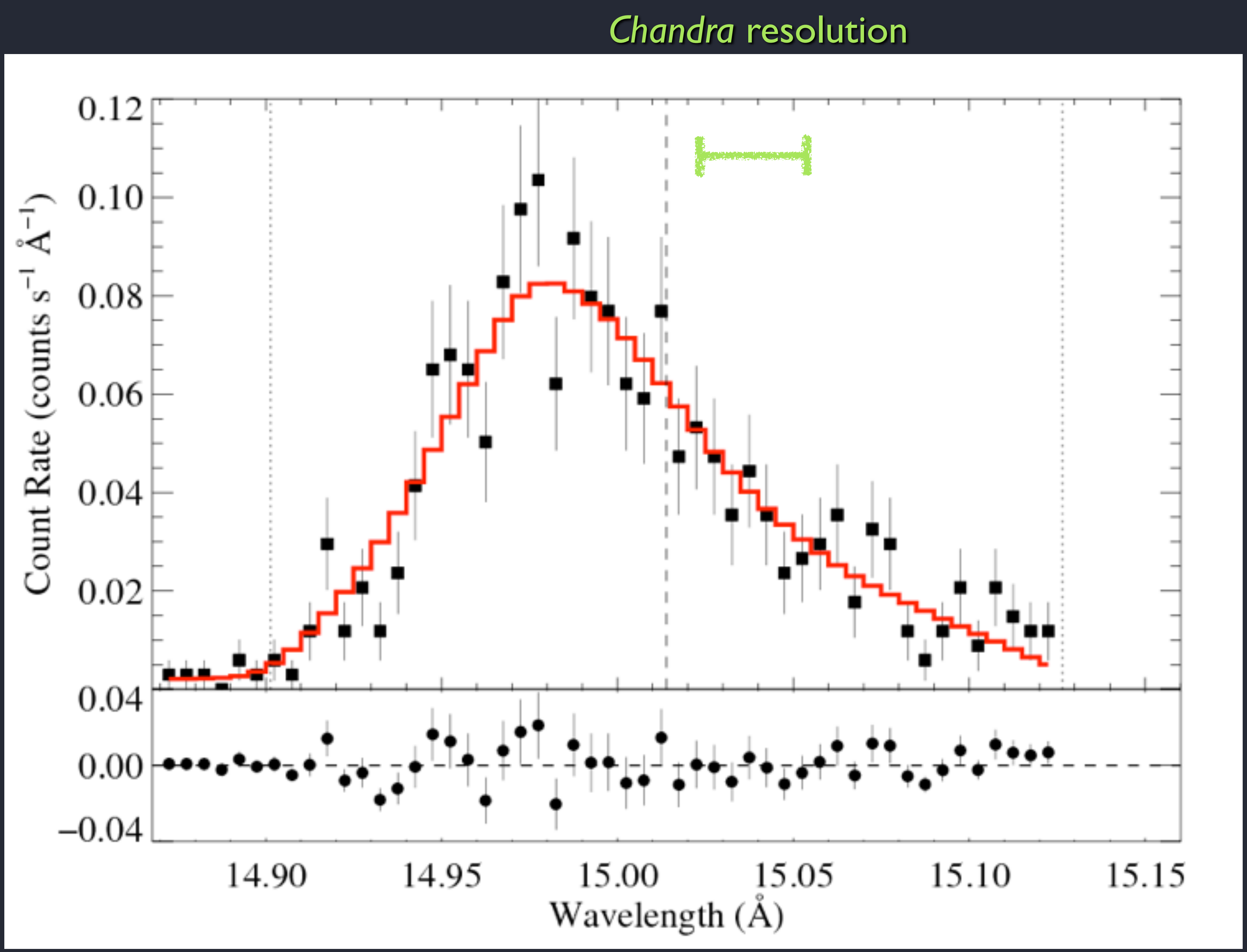

dominated by Doppler broadening due to bulk motion of the emitting plasma

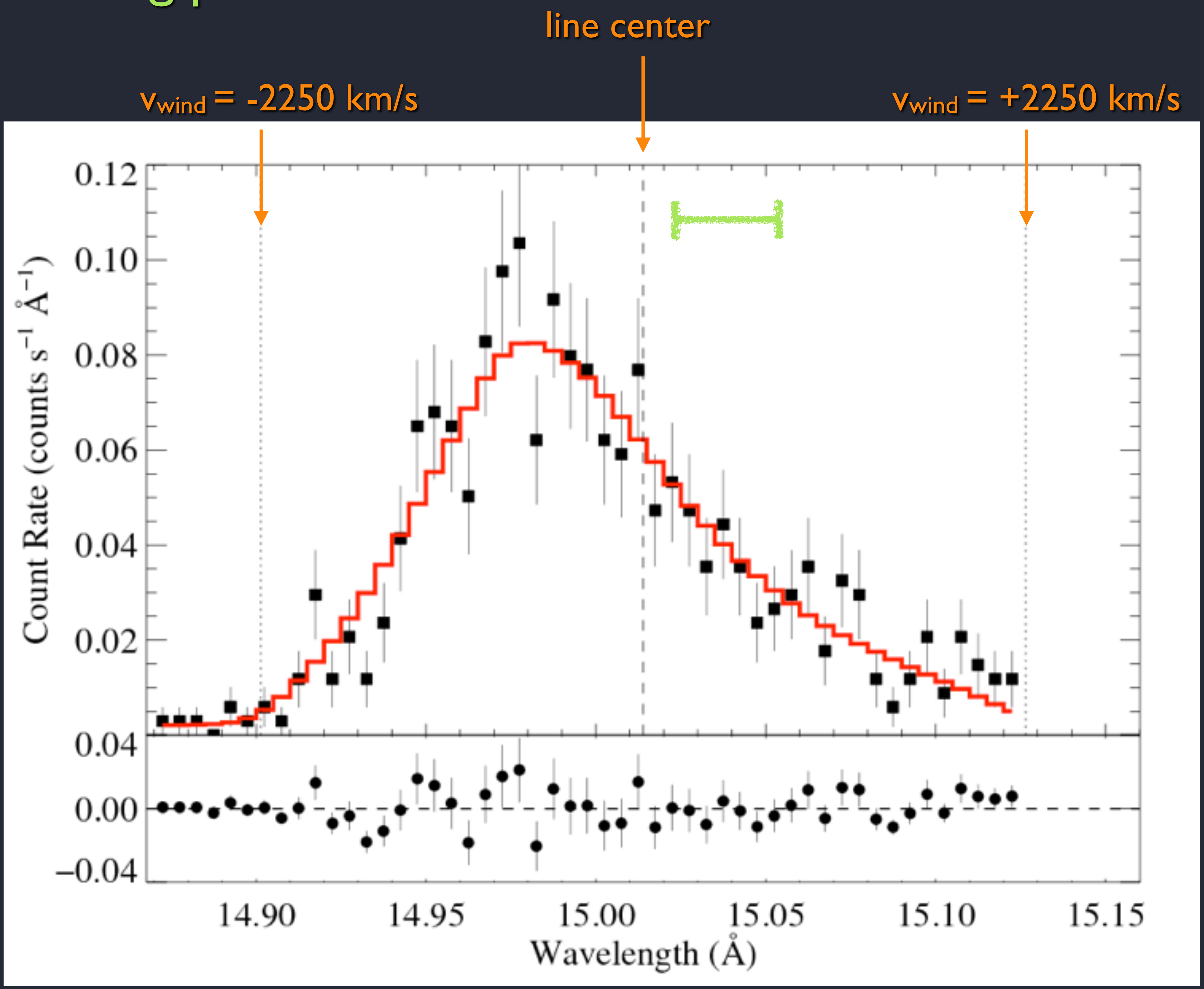

Asymmetric line shape due to continuum absorption by the cool wind component

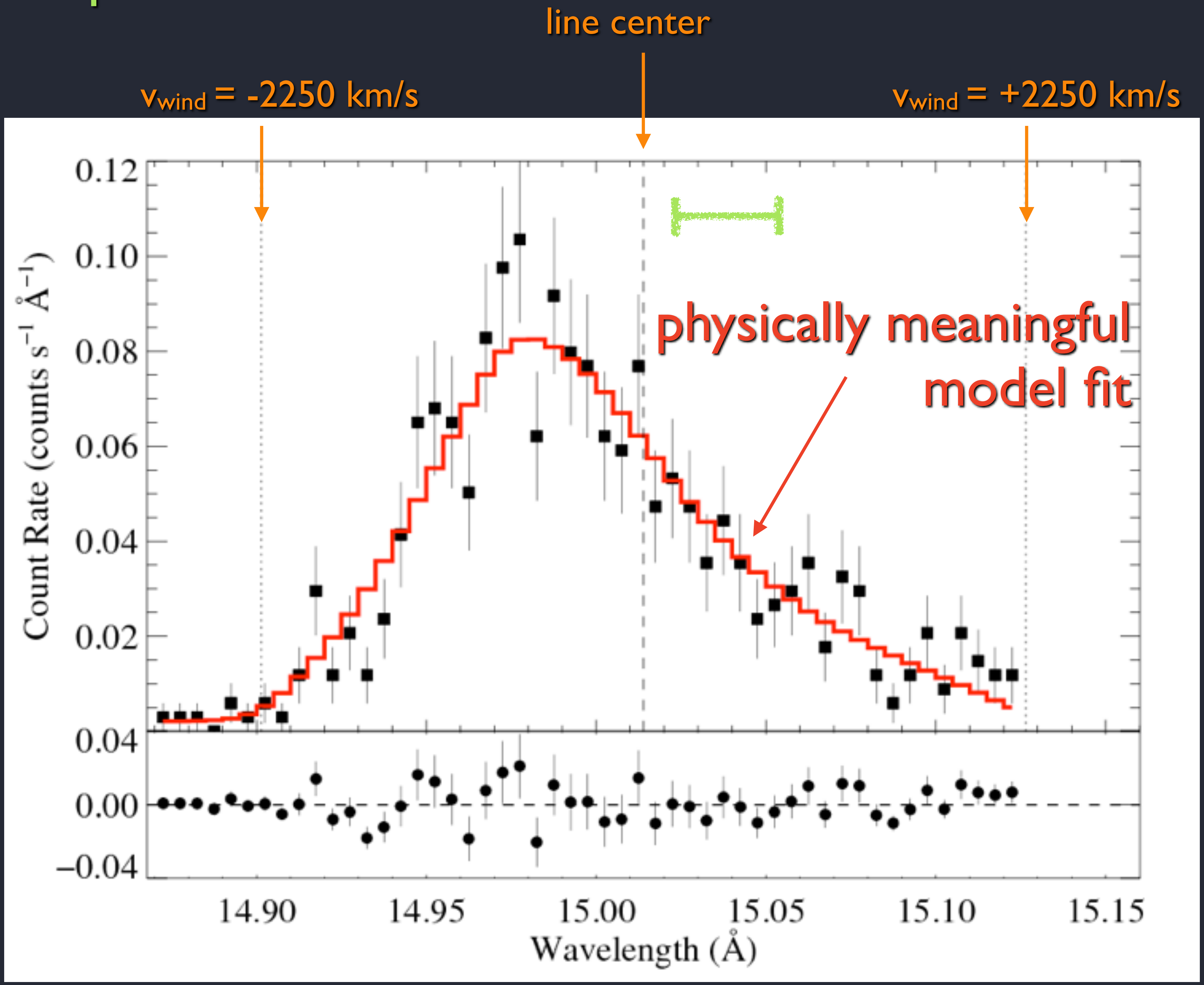

Rich diagnostics provided by HRXS

shock physics: hot plasma kinematics and spatial distribution *and* wind mass-loss rates and clumping properties

Chandra resolution

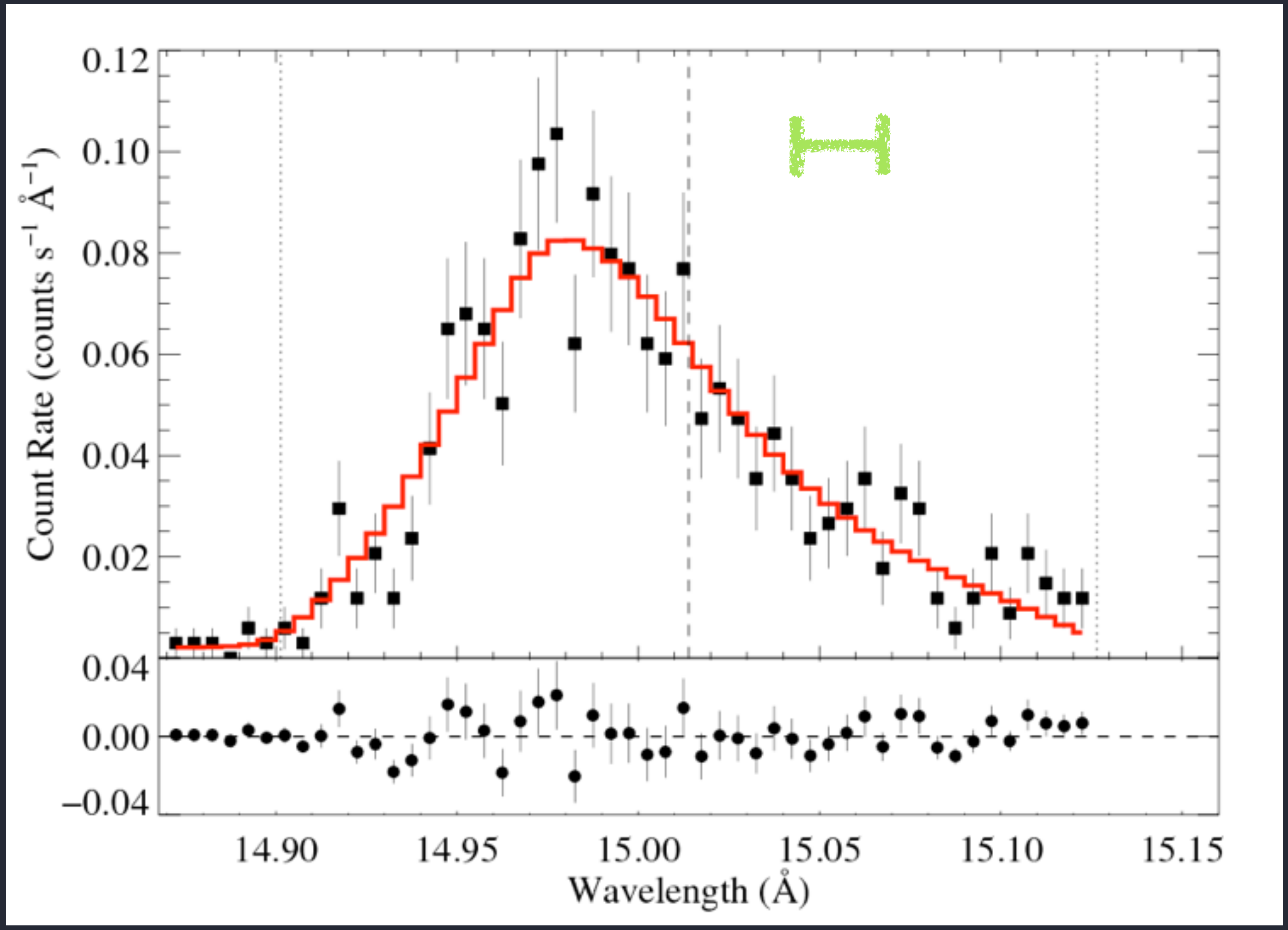

63 ks HETGS zeta Pup (O4 If)

Soft-X-ray emission is ubiquitous in O stars

$L_X \sim 10^{-7} L_{Bol}$ ($L_X \sim 10^{31}$ to 10^{33} ergs s^{-1})

soft thermal spectrum: $kT < 1$ keV

minimal time variability

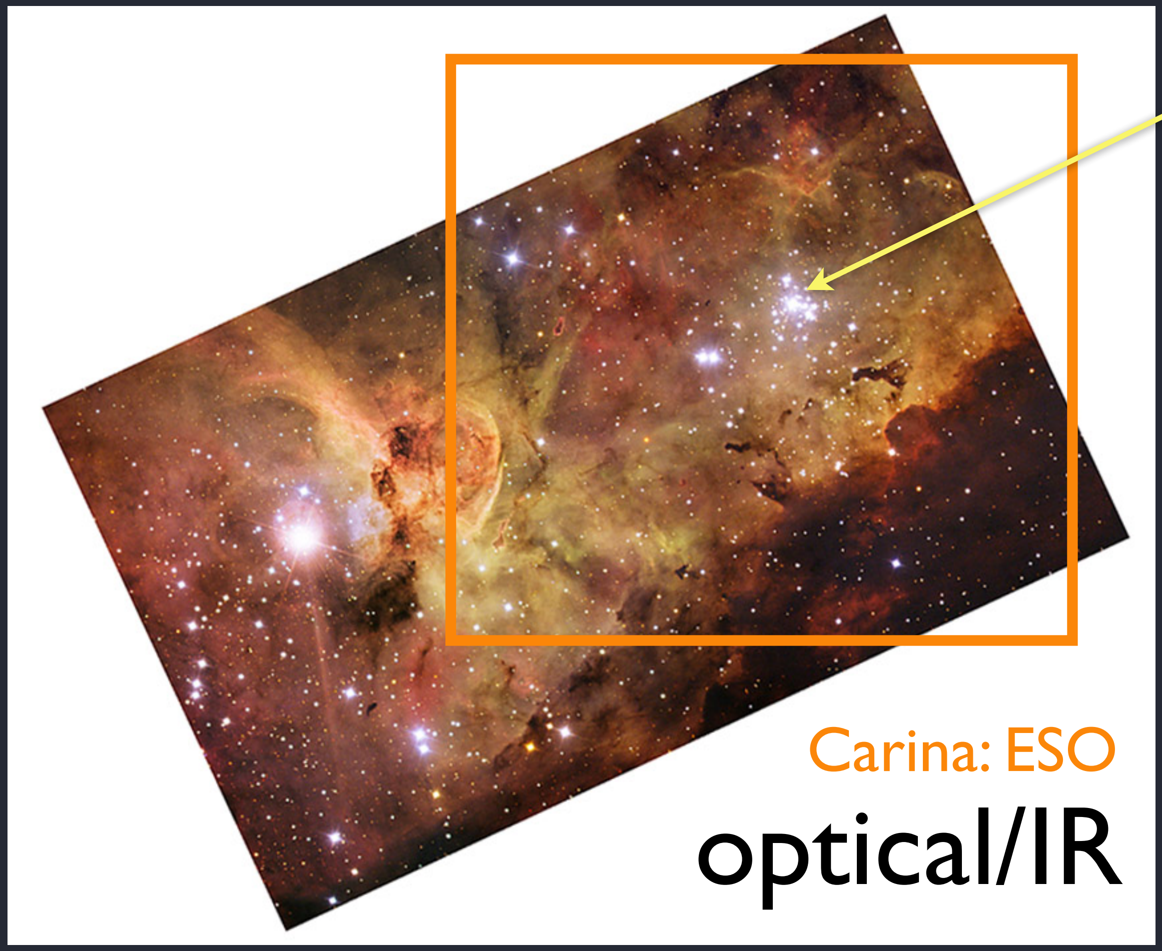

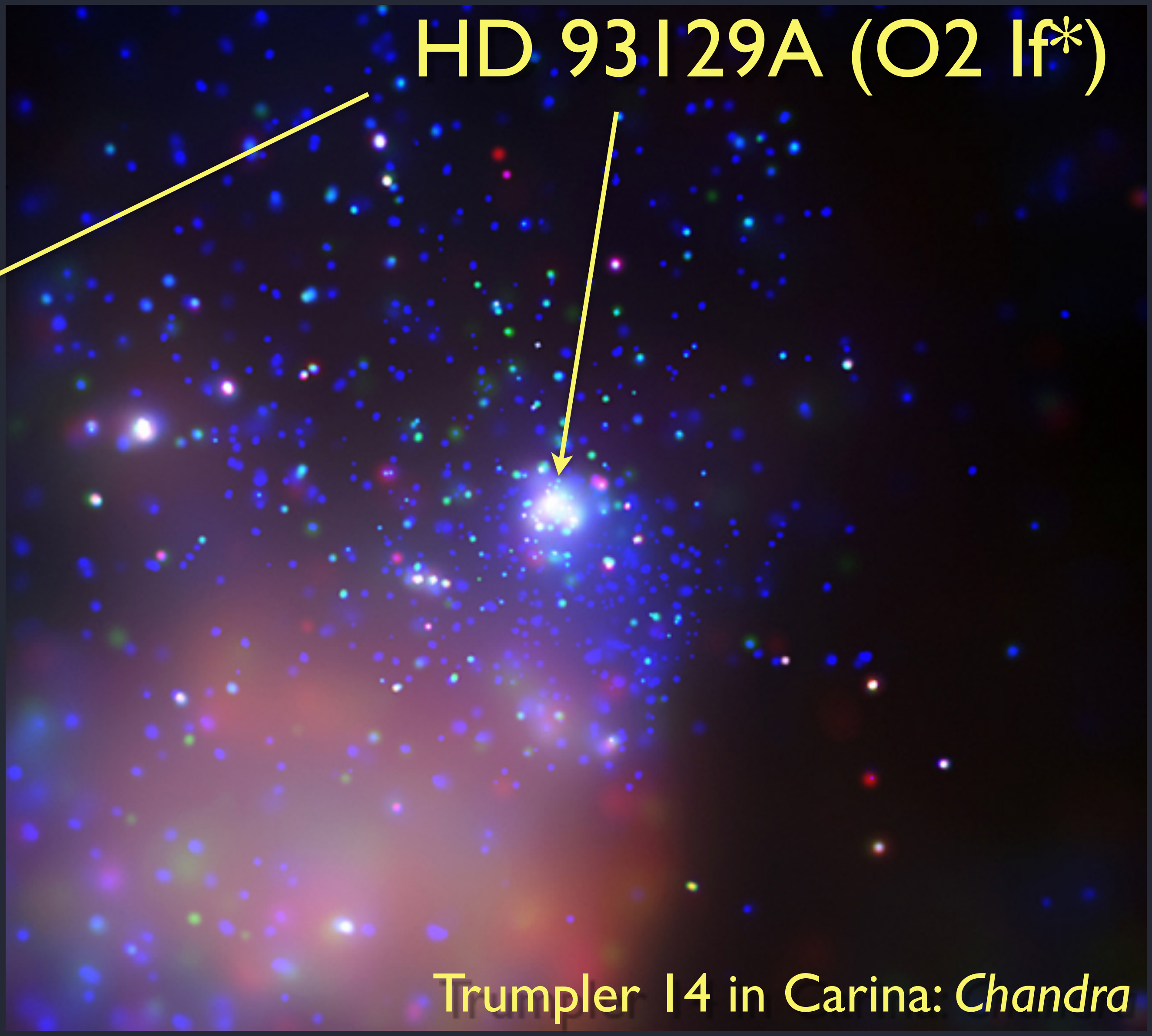

High- and low-mass stars have different X-ray production mechanisms

Massive stars show no correlation between rotation and X-ray emission
No convective envelope; no dynamo; no corona

X-ray luminosity

high mass

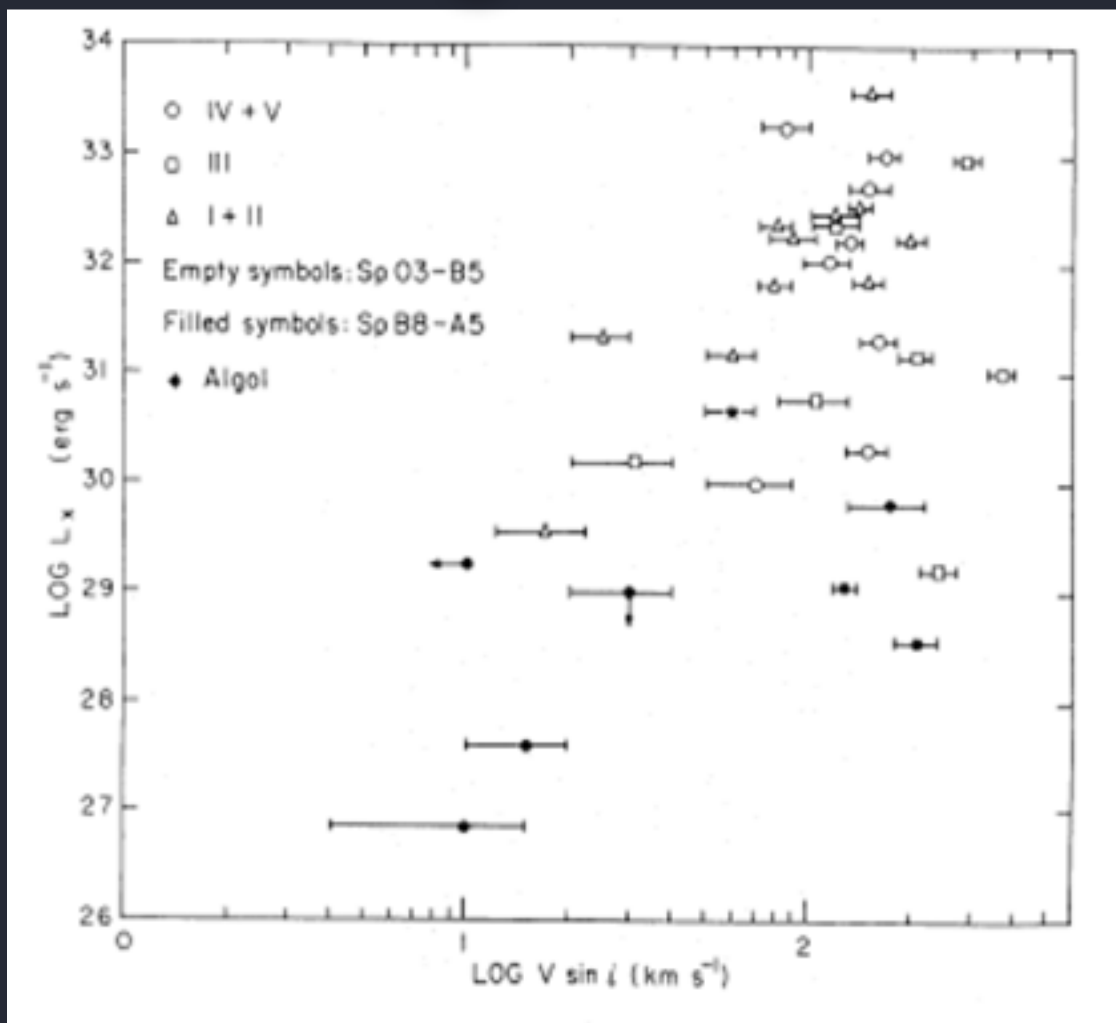

vsini

low mass

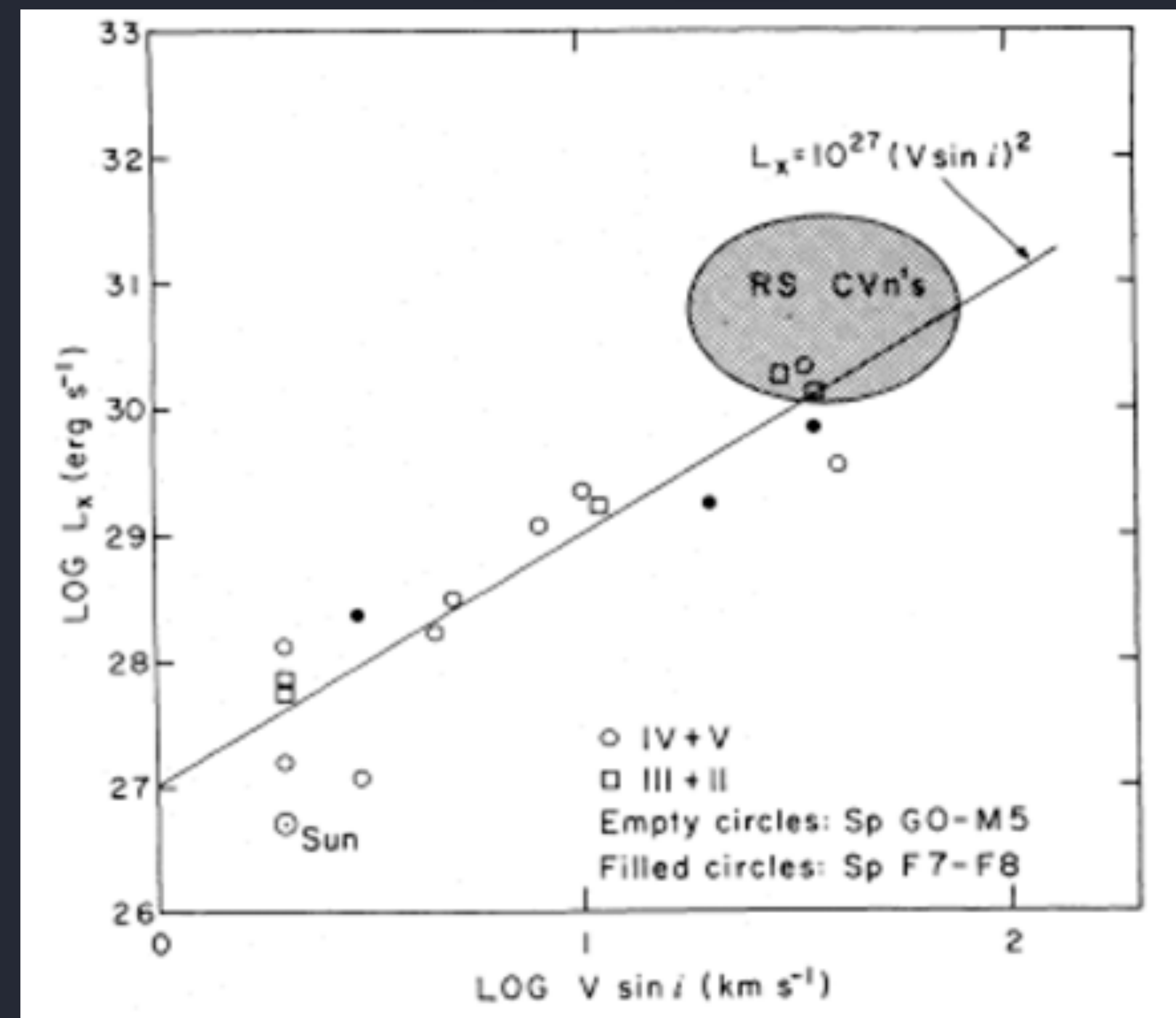

vsini

High- and low-mass stars have different X-ray production mechanisms

Massive stars produce X-rays via shock-heating of their **winds**

high mass

low mass

X-ray luminosity

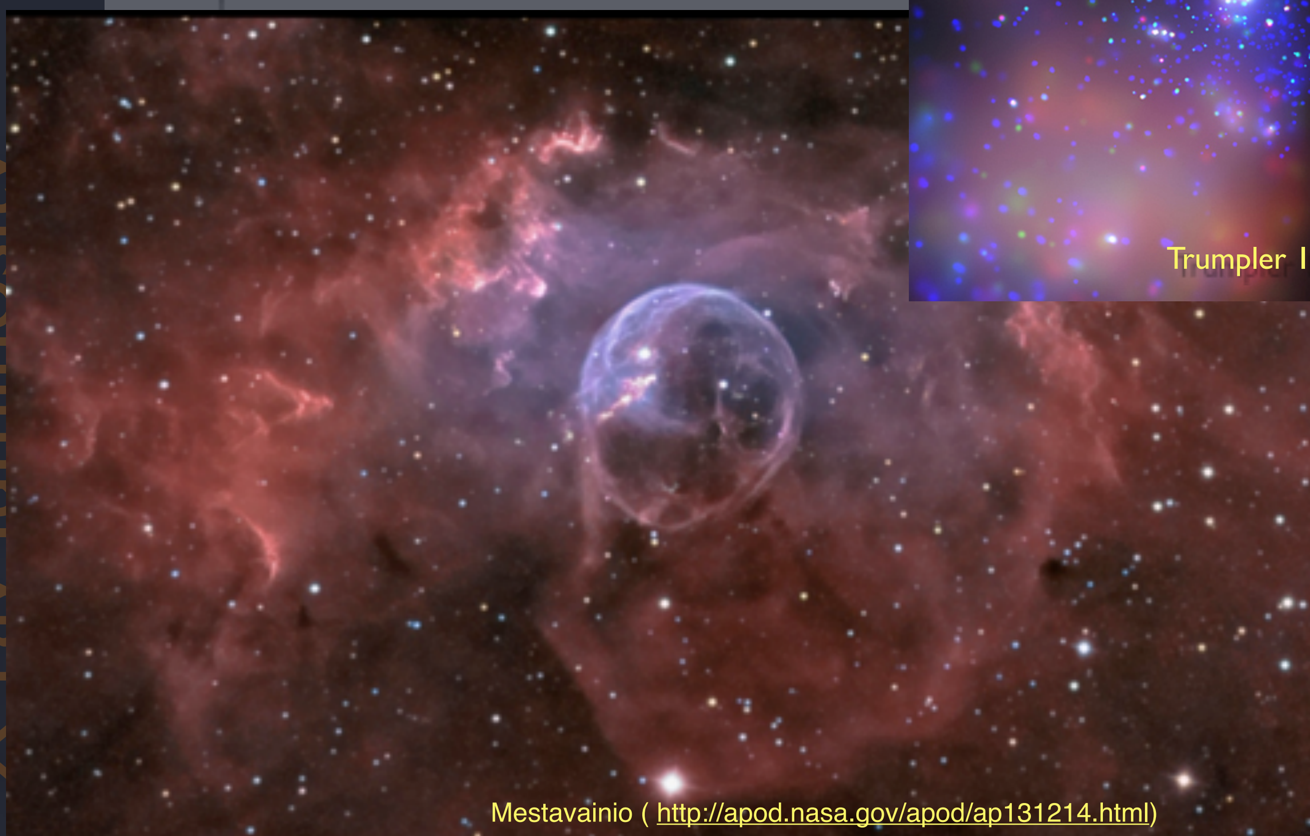
Mestavainio (http://apod.nasa.gov/apod/ap131214.html)


Trumpler 14 in Carina: *Chandra*

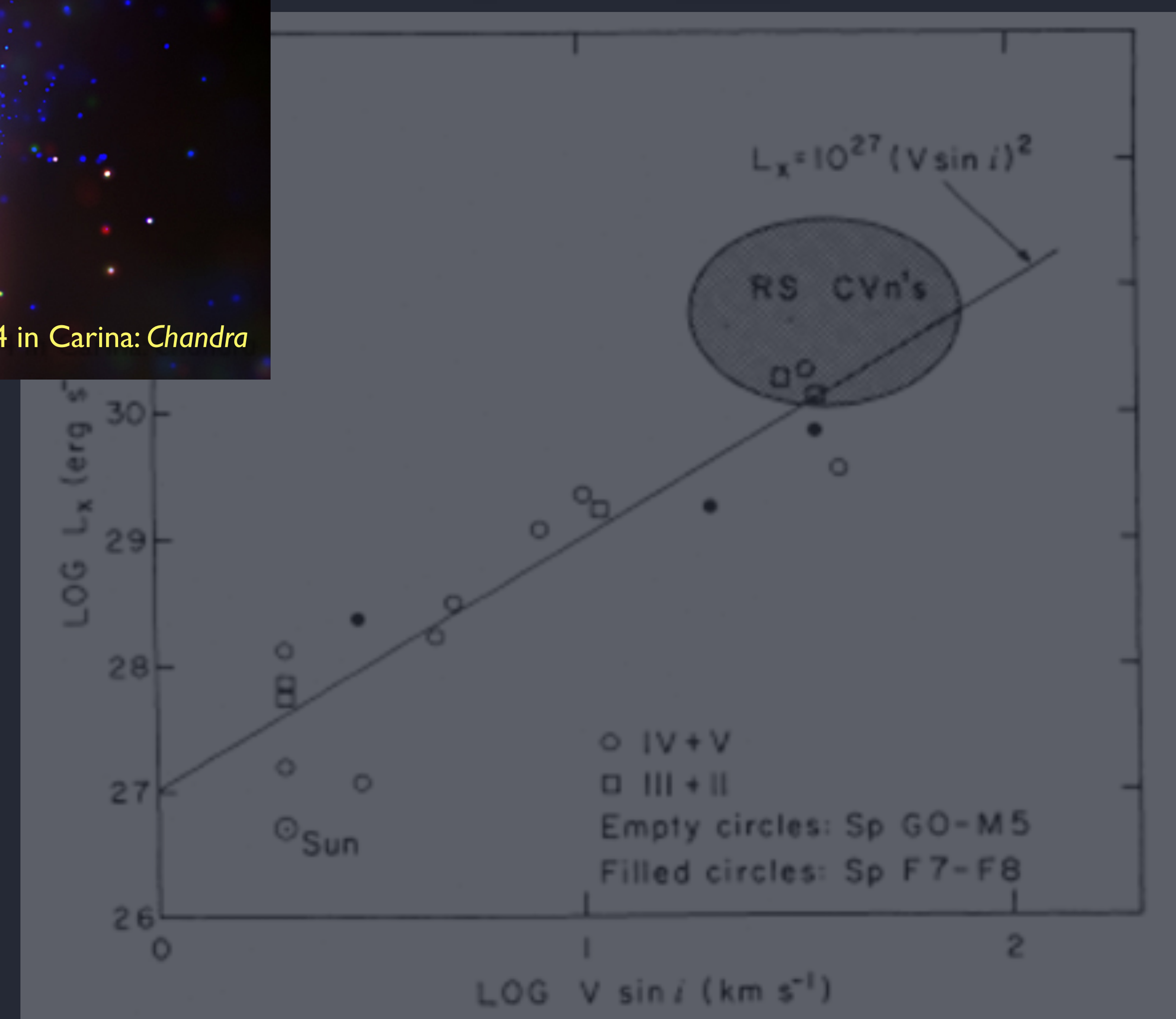

vsini

vsini

OB star winds are (line) radiation driven

& though they're very dense, they are *not* best seen via imaging

Mestavainio (http://apod.nasa.gov/apod/ap131214.html)

Radiation-driven O star winds

ζ Pup (O4 supergiant): $\dot{M} \sim$ few 10^{-6} M_{sun}/yr

UV spectrum: C IV 1548, 1551 Å

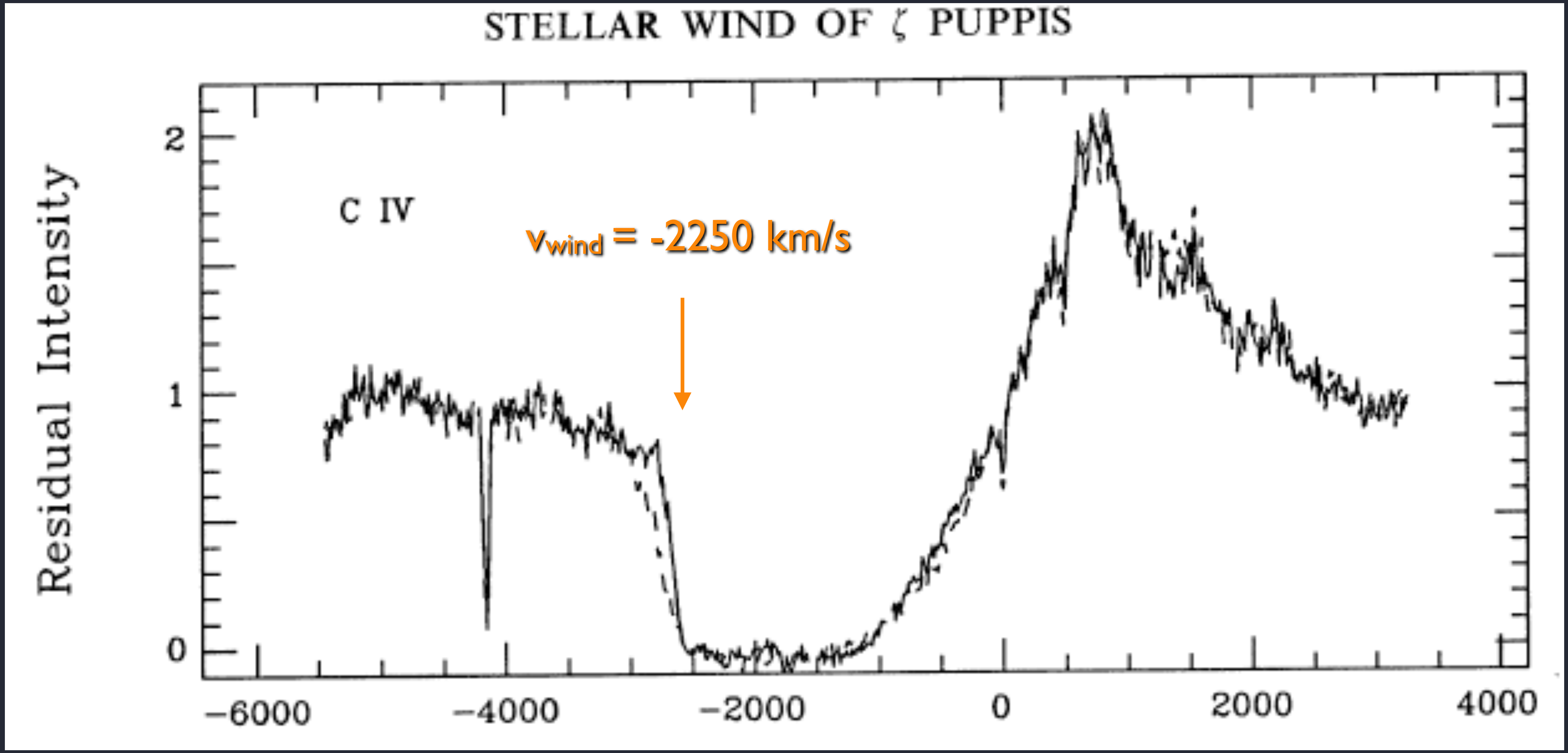

Velocity (km/s)

Prinja et al. 1992, ApJ, 390, 266

Radiation-driven O star winds

variability in wind UV lines

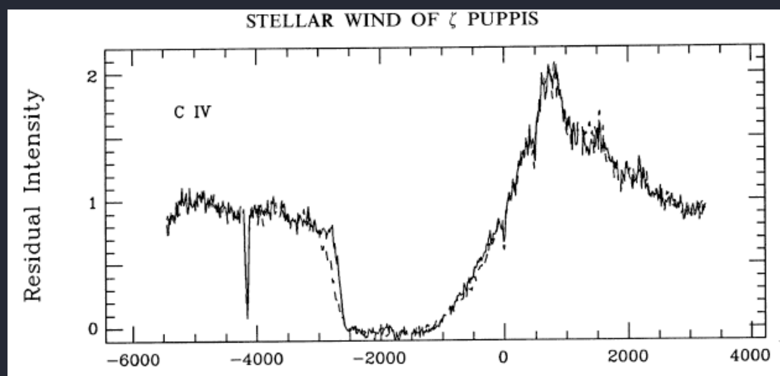

Velocity (km/s)

Prinja et al. 1992, ApJ, 390, 266

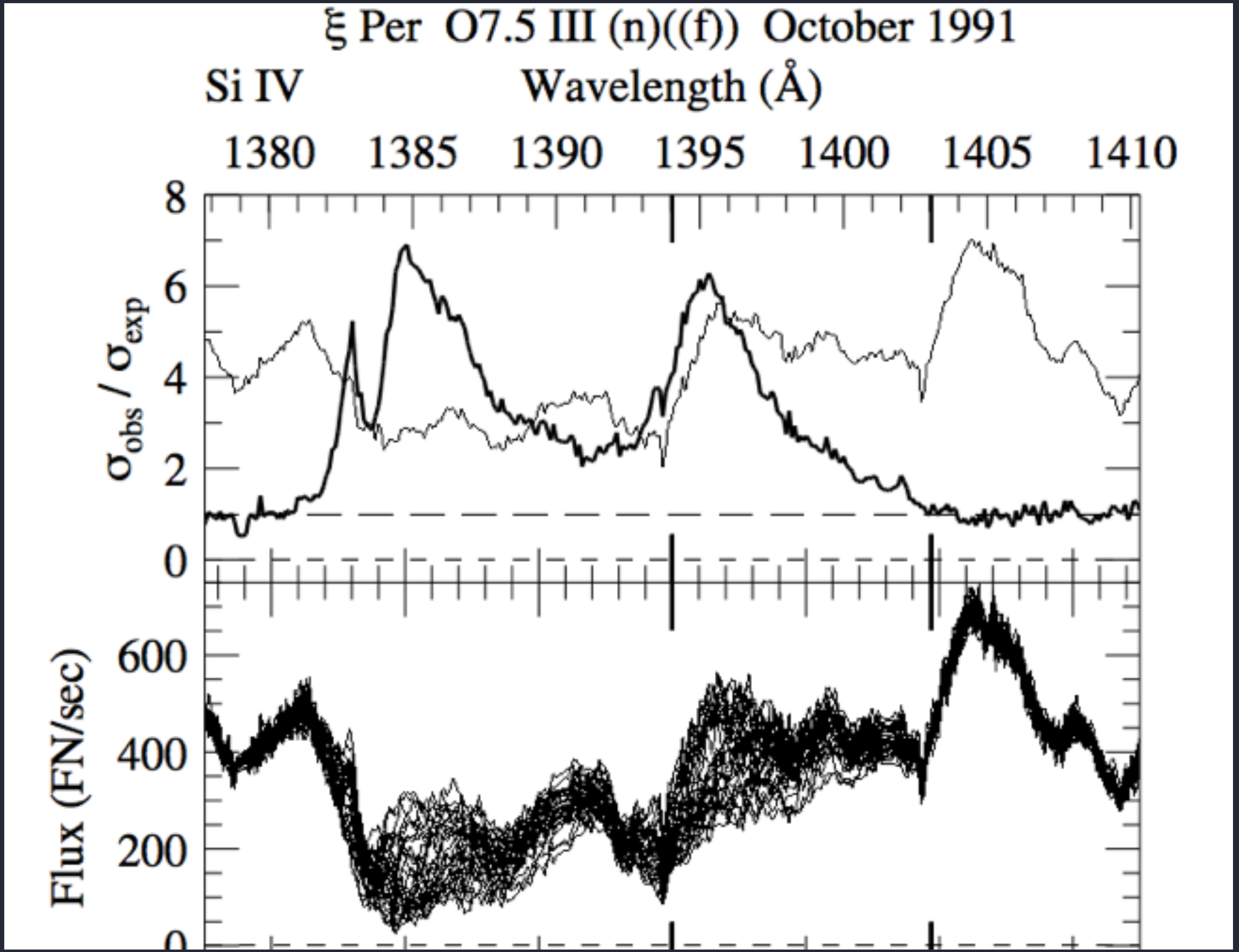

Embedded Wind Shock (EWS) paradigm

Line Deshadowing Instability (LDI) - intrinsic to line-driven flows

numerous shocks distributed throughout the wind, generally above some onset radius

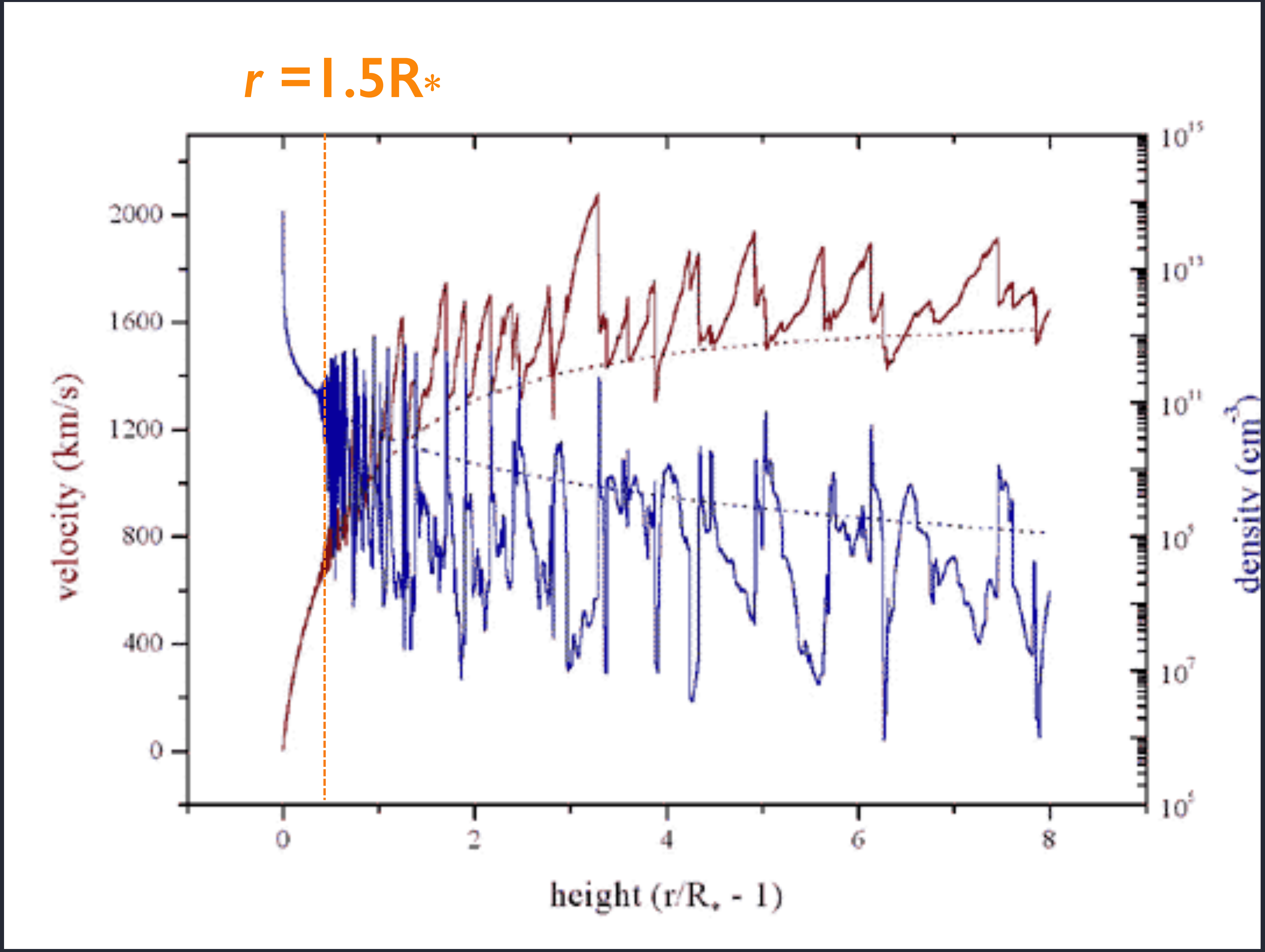

1-D radiation-hydro simulation

1-D rad-hydro simulation

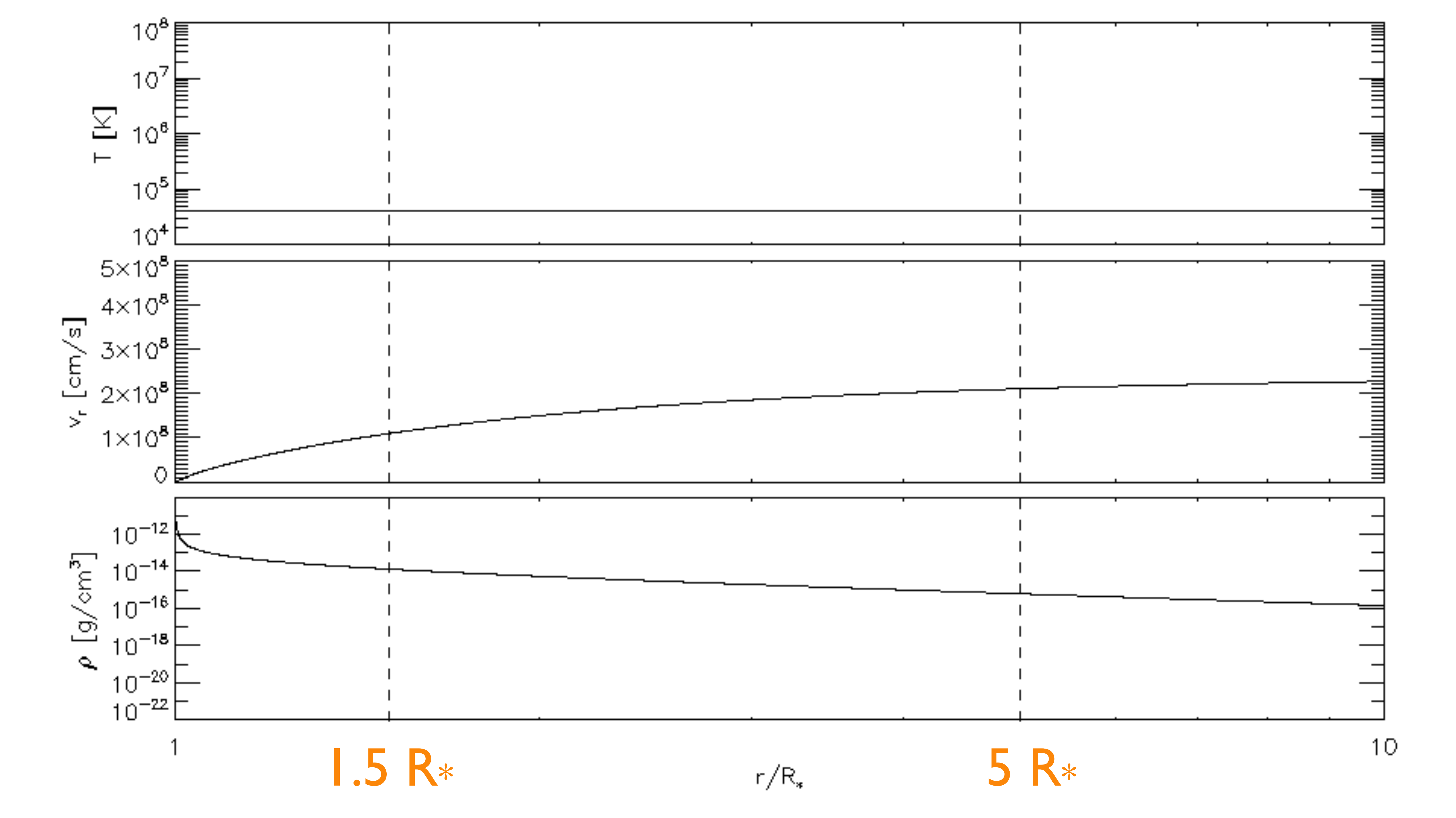

with J. Sundqvist, S. Owocki, Z. Li

movie available at http://astro.swarthmore.edu/~cohen/presentations/movies/ifrc3_abbott0.65_xkovbc350._xmbko1.e-2_epsabs-1.e-20.gif

Physics of the Line Deshadowing Instability (LDI)

Milne (1926)

radiation force depends on changes in the local wind velocity (moving out of the Doppler shadow)

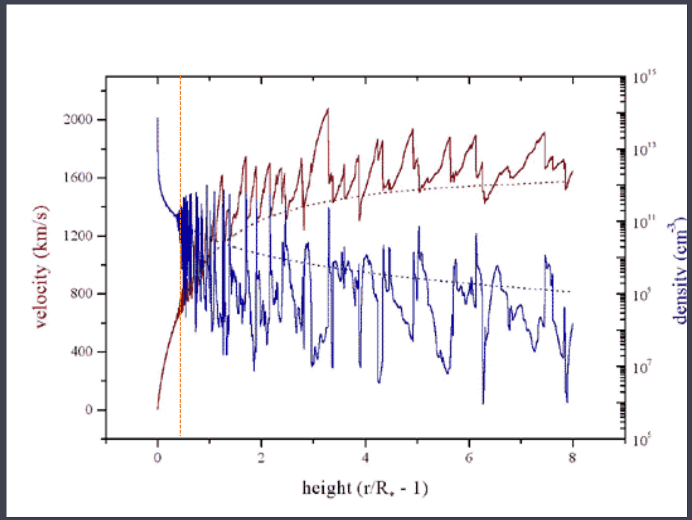

stability analysis: Owocki, Castor, Rybicki (1984,1988)

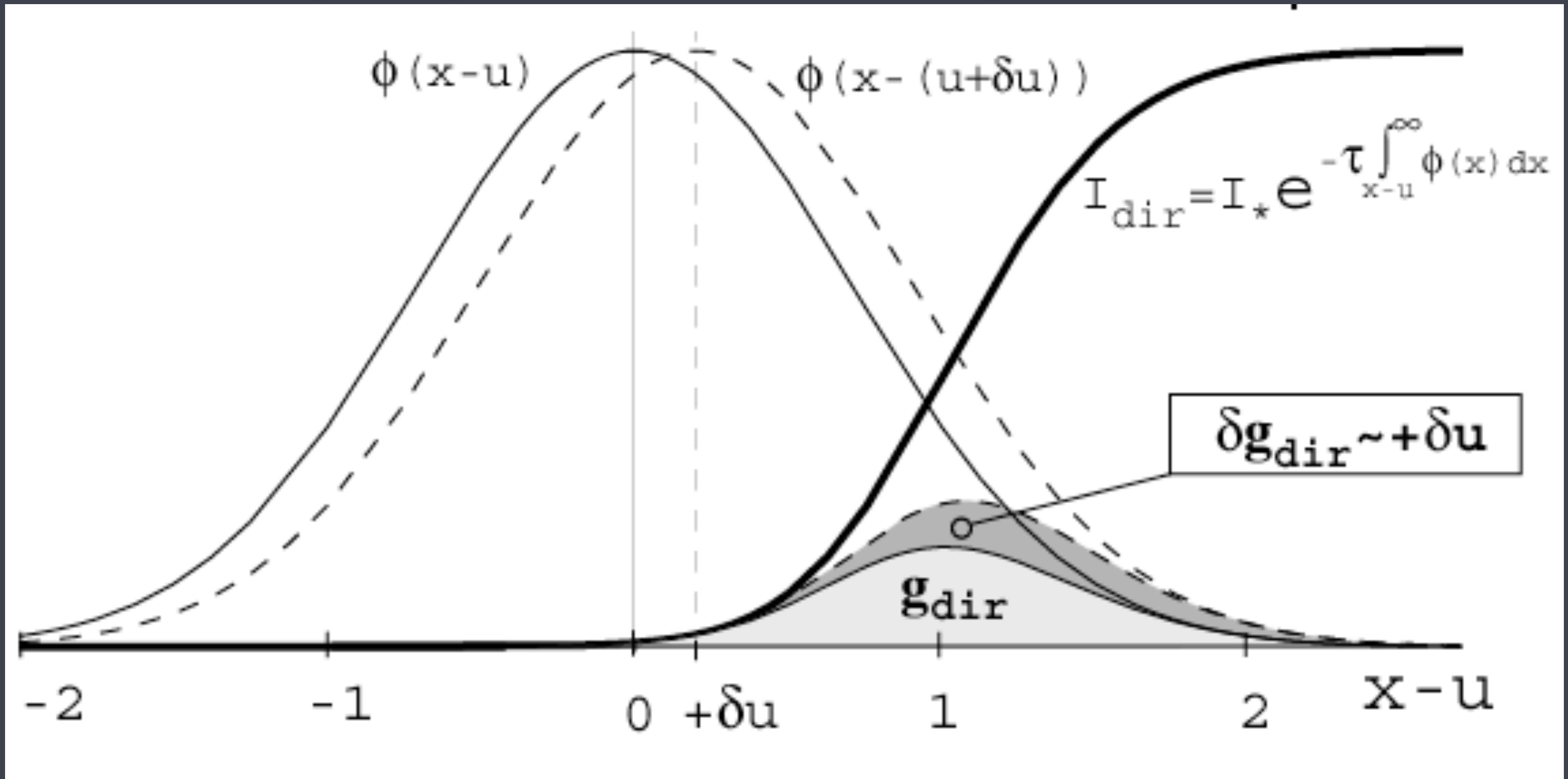

overlap between line profile and local radiation field

Embedded Wind Shock (EWS) paradigm

Less than 1% of the mass of the wind is emitting X-rays

>99% of the wind is cold and X-ray *absorbing*

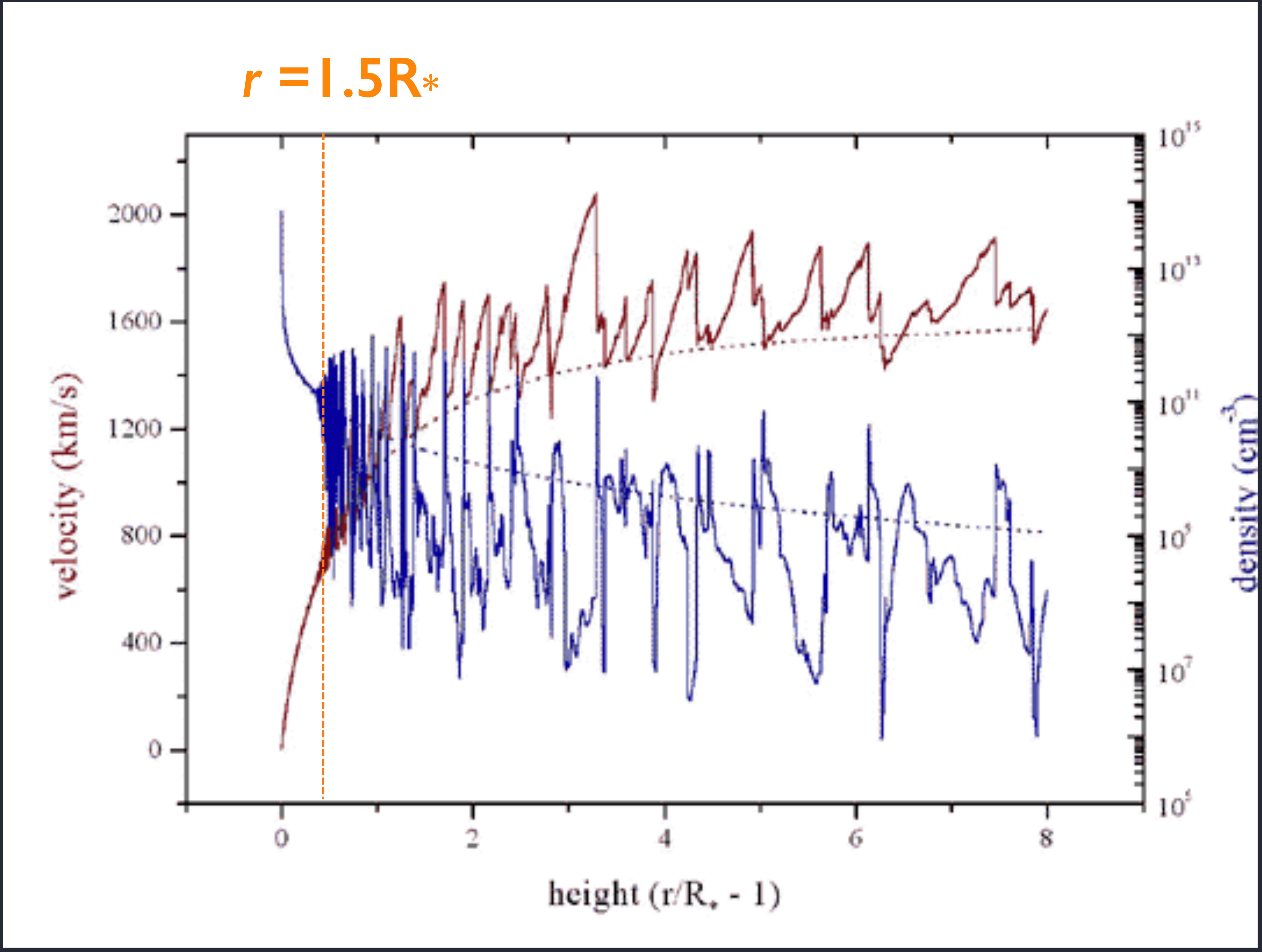

Open theoretical issues

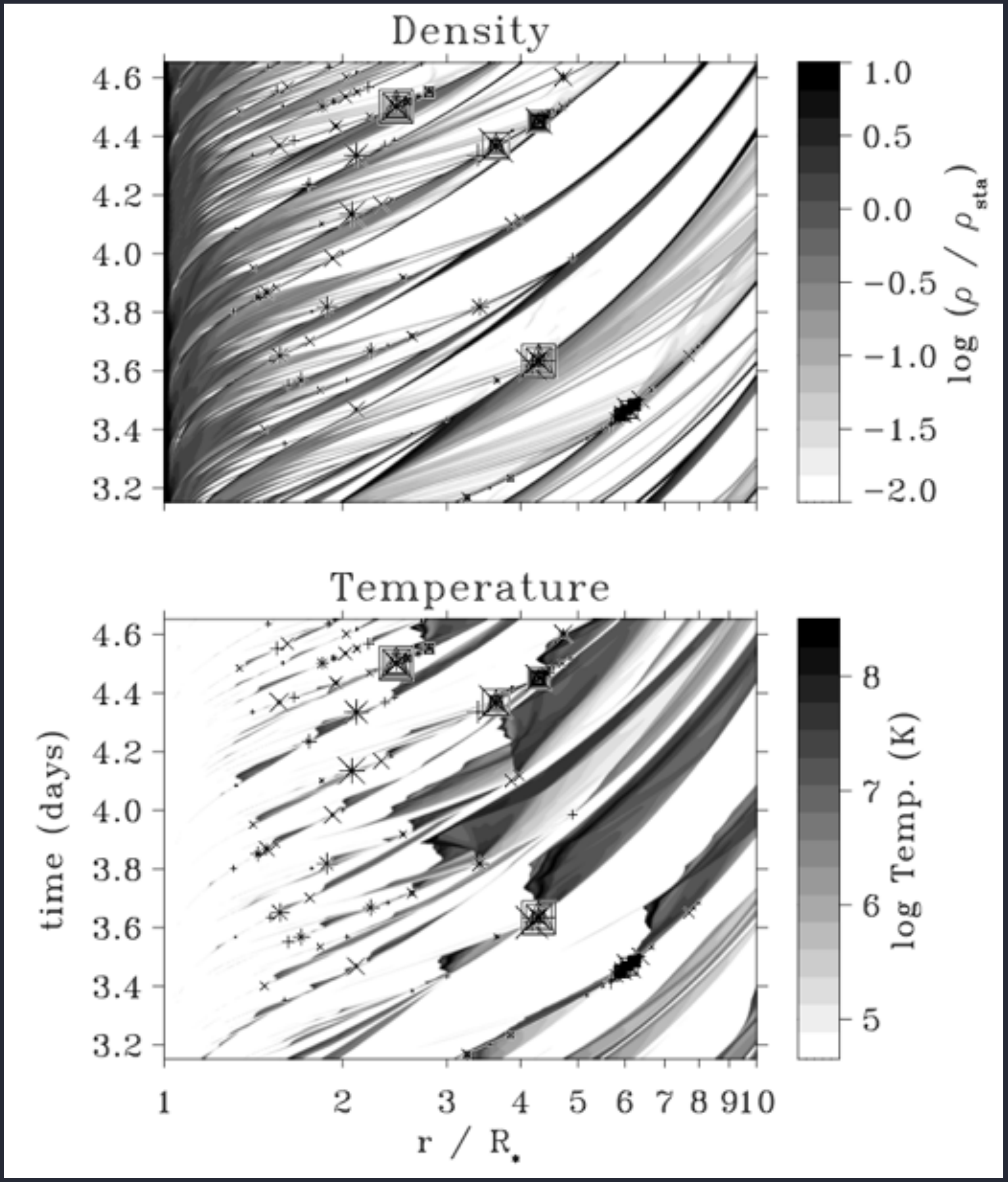

clump-clump collisions
vs.
self-excited instability

Feldmeier, Puls, & Pauldrach (1997)

Lower boundary conditions

self-excited

photospheric perturbations + limb darkening

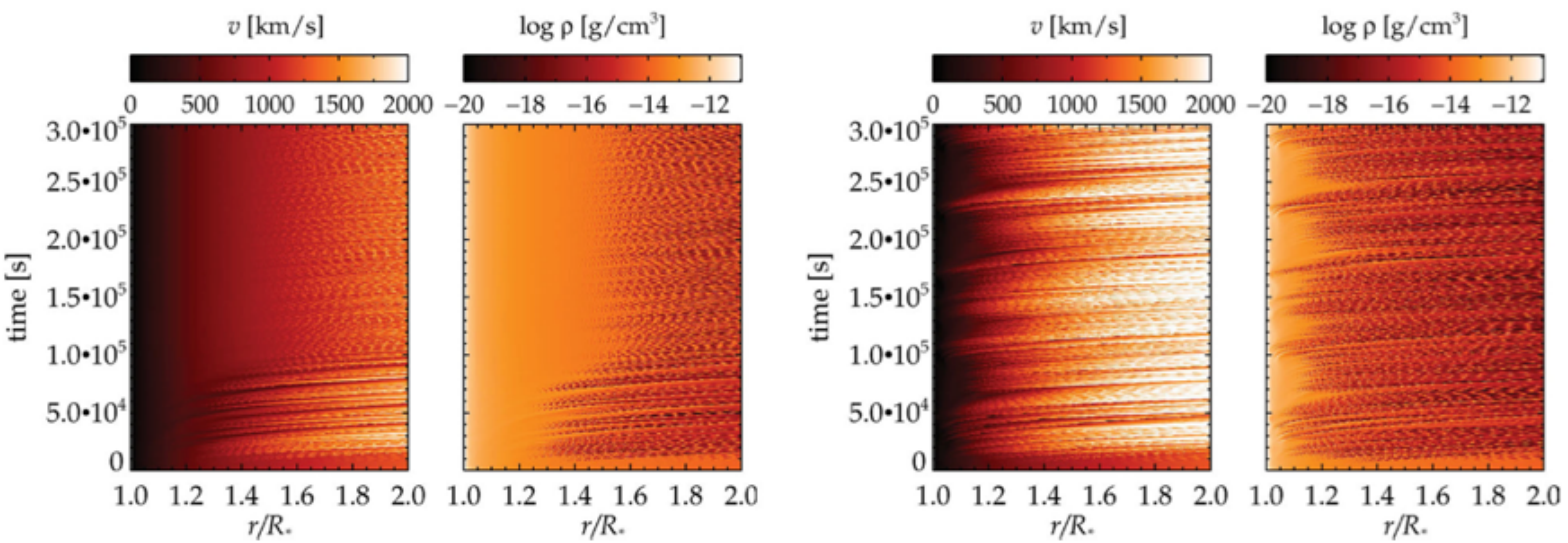

Figure 4. Inner wind time evolutions of a simulation without limb darkening and photospheric perturbations (left) and one including both effects (right).

Sundqvist & Owocki (2013)

2-D radiation-hydro simulations

initial work; line transport is expensive

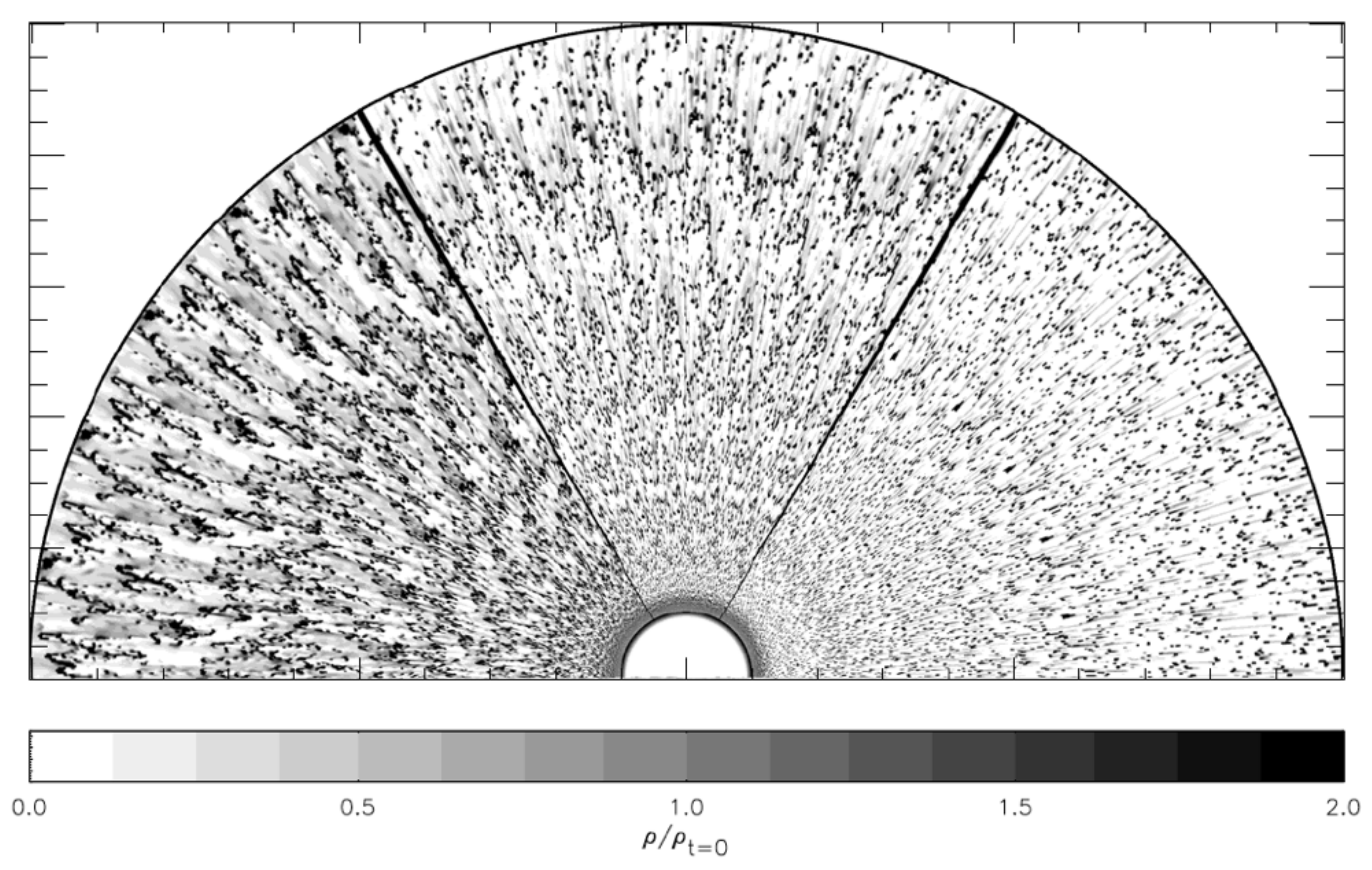

Dessart & Owocki 2003

Simulations constrained by data?

In addition to explaining the overall X-ray emission levels, the LDI physics generating embedded wind shocks makes predictions that can be tested by high-resolution X-ray spectroscopy:

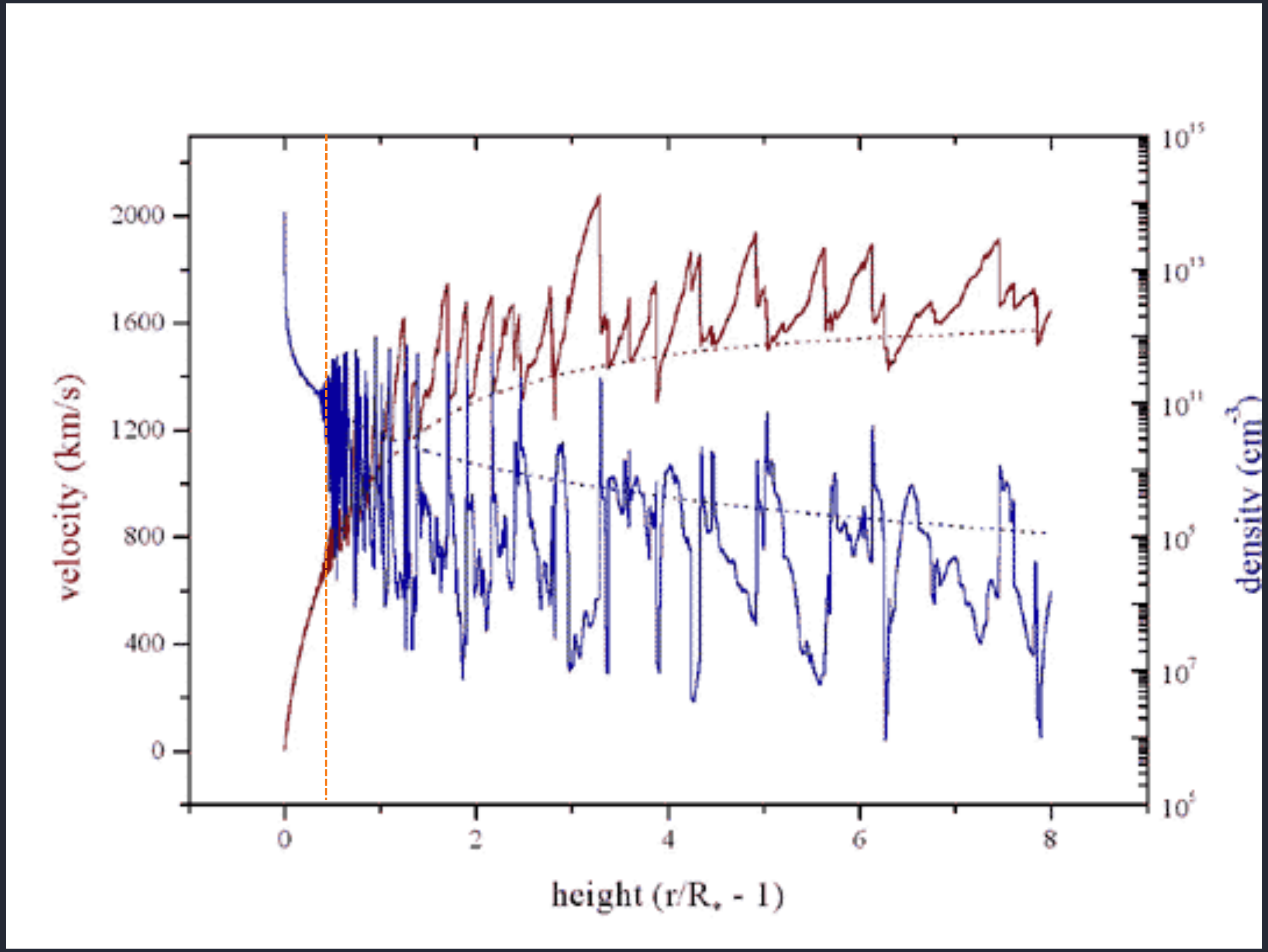

Spatial distribution of X-ray emitting plasma

Kinematics

Degree of absorption by the wind in which it's embedded

…clumping

Chandra grating spectra confirmed the EWS scenario

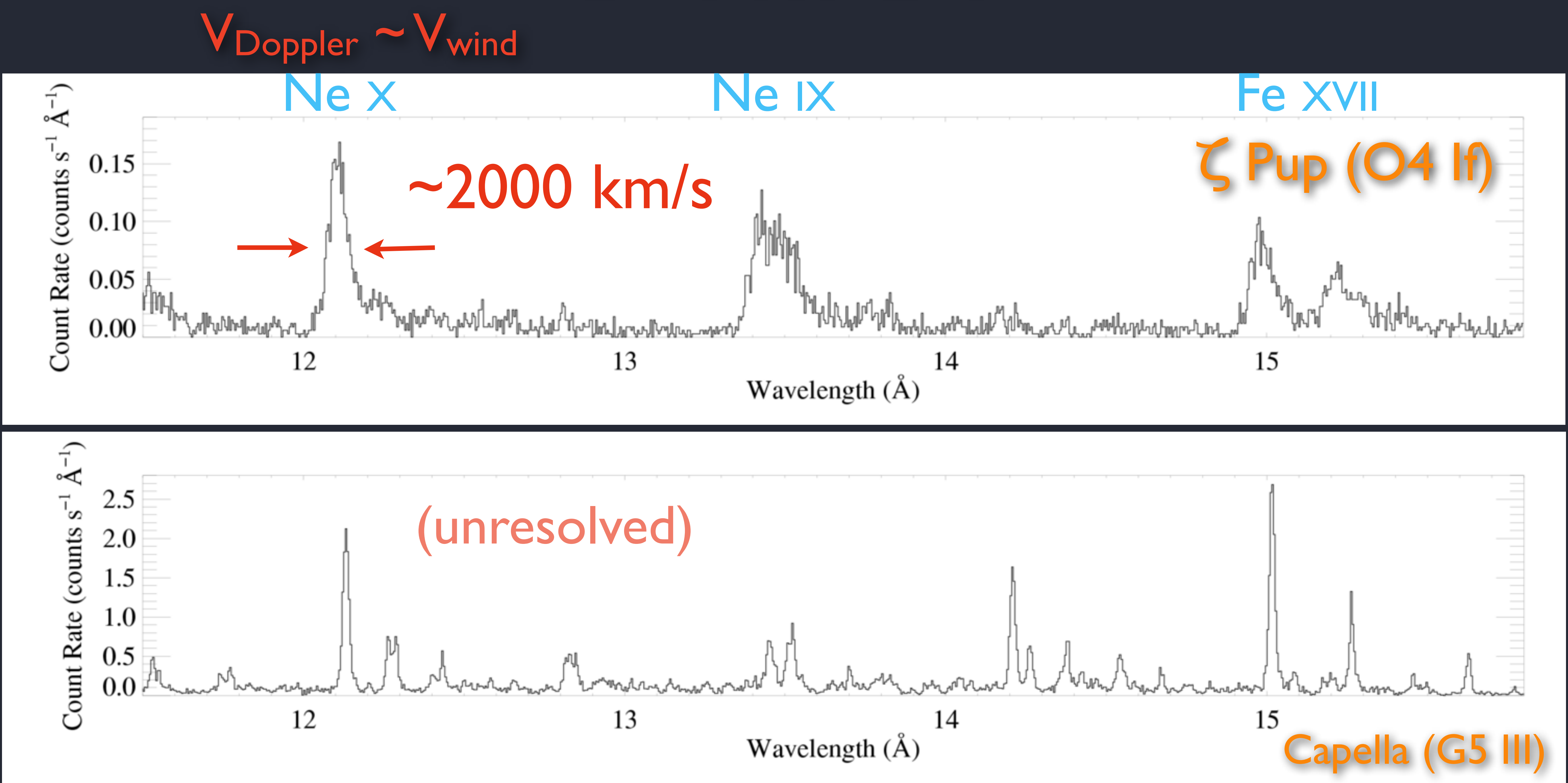

Chandra easily resolves the wind-broadened X-ray emission lines

lines are *asymmetric:*

this is a signature of wind absorption, and enables us to *measure the wind mass-loss rate*

ζ Pup (O4If)

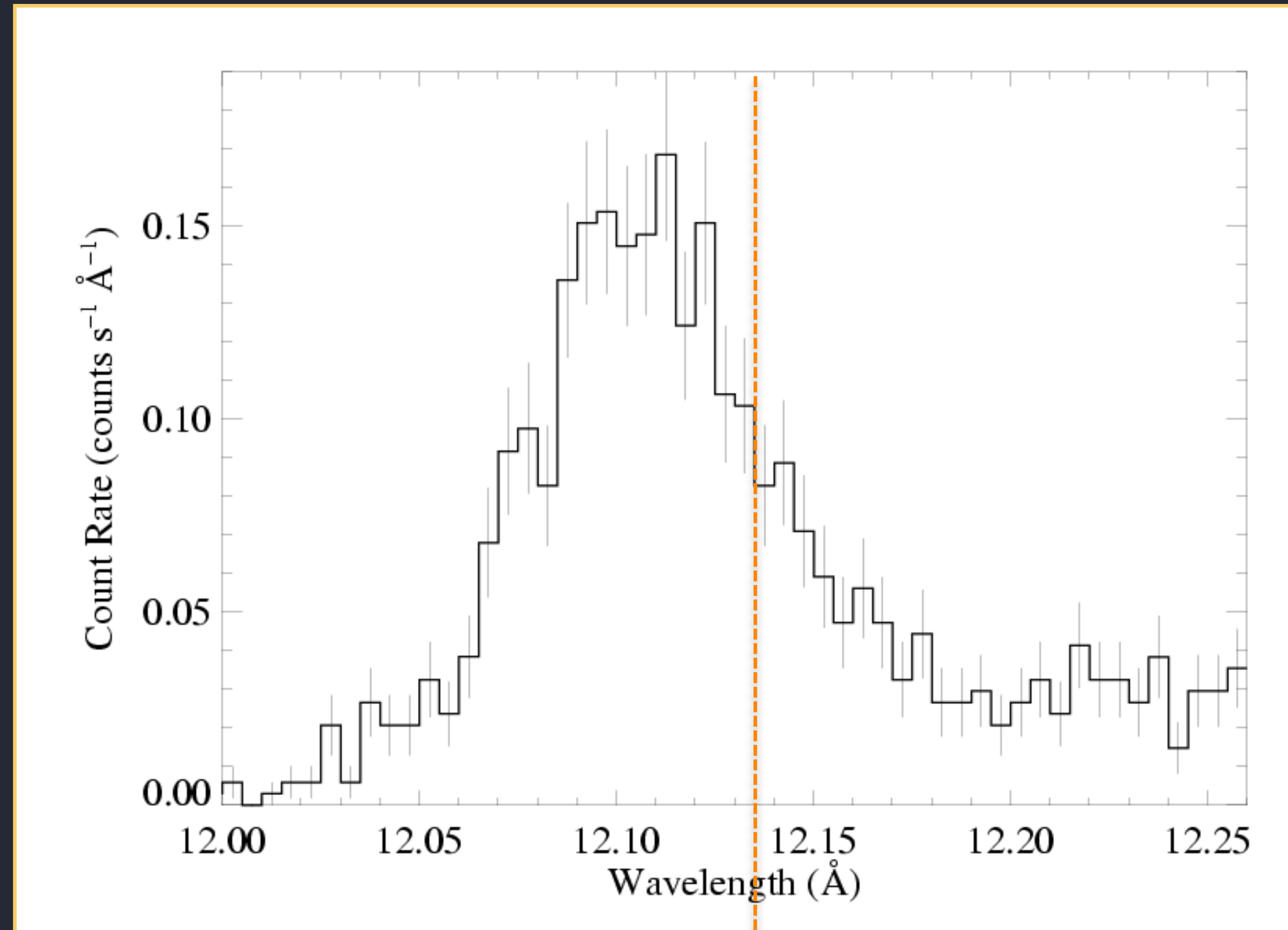

Capella (G5 III)

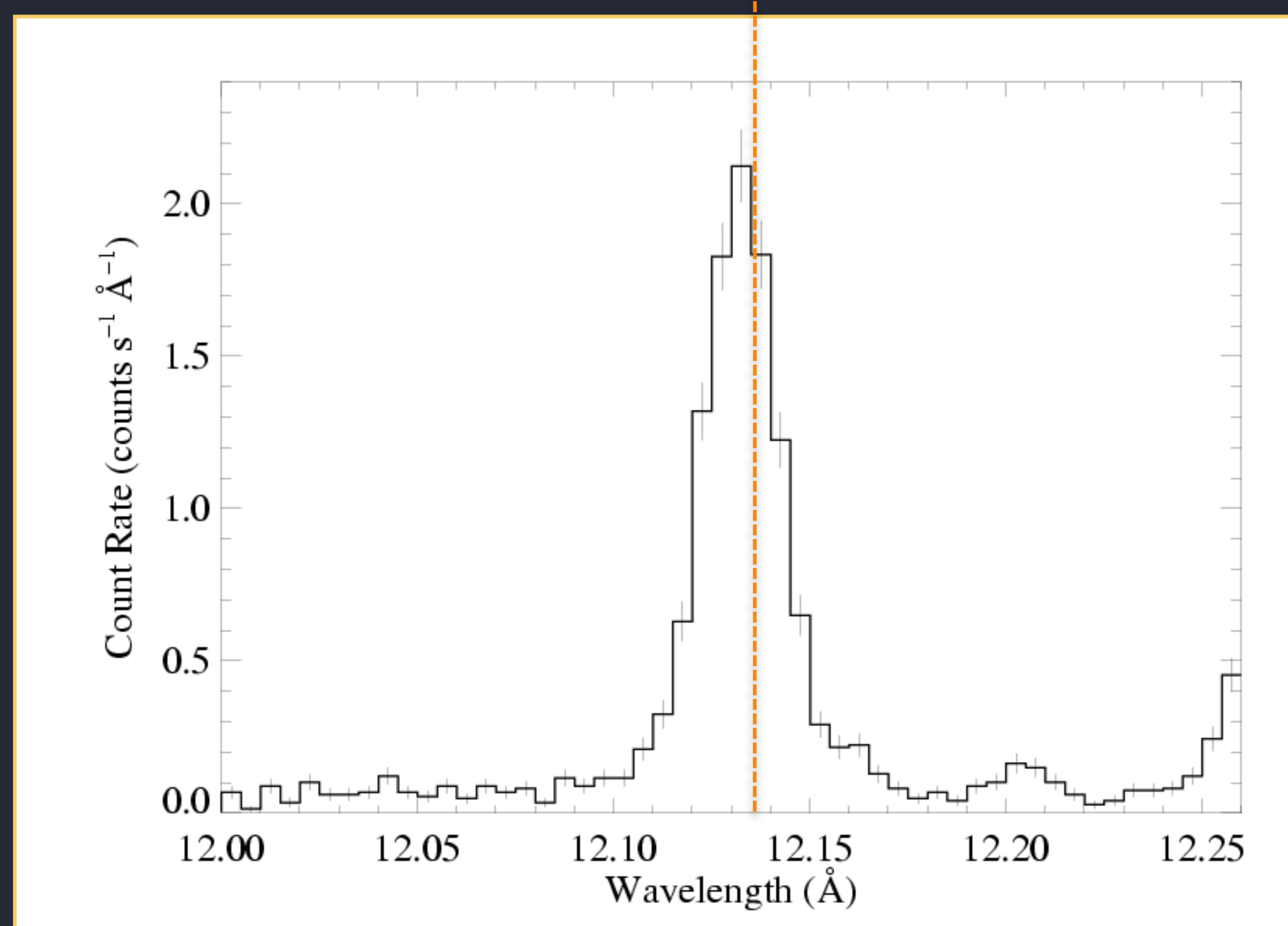

Build a model

to fit data

that captures the physics of the EWS/LDI

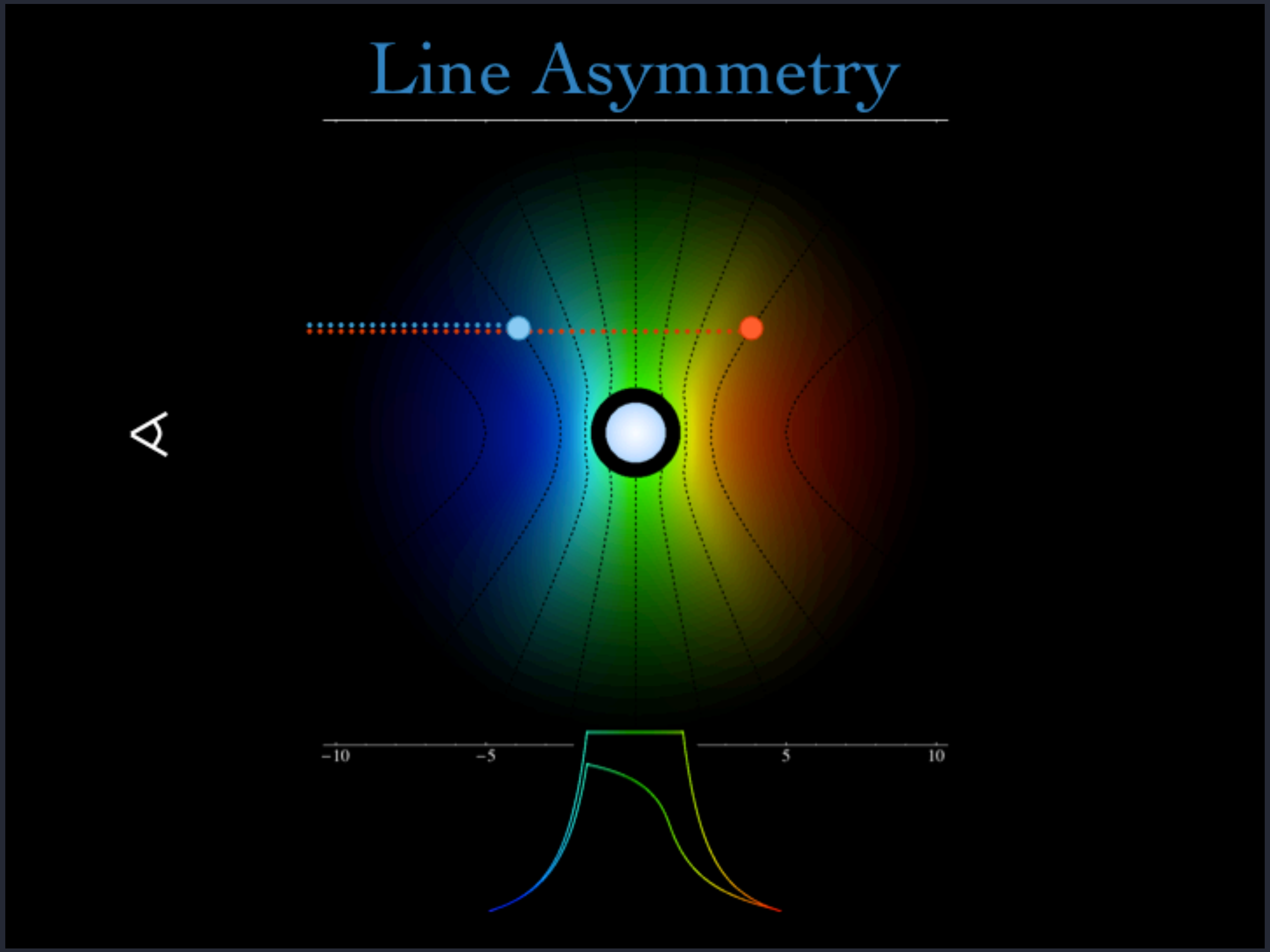

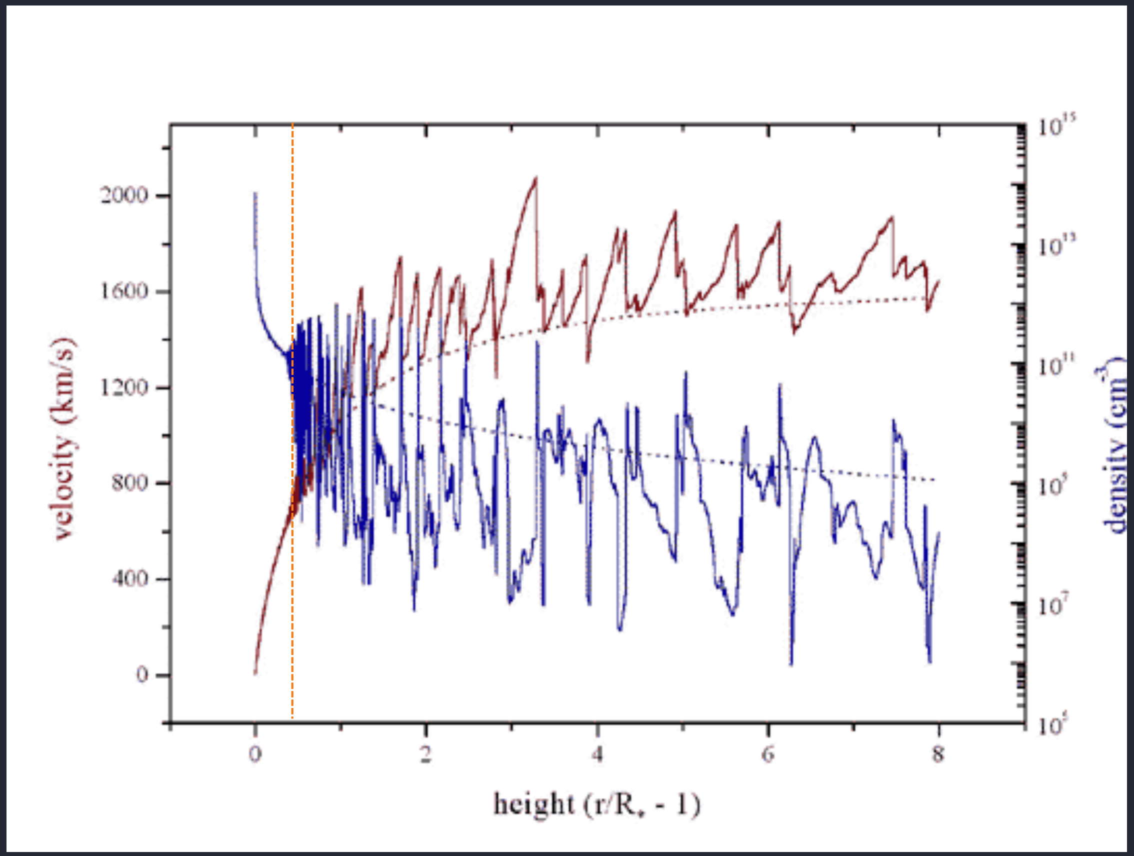

$v = v_\infty(1 - r/R_\star)^\beta$

beta velocity law assumed

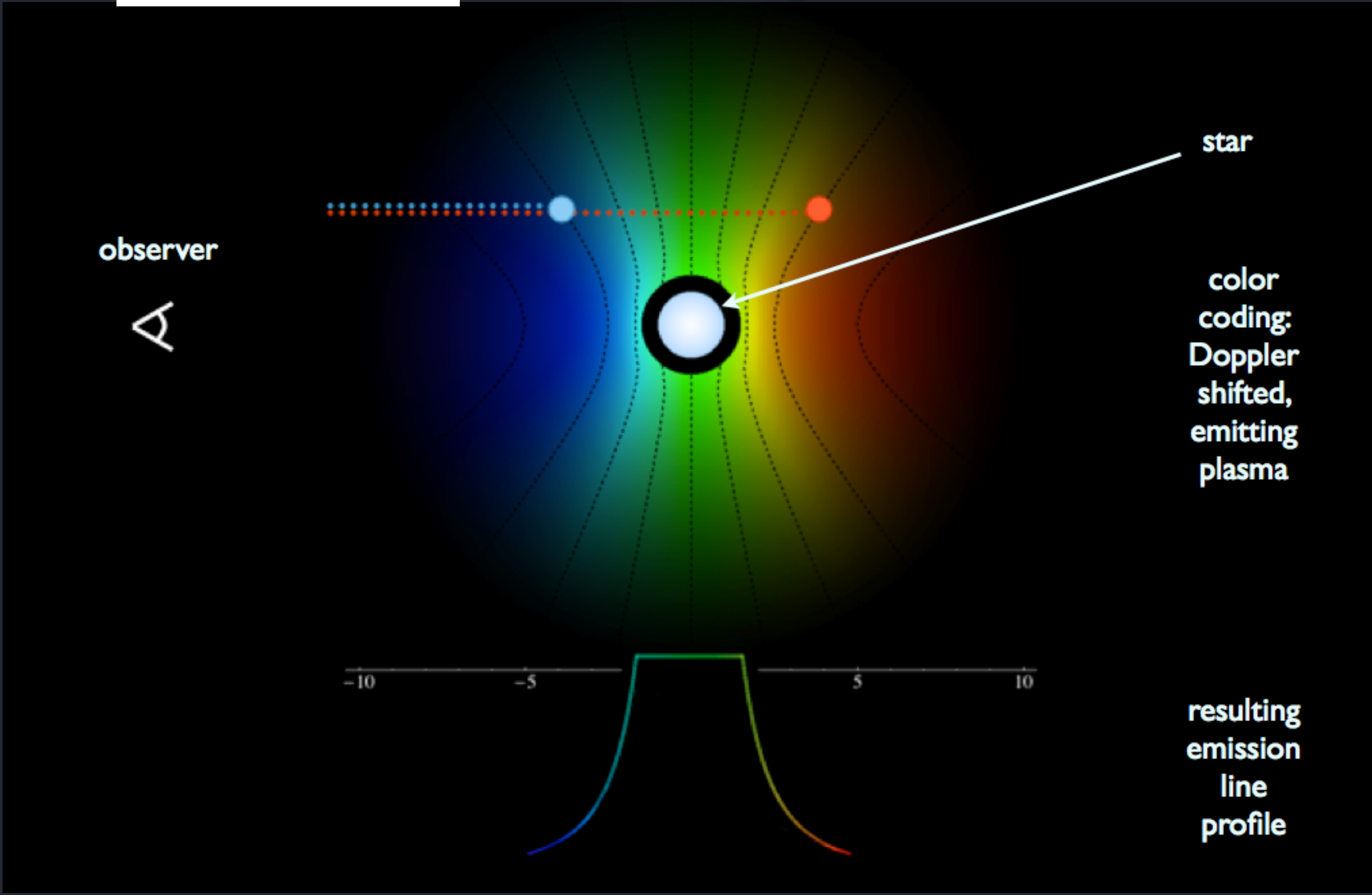

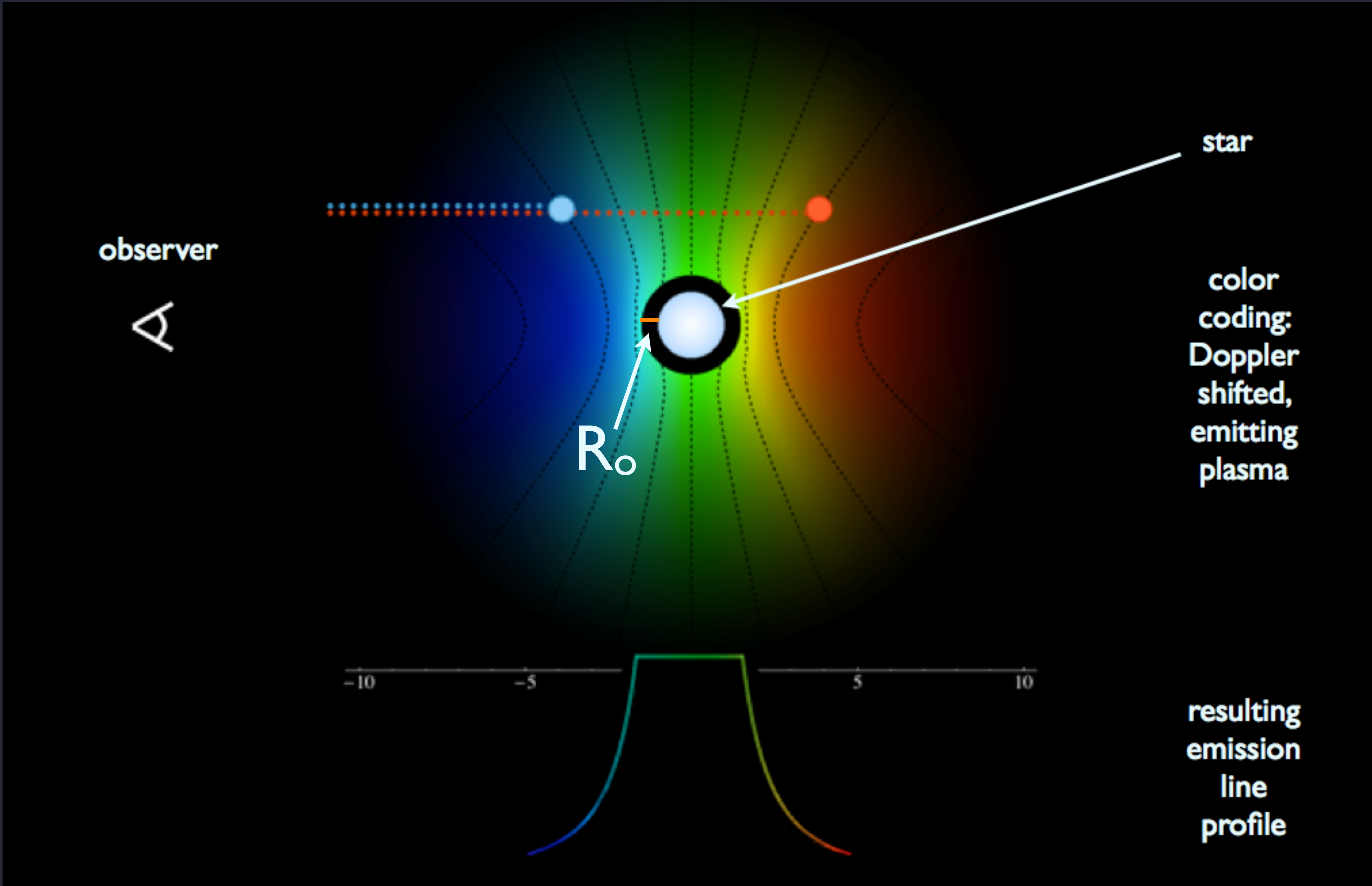
star
observer
color coding: Doppler shifted, emitting plasma
R_o
-10
-5
5
10
resulting emission line profile

Line Asymmetry

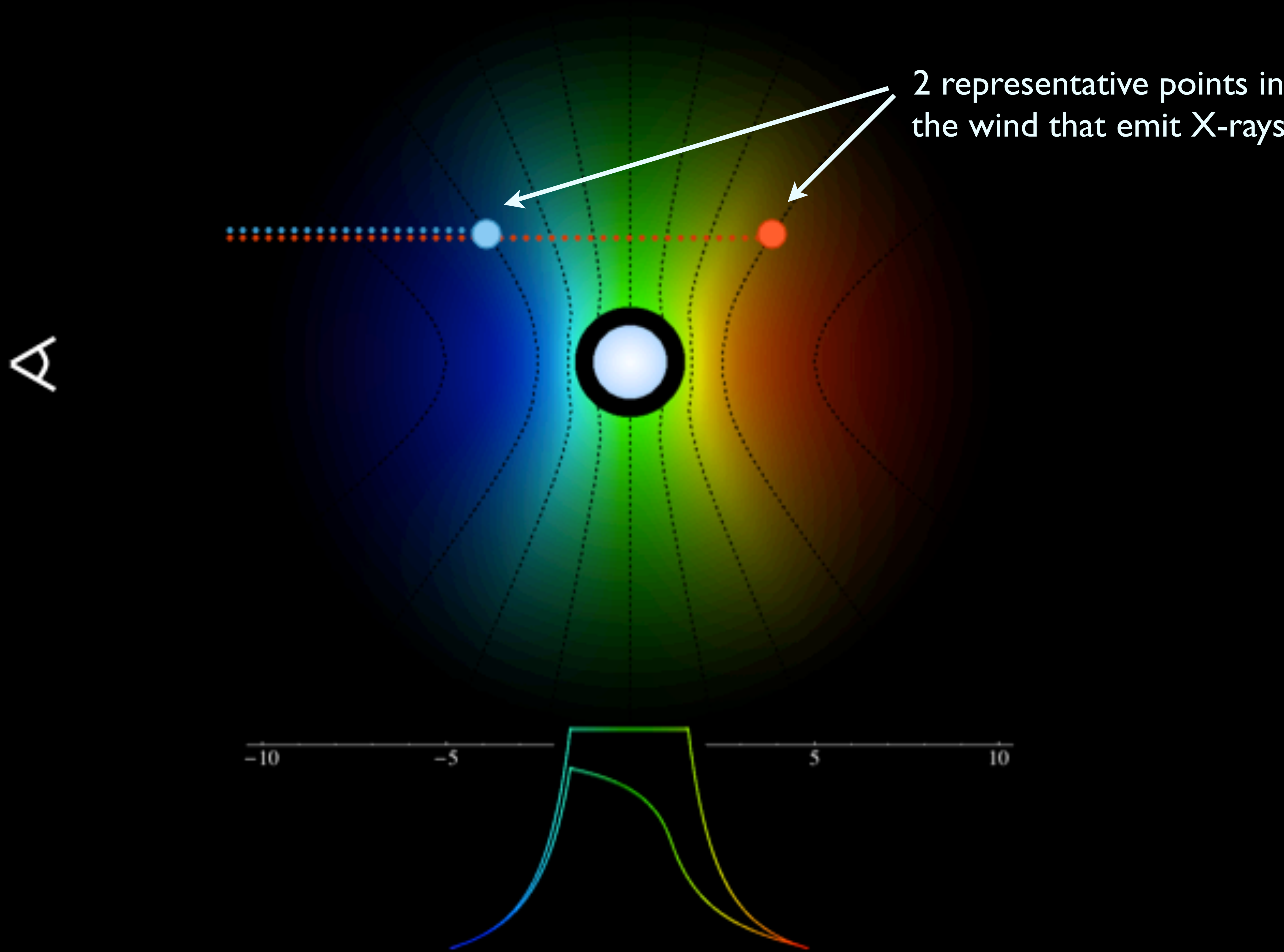

Line Asymmetry

2 representative points in the wind that emit X-rays

absorption along the ray

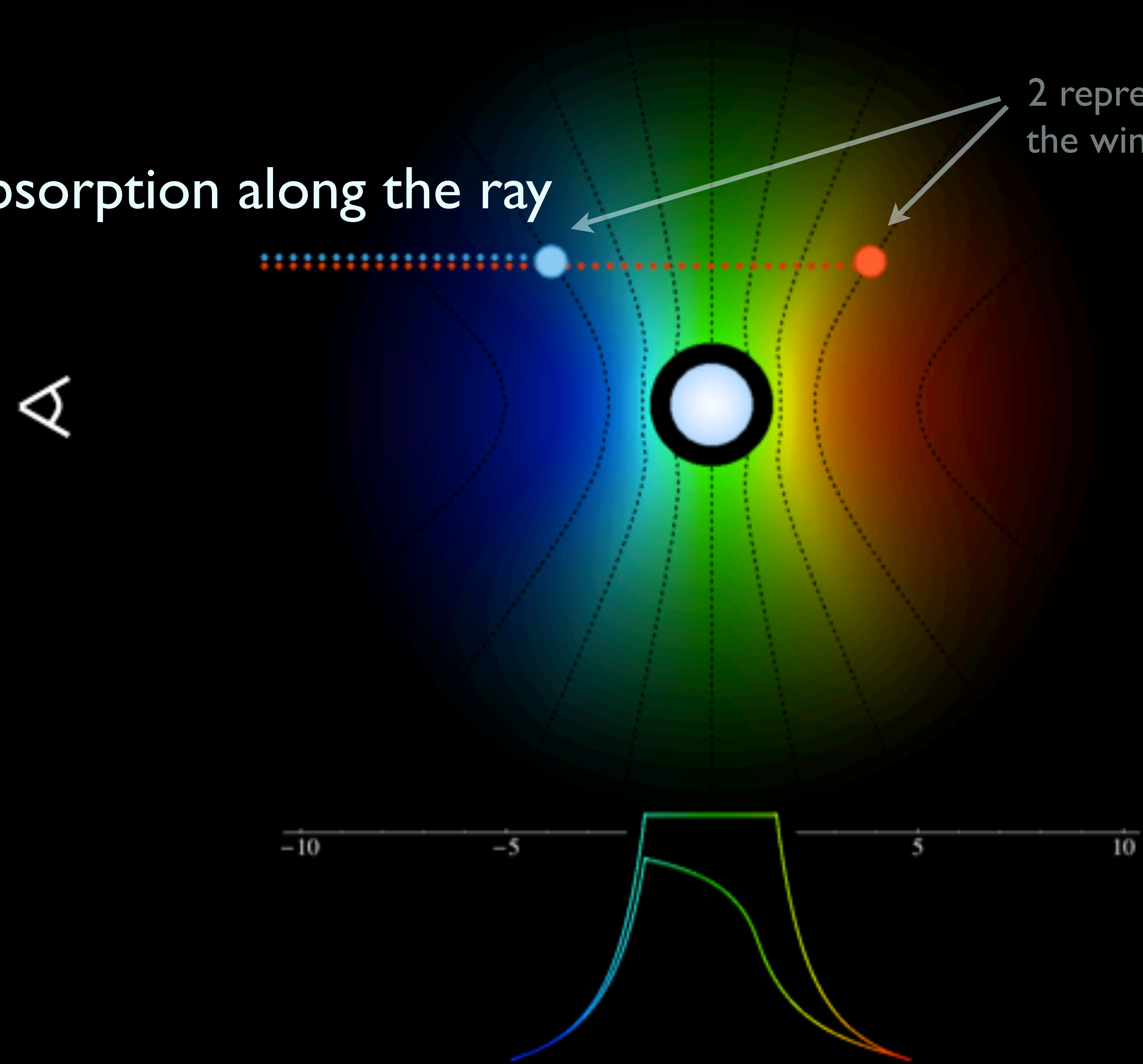

Line Asymmetry

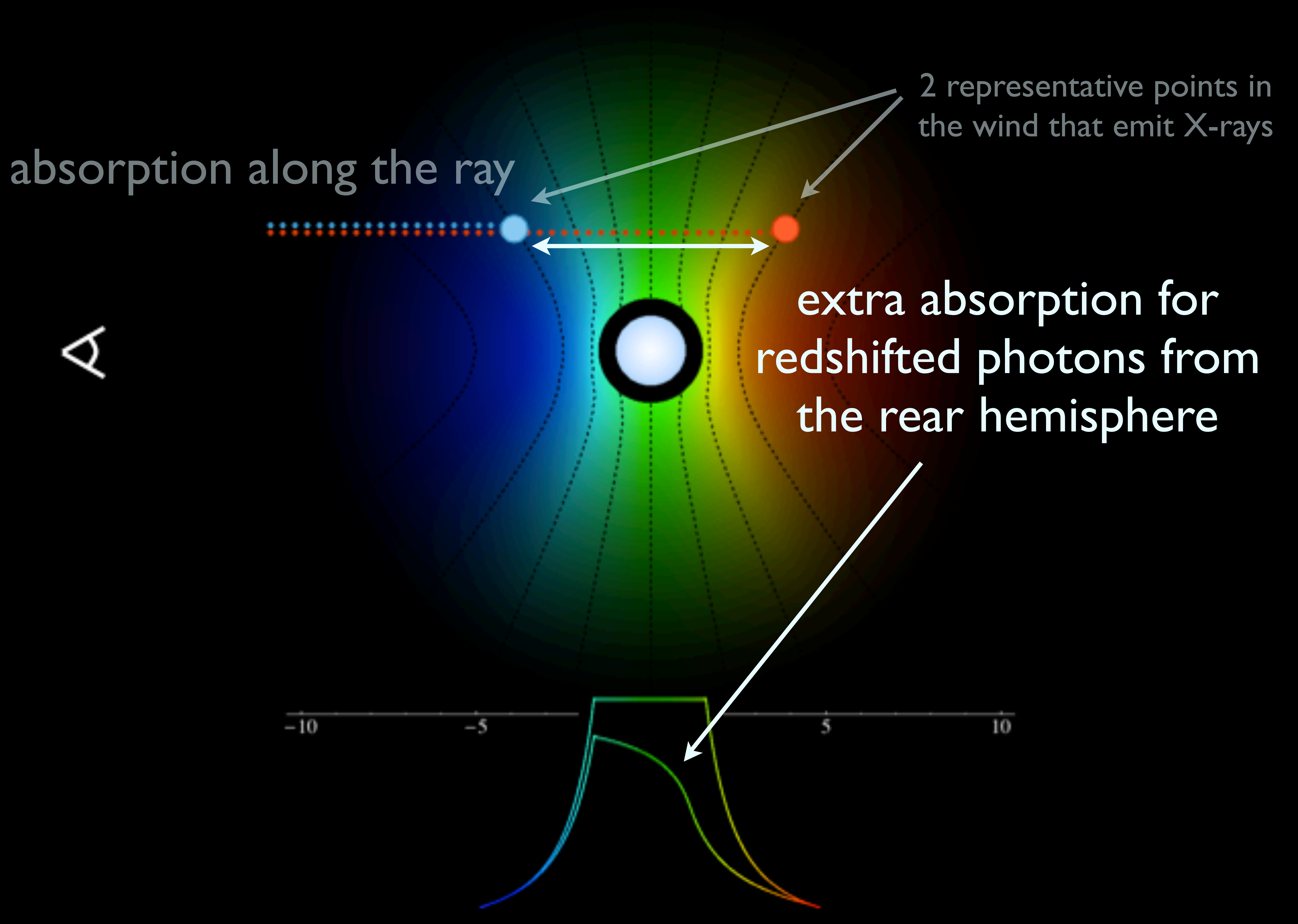

Wind Profile Model

mass-loss rates ~10^{-6}: expect wind to be modestly optically thick

$$\tau_* = \frac{\kappa \dot{M}}{4\pi R_* v_\infty}$$

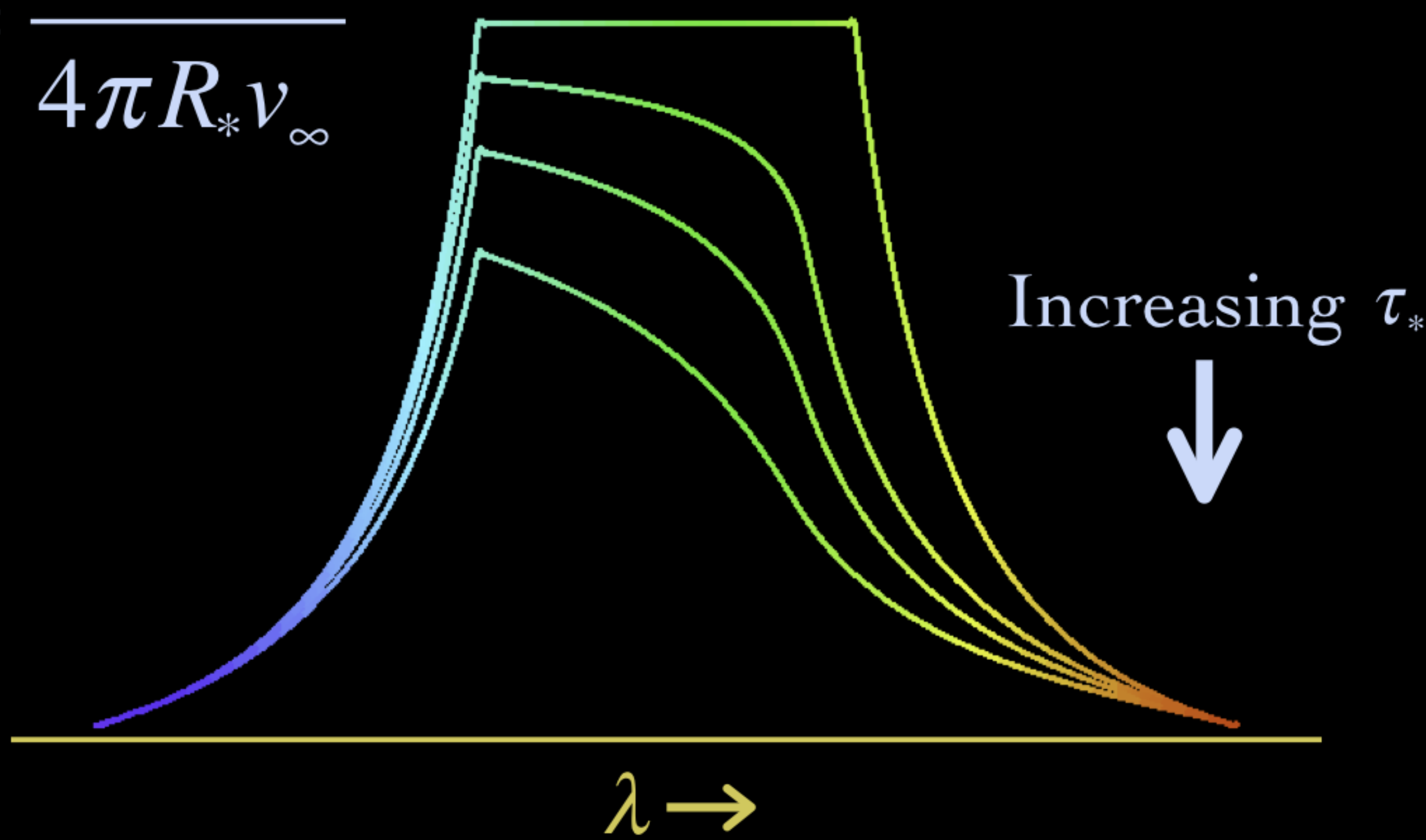

Line profile shapes

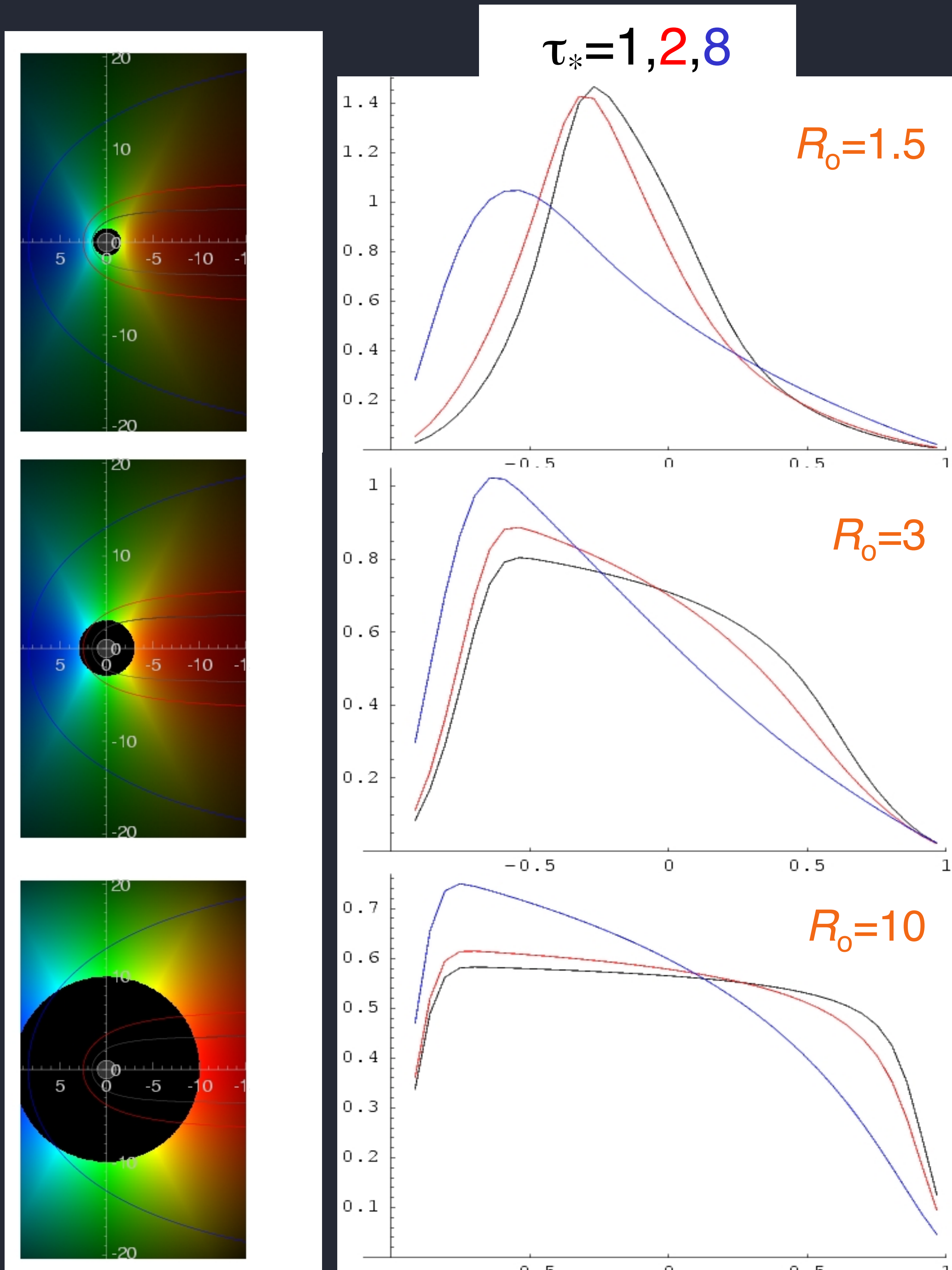

key parameters: R_o & $\tau_\star$

$$v = v_\infty (1 - r/R_\star)^\beta$$

$$j \sim \rho^2 \text{ for } r/R_* > R_o, \quad = 0 \text{ otherwise}$$

$$\tau = \tau_* \int_z^\infty \frac{R_* dz'}{r'^2 (1 - R_*/r')^\beta}$$

$$\tau_* \equiv \frac{\kappa \dot{M}}{4\pi R_* v_\infty}$$

Owocki & Cohen 2001

custom model in XSPEC (*windprofile*)

Fit the model to data

ζ Pup: *Chandra*

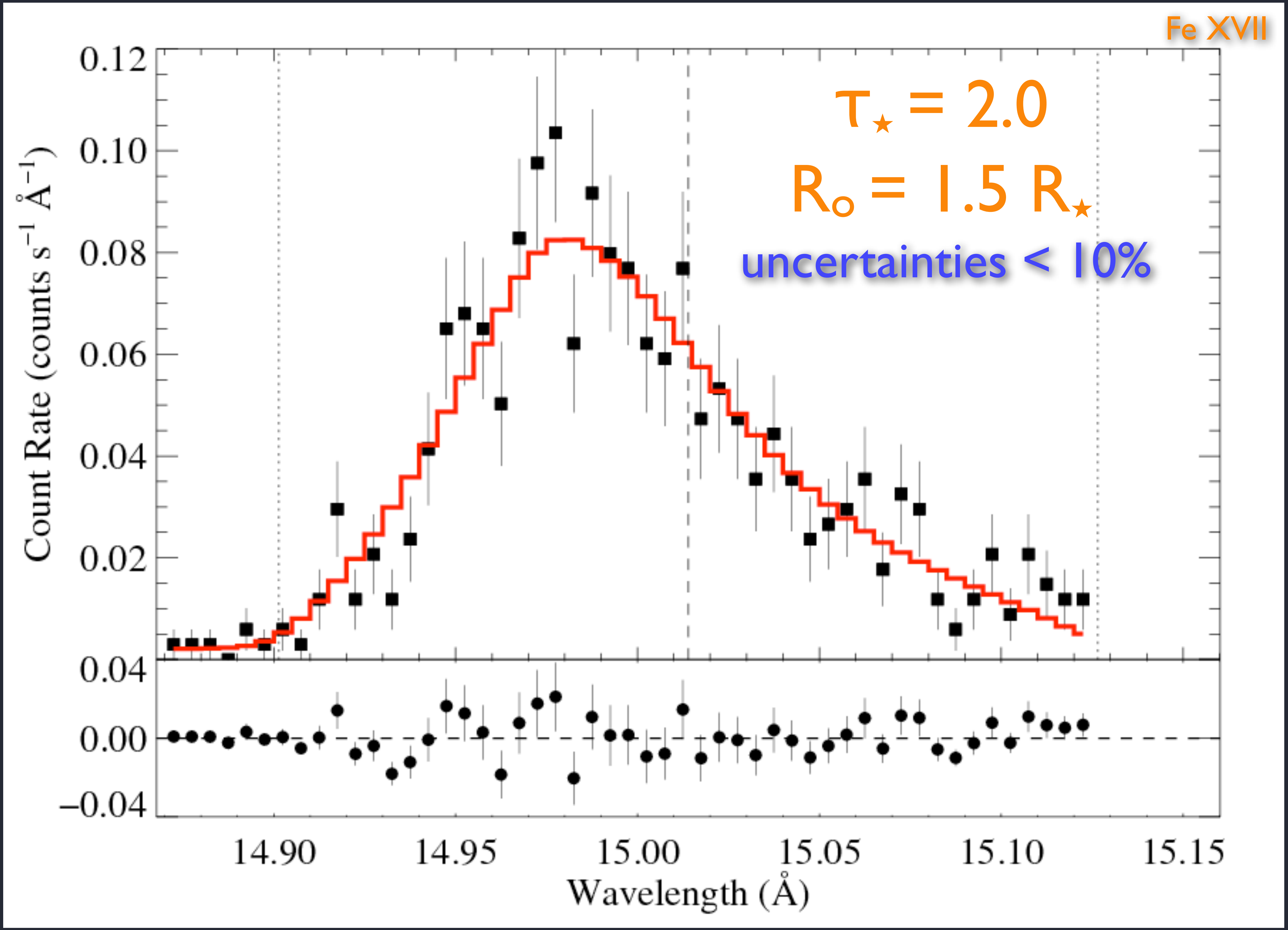

Spatial distribution and kinematics of shocked wind plasma

Look at all unblended lines in the *Chandra* HETGS spectrum of ζ Pup

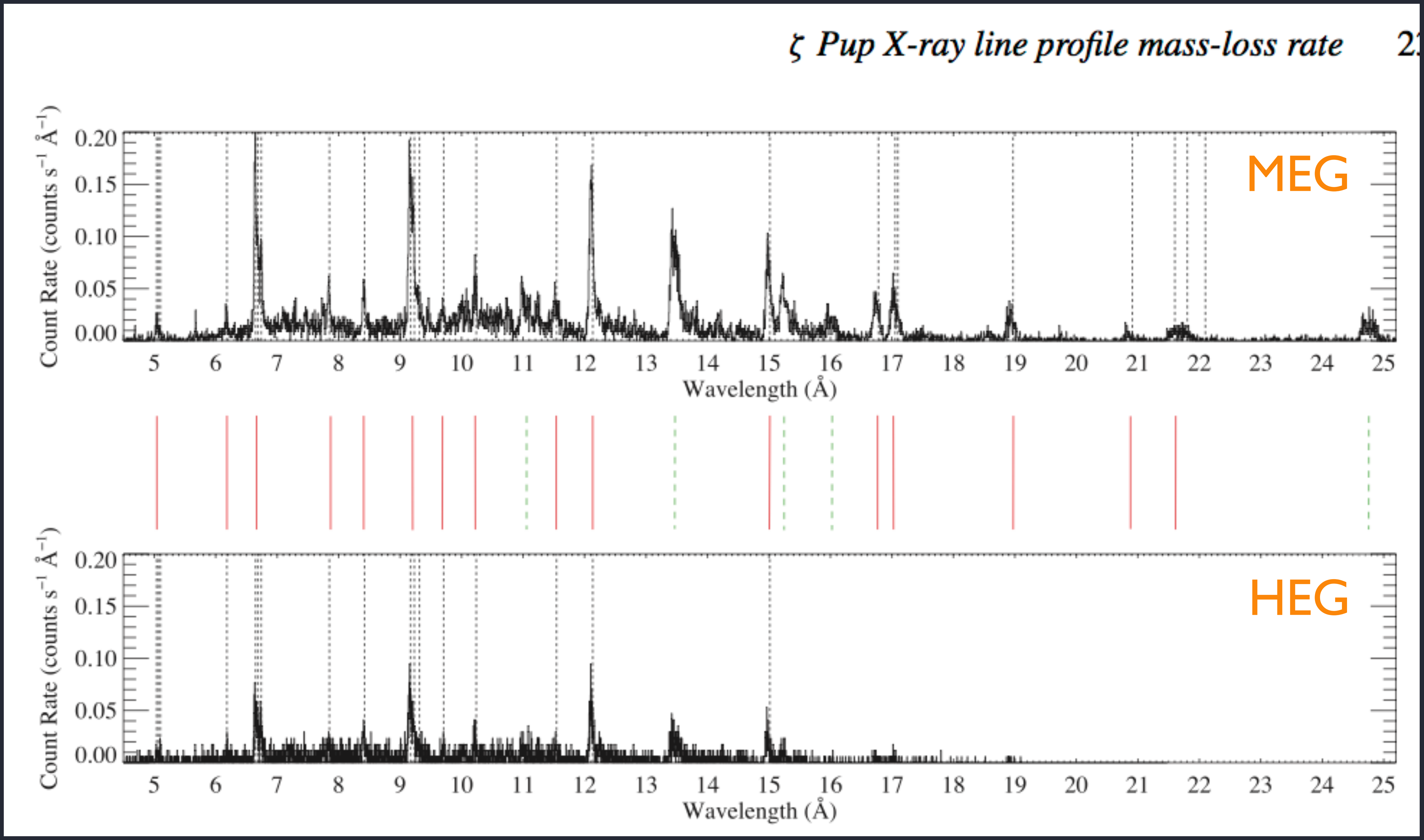

Distribution of R_o values for ζ Pup

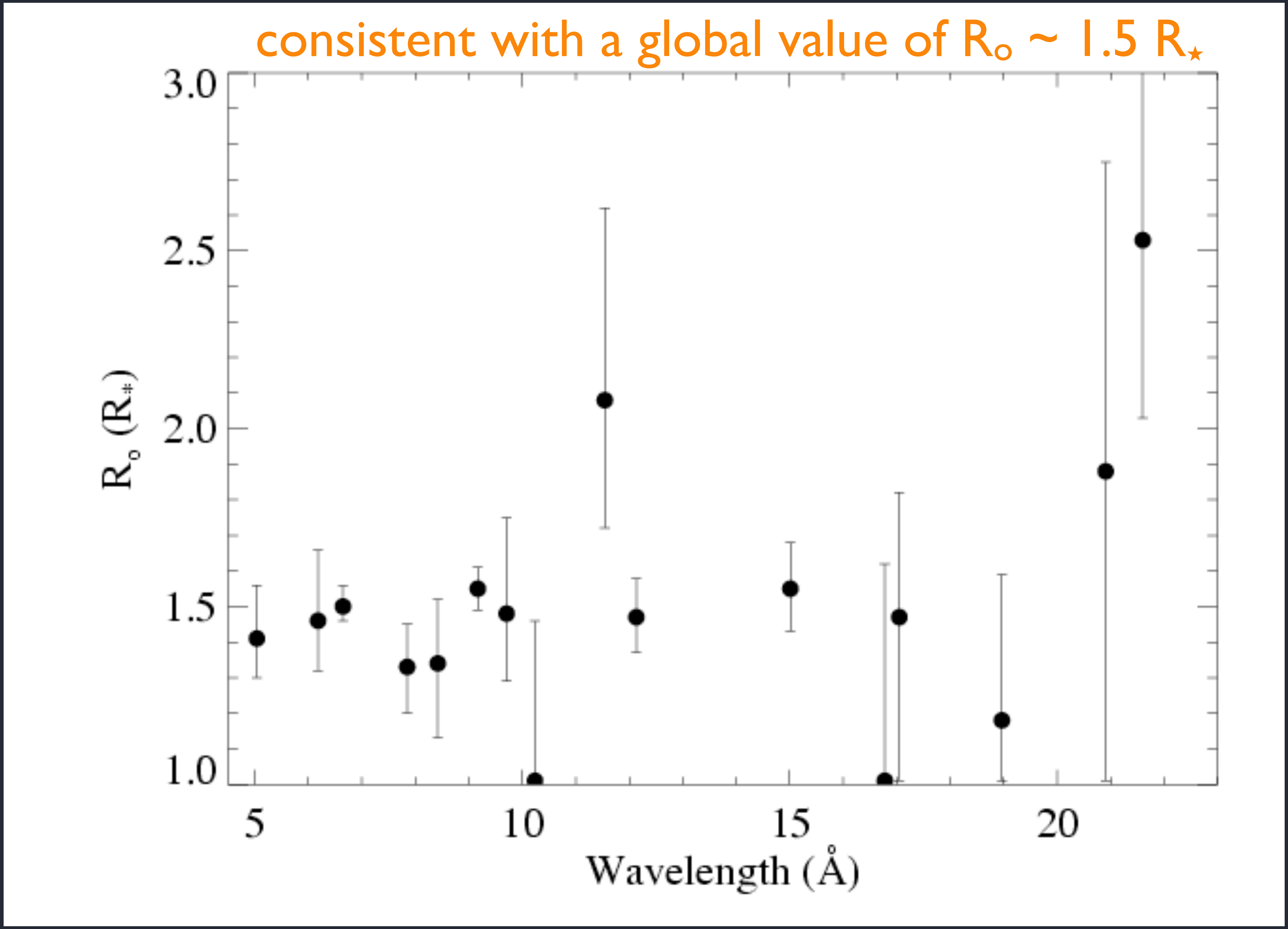

v_∞ can be constrained by the line fitting too

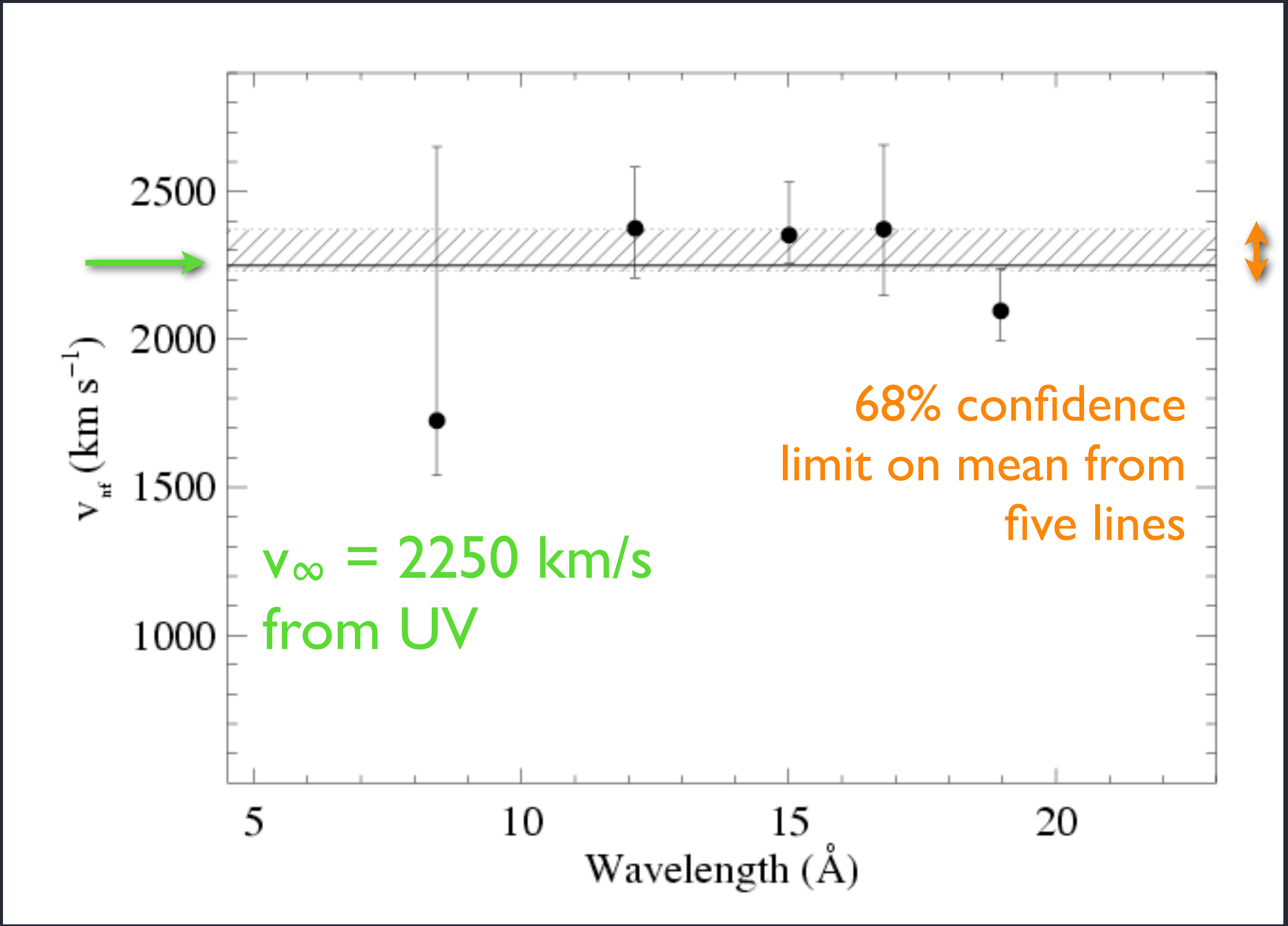

X-ray plasma and mean wind have same kinematics

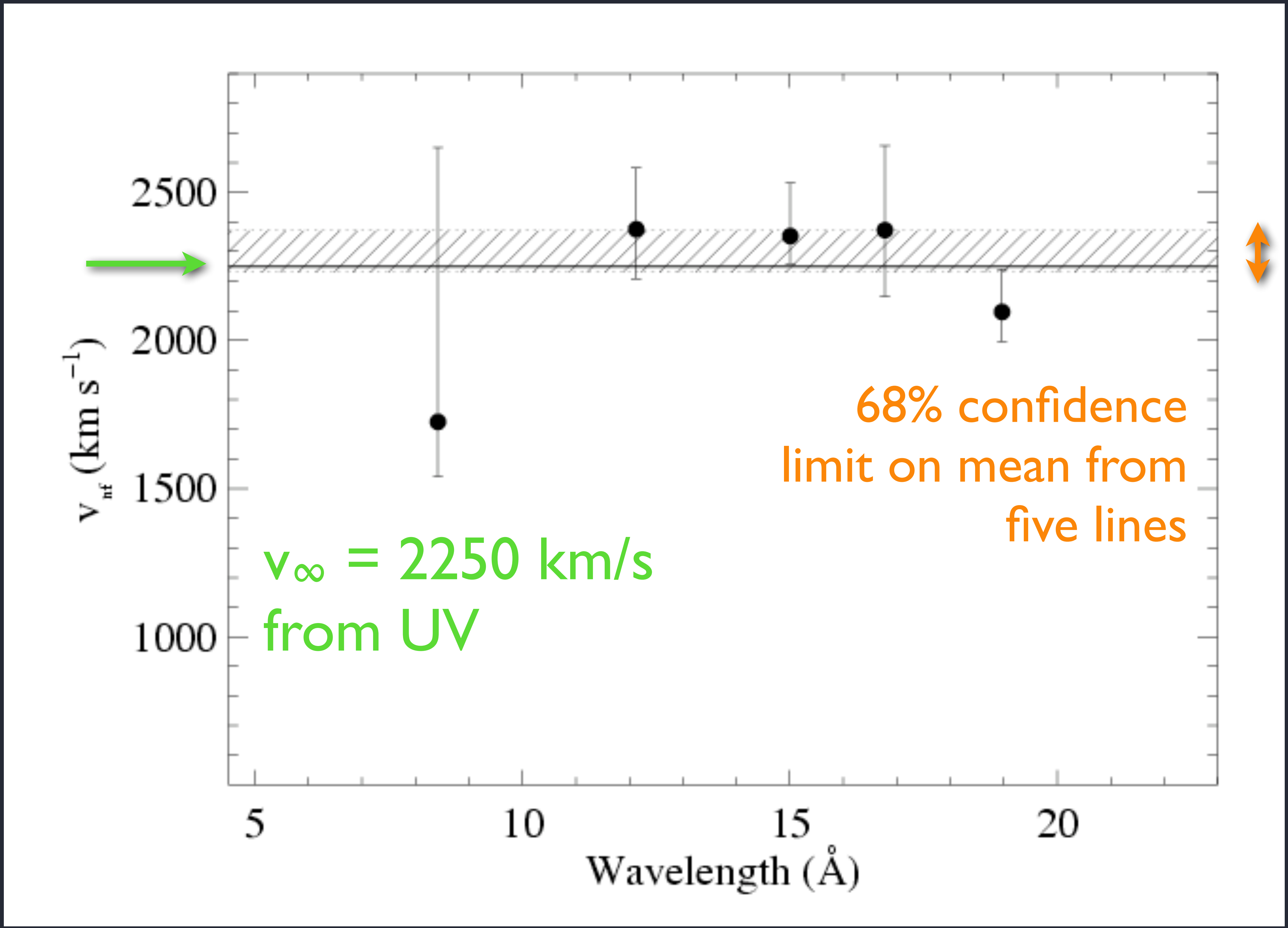

Absorption signatures in the X-ray line profiles

Fit the model to data

ζ Pup: *Chandra*

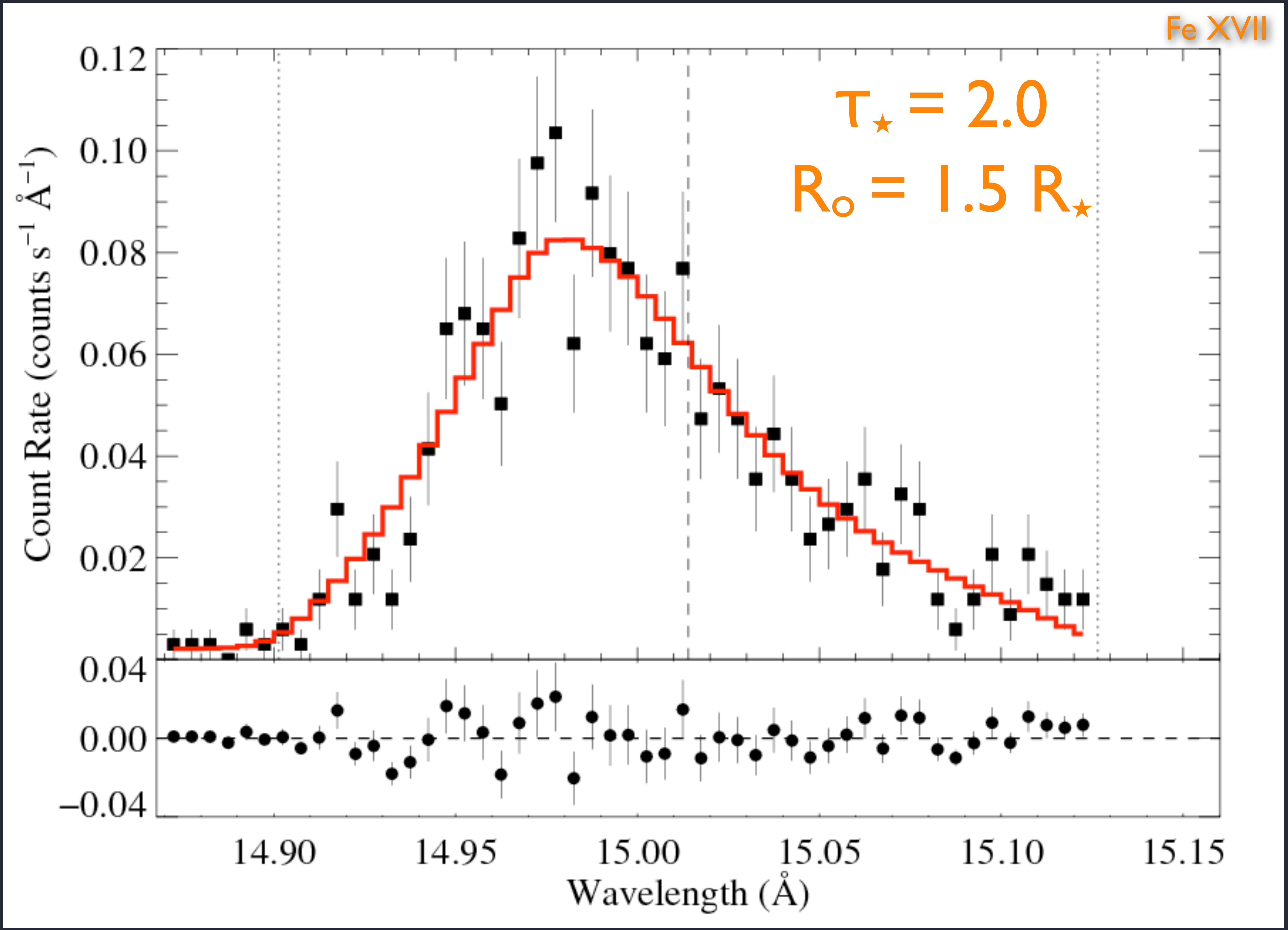

Quantifying the wind optical depth

opacity of the cold wind component (due to photoionization of C, N, O, Ne, Fe)

wind mass-loss rate

$$\dot{M} = 4\pi r^2 v \rho$$

$$\tau_* \equiv \frac{\kappa \dot{M}}{4\pi R_* v_\infty}$$

stellar radius

wind terminal velocity

soft X-ray wind opacity

note: absorption arises in the dominant, cool wind component

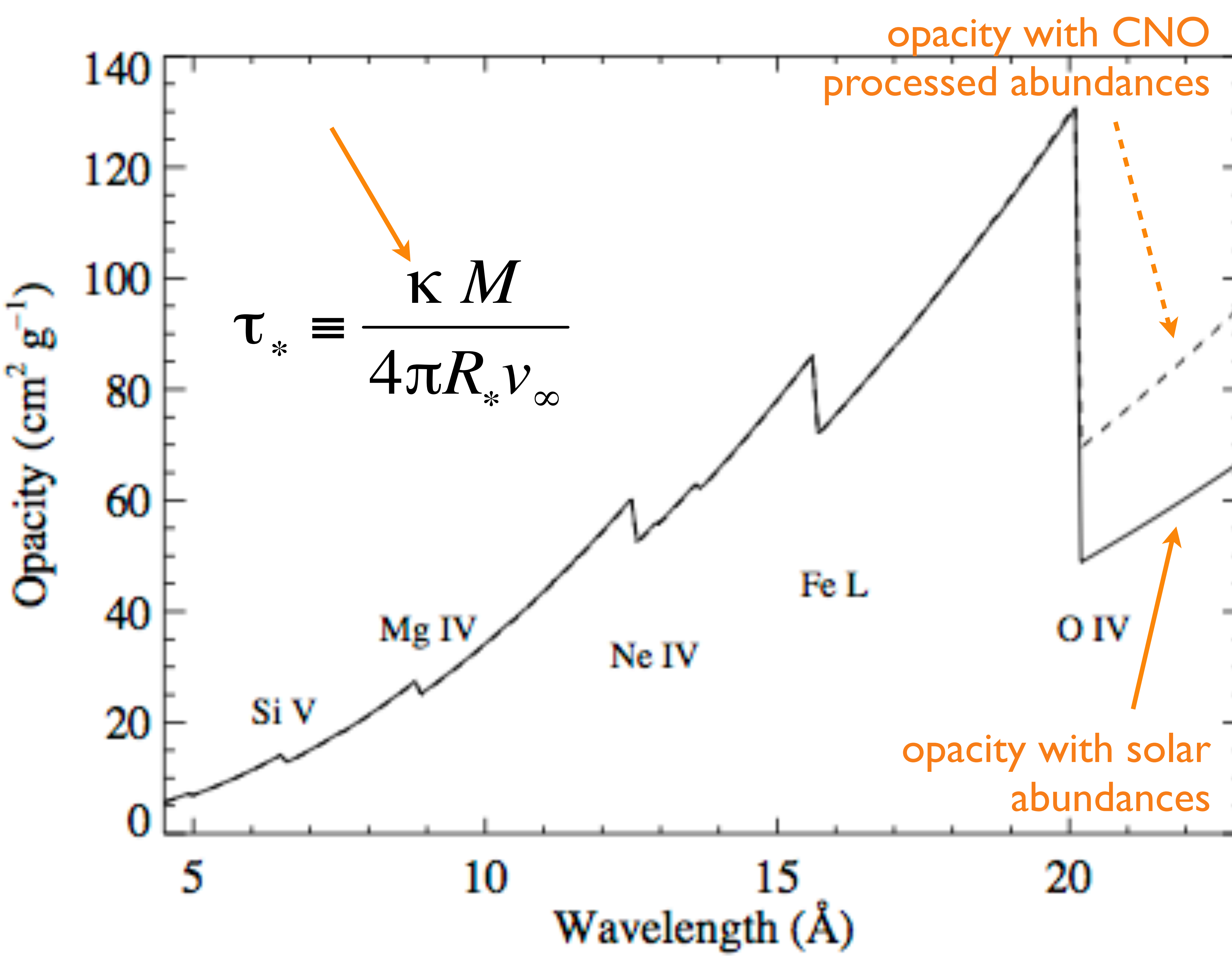

$$\tau_* \equiv \frac{\kappa M}{4\pi R_* v_\infty}$$

ζ Pup *Chandra*: three emission lines

Mg Lyα: 8.42 Å | Ne Lyα: 12.13 Å | O Lyα: 18.97 Å

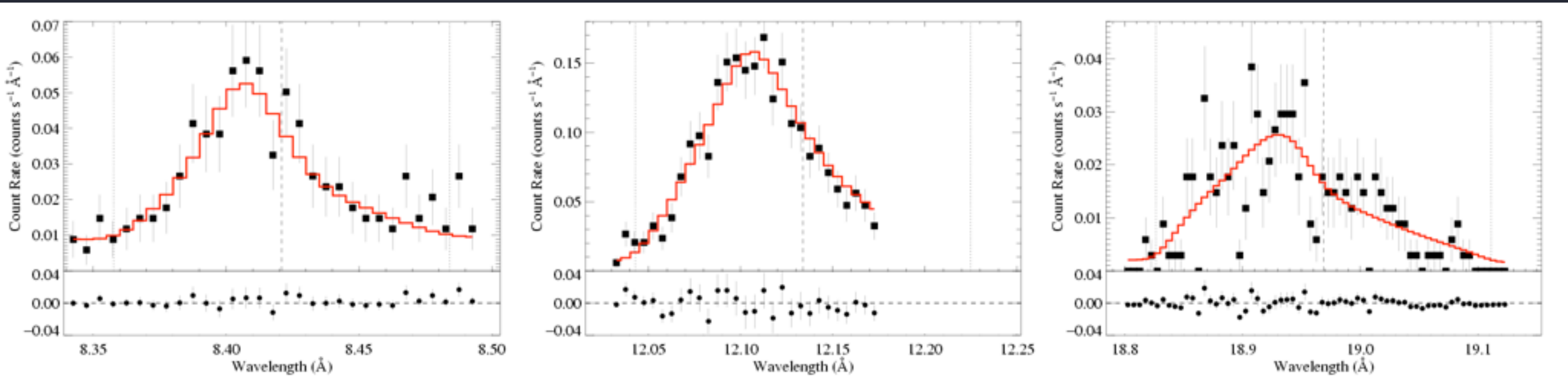

$\tau_* \sim 1$ | $\tau_* \sim 2$ | $\tau_* \sim 3$

Recall:

$$\tau_* \equiv \frac{\kappa \dot{M}}{4\pi R_* v_\infty}$$

Results from the 3 line fits shown previously

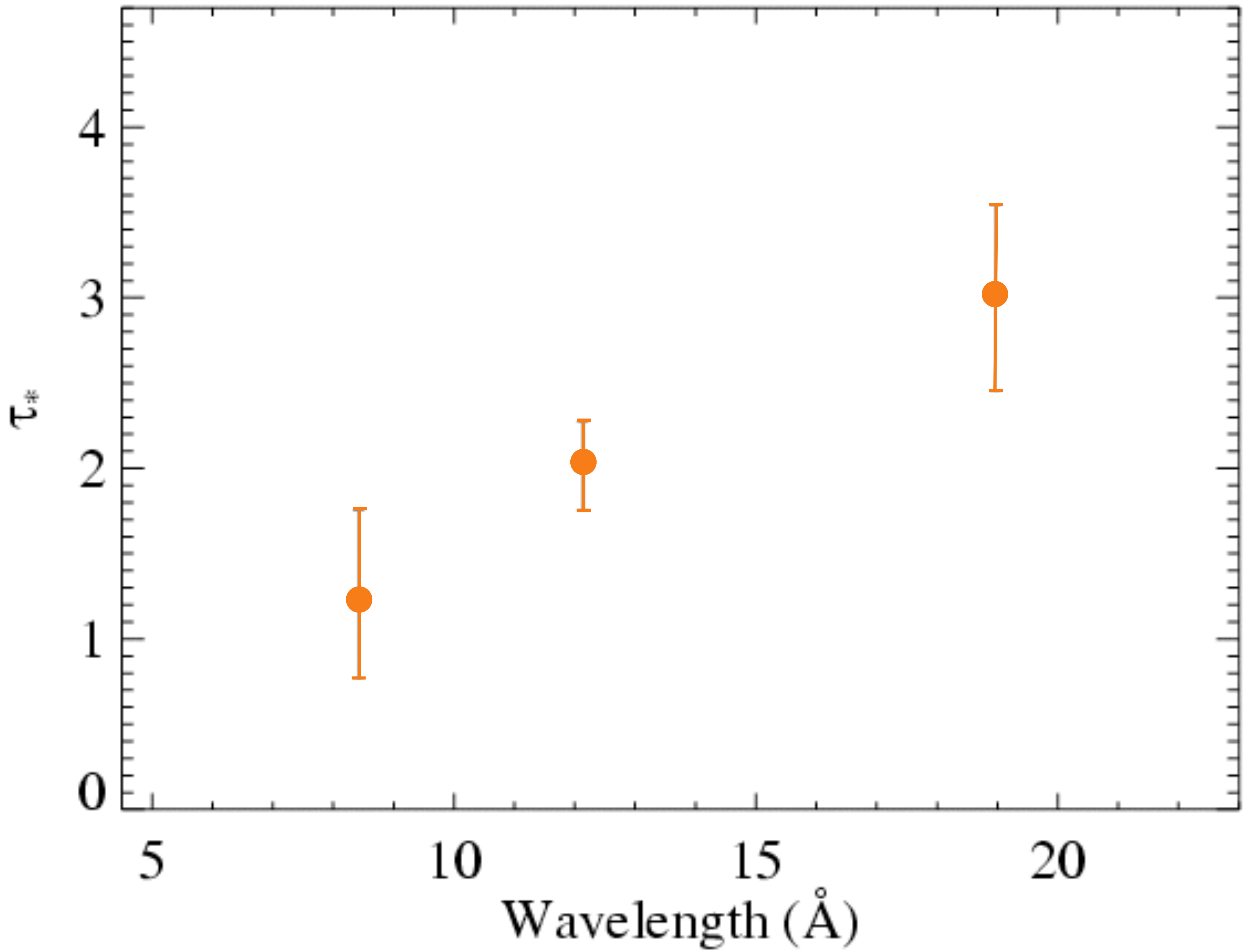

Fits to 16 lines in the *Chandra* spectrum of ζ Pup

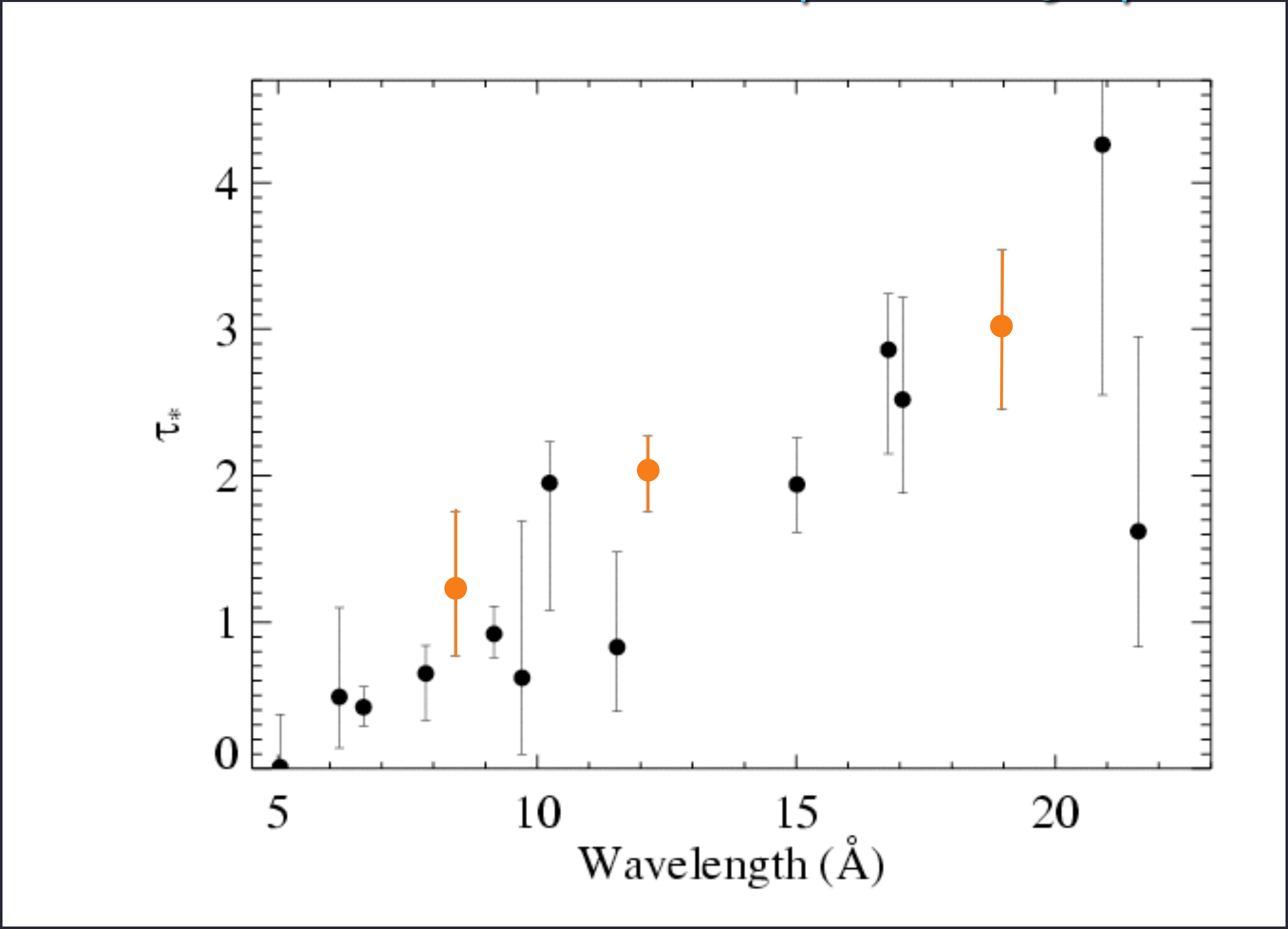

Fits to 16 lines in the *Chandra* spectrum of ζ Pup

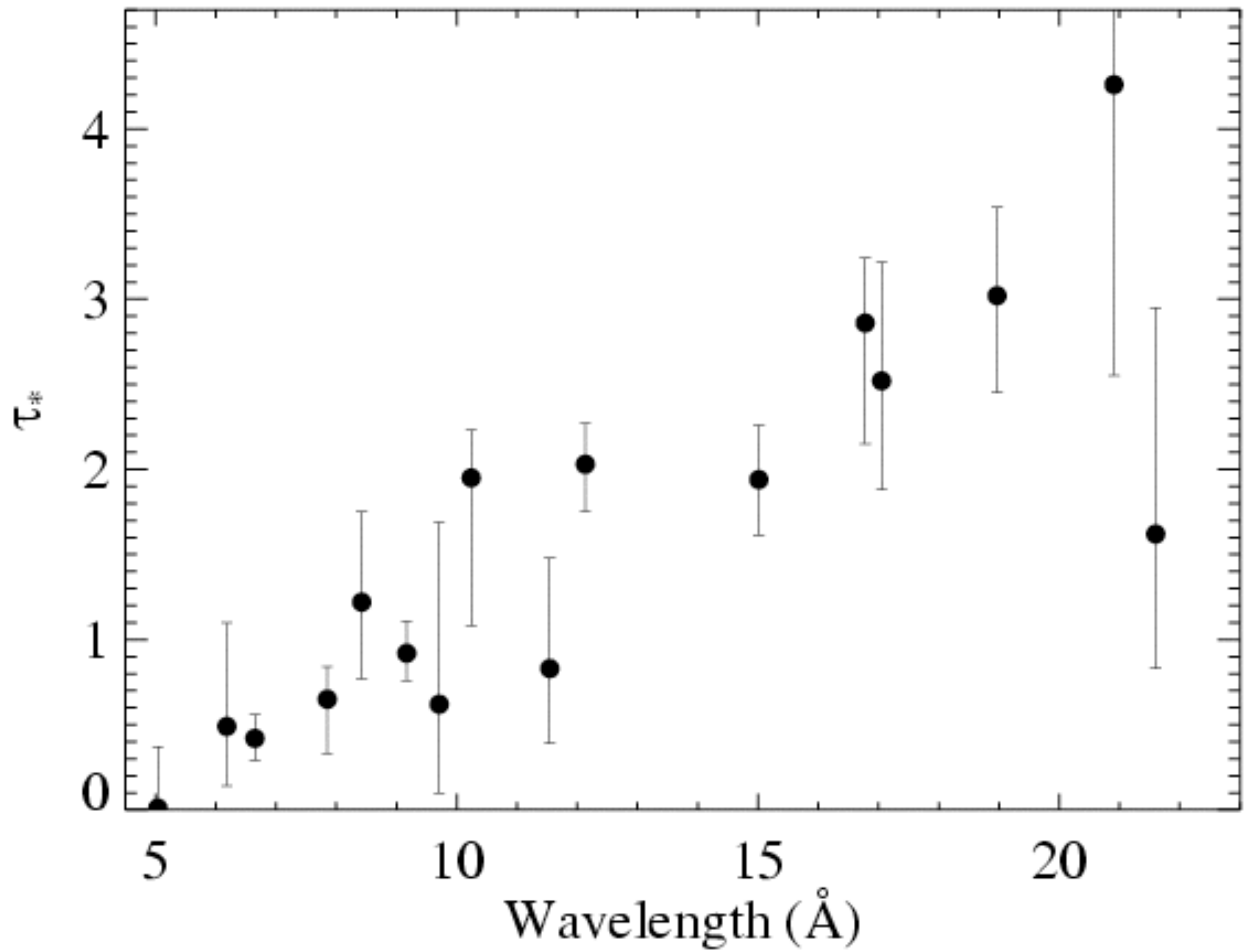

Fits to 16 lines in the *Chandra* spectrum of ζ Pup

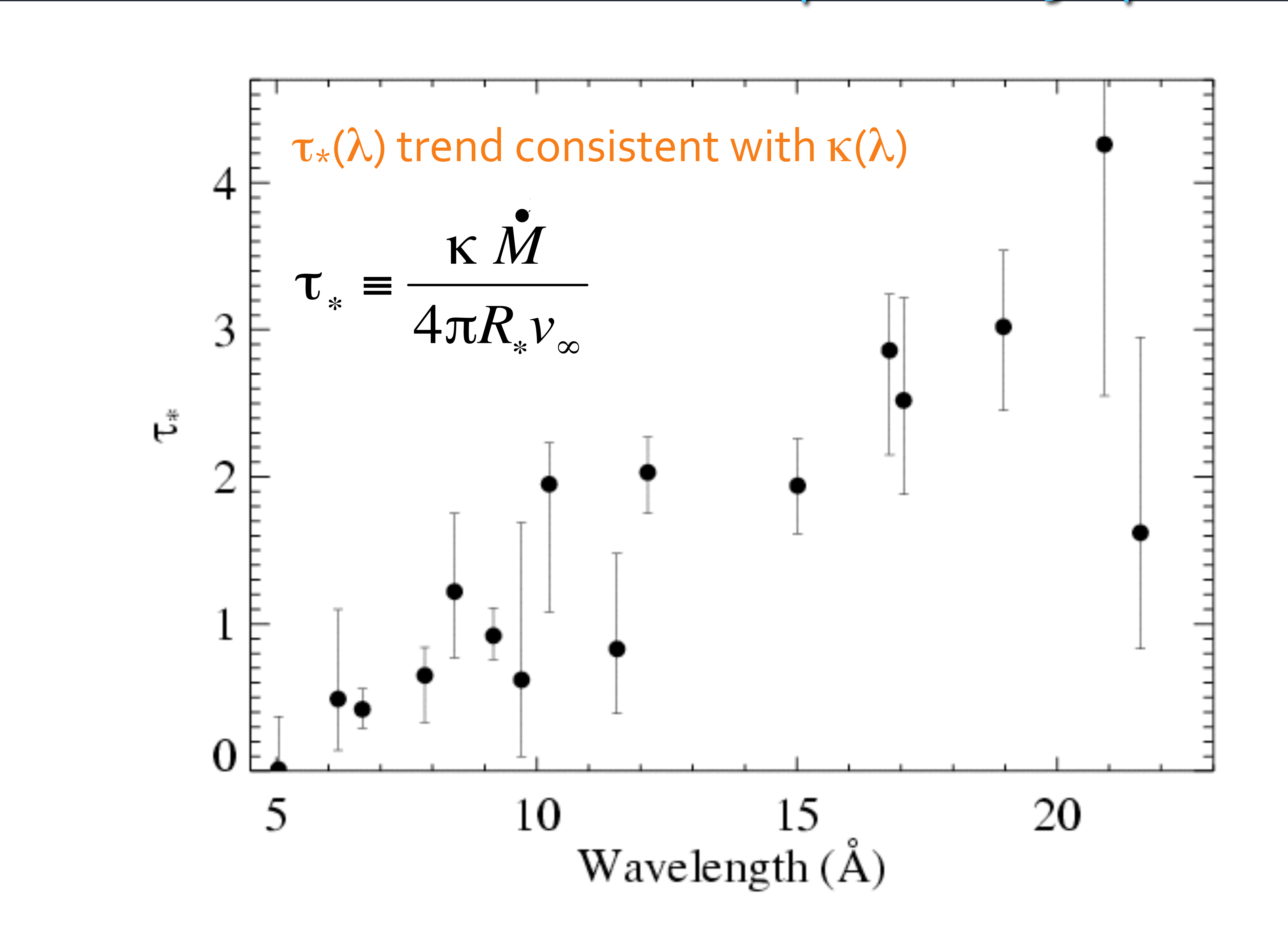

$$\tau_* \equiv \frac{\kappa \dot{M}}{4\pi R_* v_\infty}$$

$\dot{M}$ becomes the free parameter of the fit to the $\tau_*(\lambda)$ trend

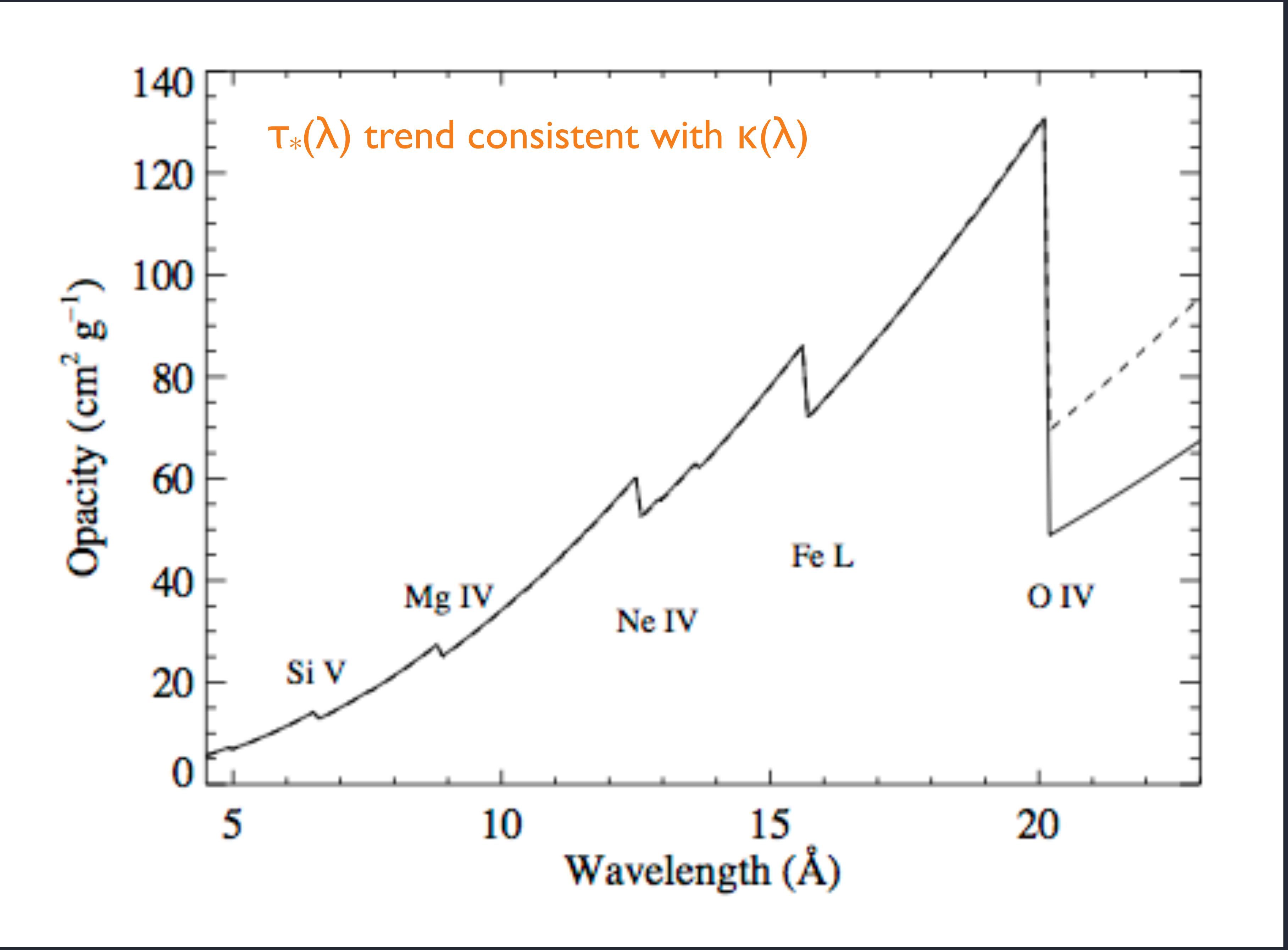

$$\tau_* \equiv \frac{\kappa \dot{M}}{4\pi R_* v_\infty}$$

$\dot{M}$ becomes the free parameter of the fit to the $\tau_*(\lambda)$ trend

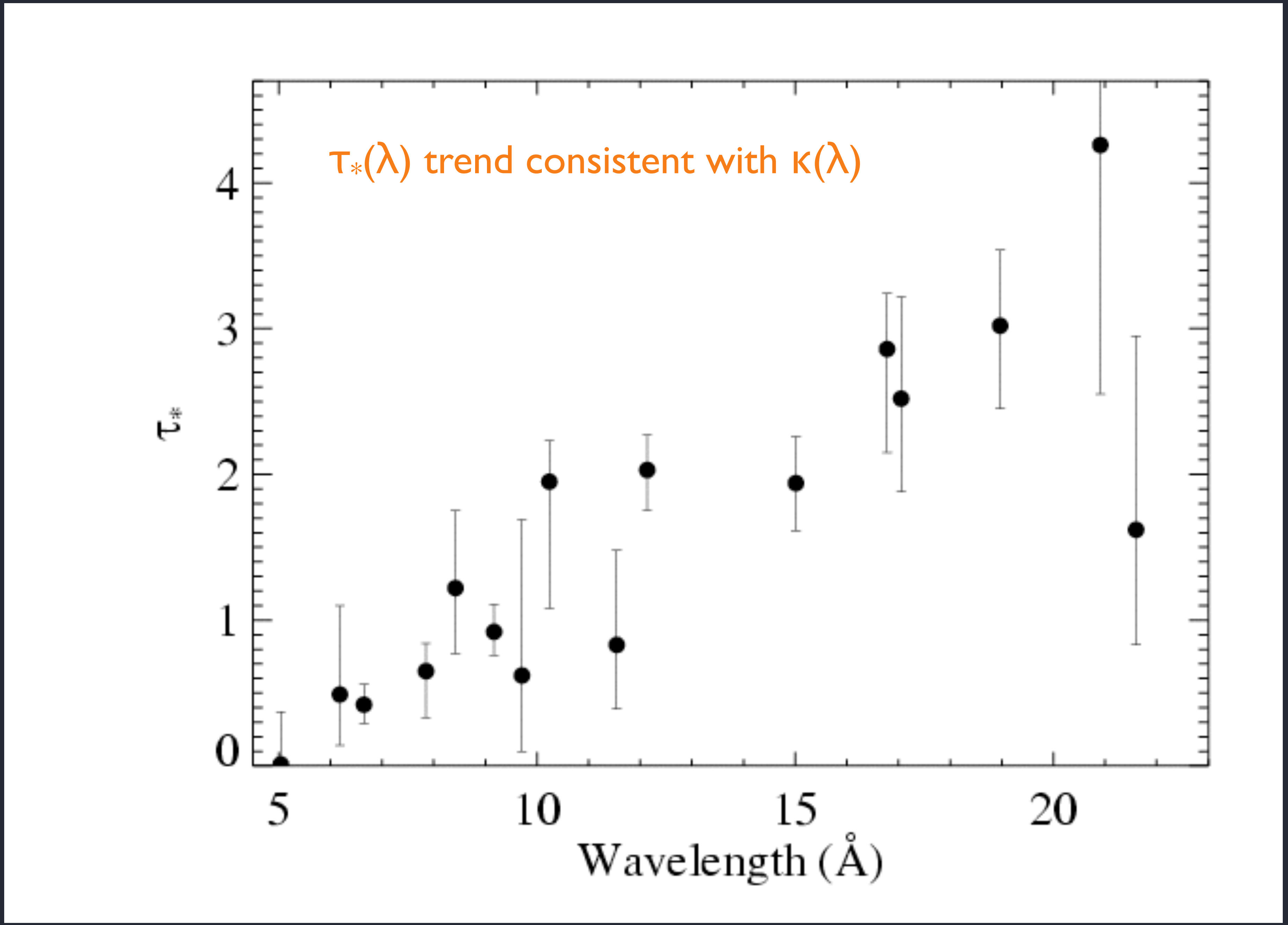

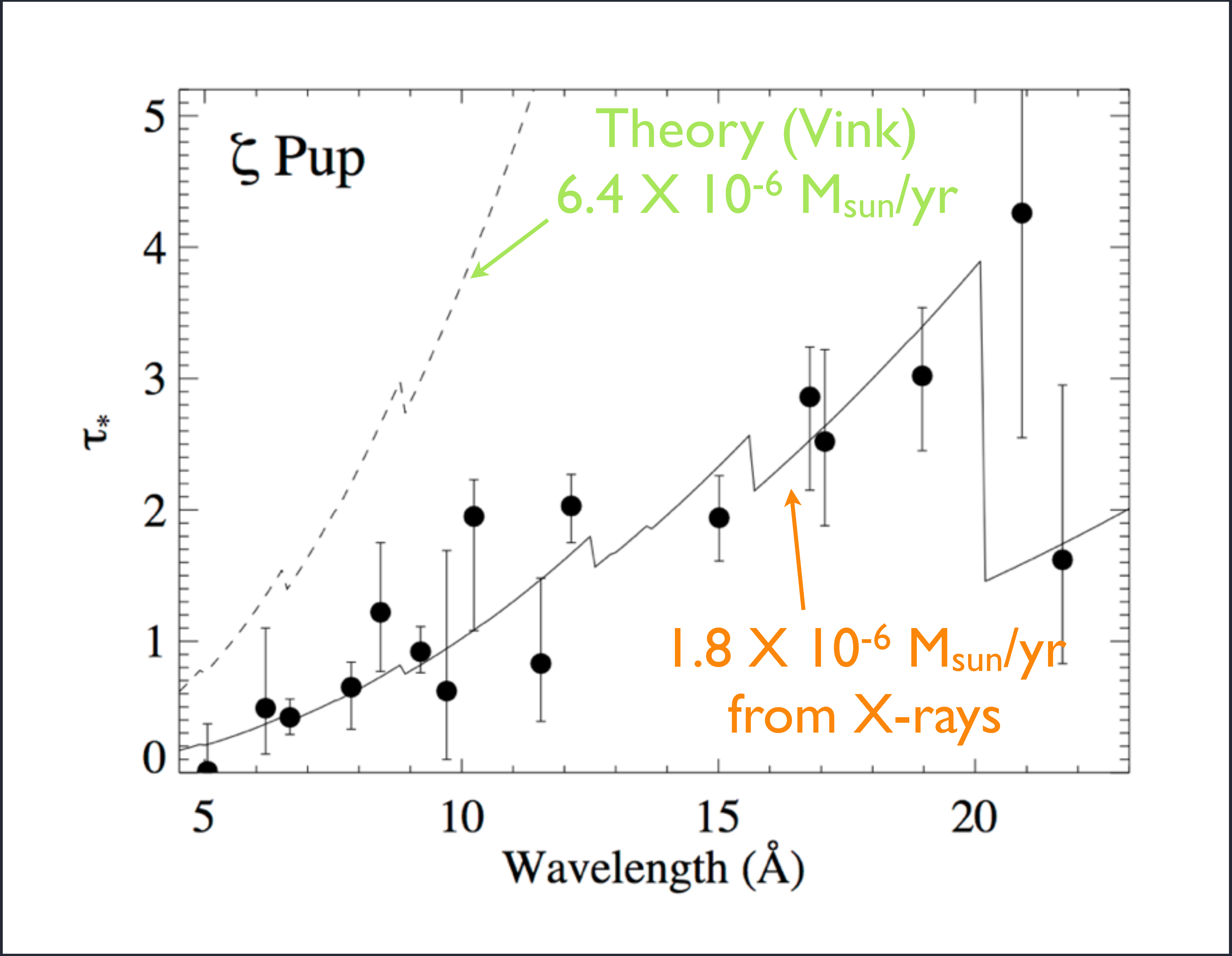

ζ Pup
Theory (Vink)
6.4 X 10-6 Msun/yr
1.8 X 10-6 Msun/yr
from X-rays
τ*
Wavelength (Å)
0
1
2
3
4
5
5
10
15
20

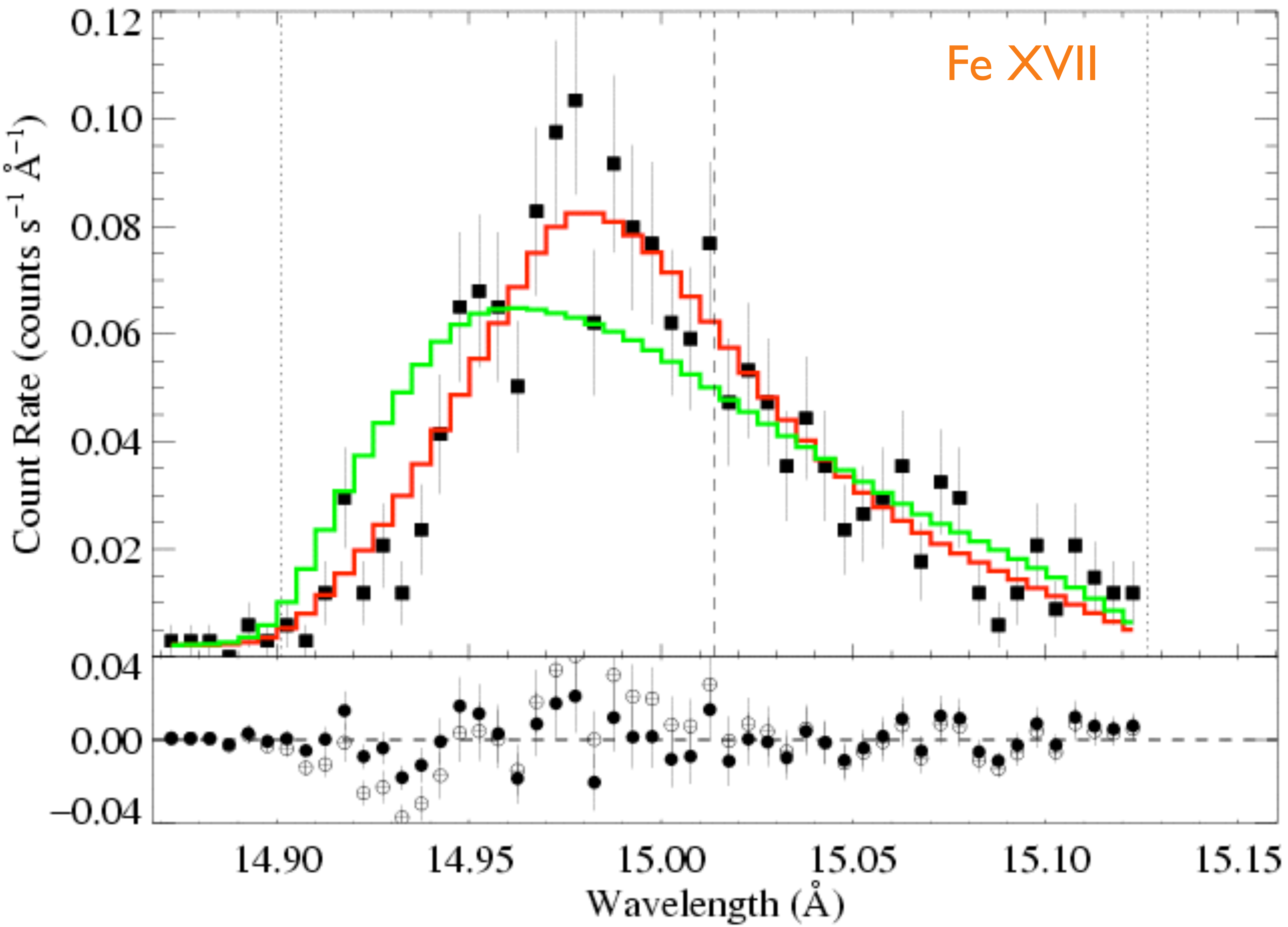

Fe XVII
Count Rate (counts s^{-1} Å^{-1})
0.12
0.10
0.08
0.06
0.04
0.02
0.04
0.00
−0.04
14.90
14.95
15.00
15.05
15.10
15.15
Wavelength (Å)

consistent with new UV&IR measurements that model the wind clumping (Bouret et al. 2012, Najarro et al. 2011)

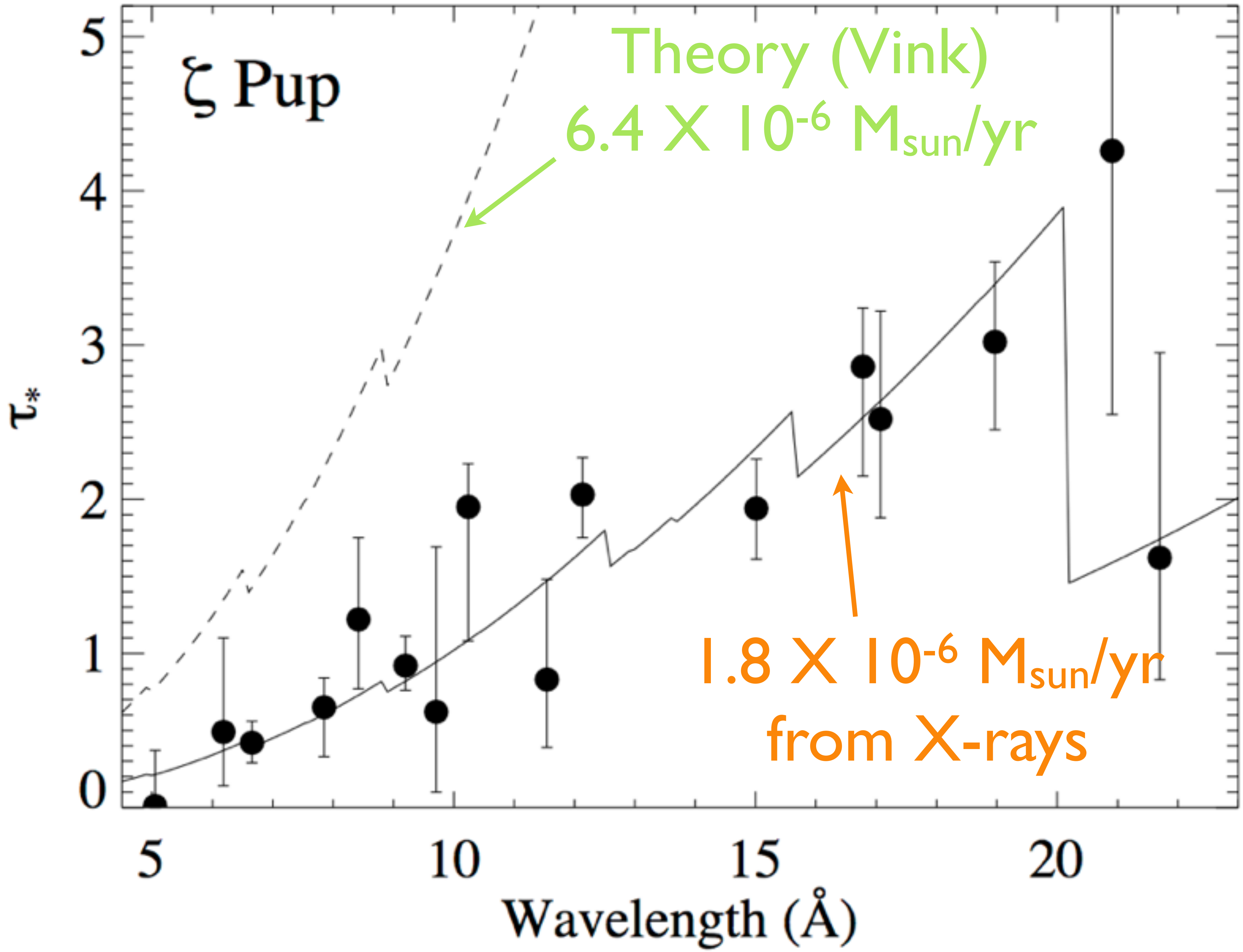

X-ray line profile based mass-loss rate: implications for clumping

basic definition: $f_{cl} \equiv \langle\rho^2\rangle / \langle\rho\rangle^2$

$= \langle\rho^2\rangle^{0.5} / \langle\rho\rangle$

clumping factor

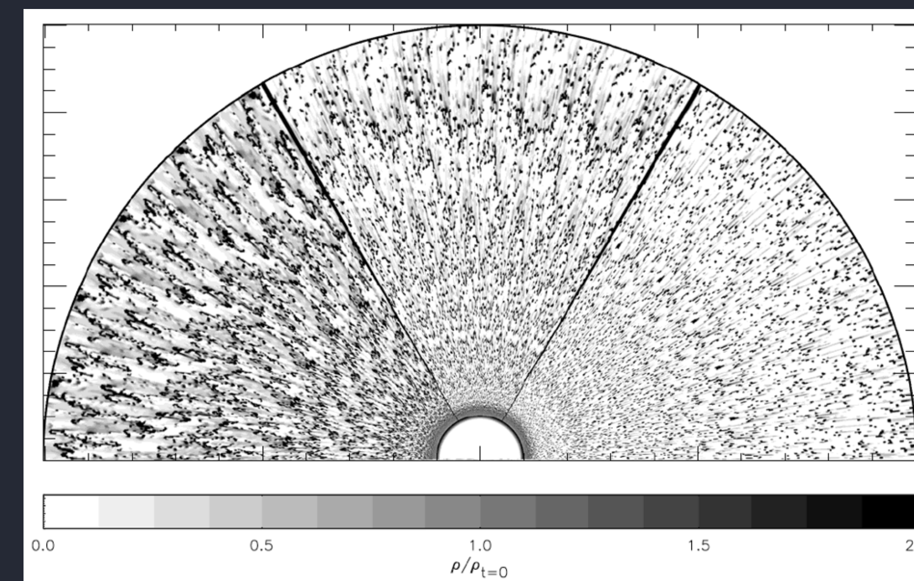

optical: $F_{H\alpha} \sim f_{cl}\rho^2 \sim f_{cl}\dot{M}^2$

$(f_{cl})^{0.5}\dot{M}$ is the invariant for $H\alpha$

ignoring clumping will cause you to *overestimate* the mass-loss rate…for density-squared diagnostics

X-ray combined with Hα

optical: $F_{H\alpha} \sim f_{cl}\rho^2 \sim f_{cl}\dot{M}^2$

X-ray: $\tau_\star \sim \rho \sim \dot{M}$

$(f_{cl})^{0.5}\dot{M}$ is the invariant for Hα

optical Hα: $(f_{cl})^{0.5}\dot{M} = 8.3 \times 10^{-6}$ for ζ Pup

X-ray: $\dot{M} = 1.8 \times 10^{-6}$ for ζ Pup (this work)

$f_{cl} \sim 20$ for ζ Pup

but see Puls et al. 2006, Najarro et al. 2011:
radial variation of clumping factor

clumping factor ~10 to ~20 (Najarro et al. 2011)

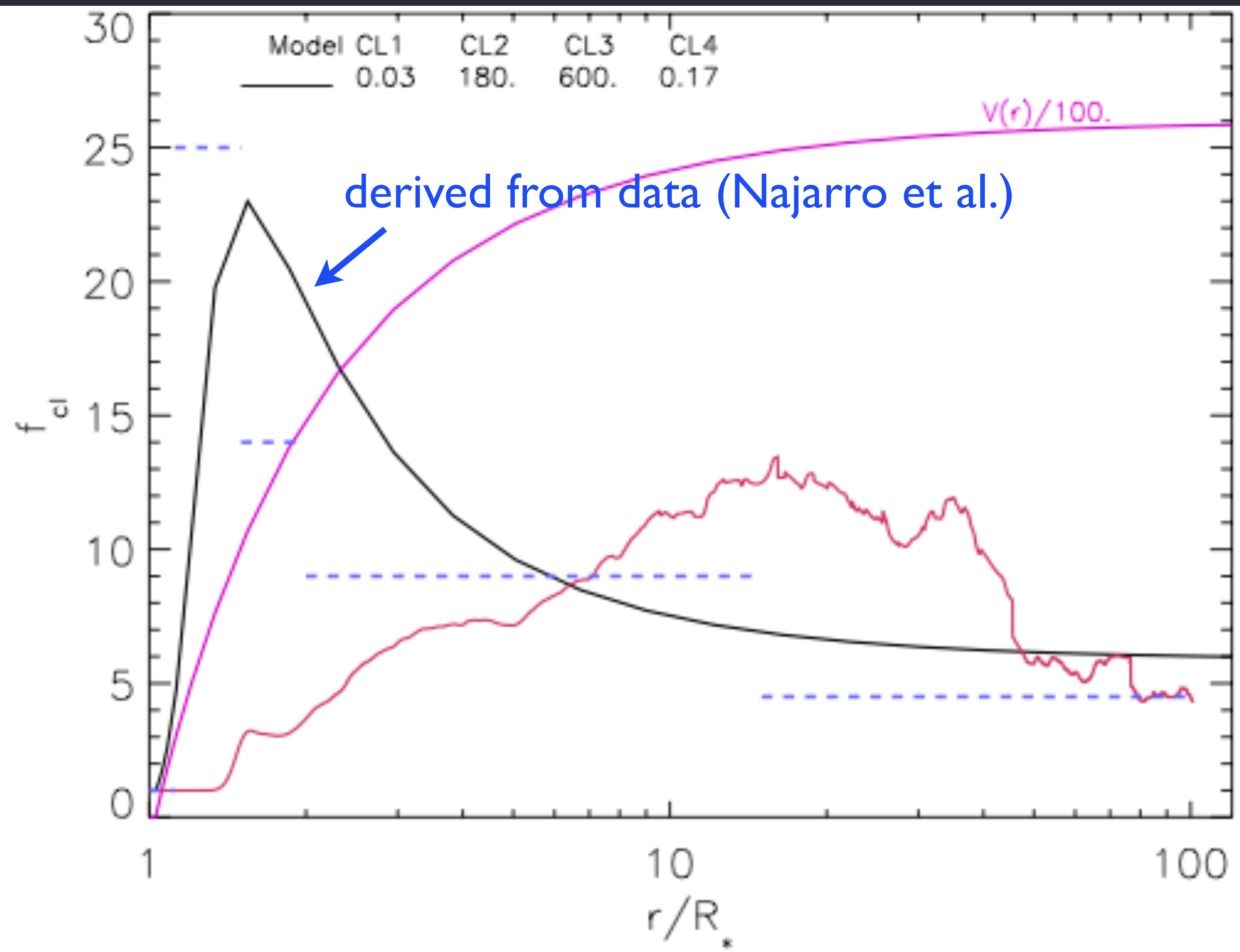

Fig. 18. Radial stratification of the clumping factor, f_{cl}, for ζ Pup. Black solid: clumping law derived from our model fits. Red solid: Theoretical predictions by Runacres & Owocki (2002) from hydrodynamical models, with self-excited line driven instability. Dashed: Average clumping factors derived by Puls et al. (2006) assuming an outer wind matching the theoretical predictions. Magenta solid: run of the velocity field in units of 100 km s^{-1}. See also Sect. 4.

2-D radiation-hydro simulations

clumps break up to the grid scale; $f_{cl} \sim 10$

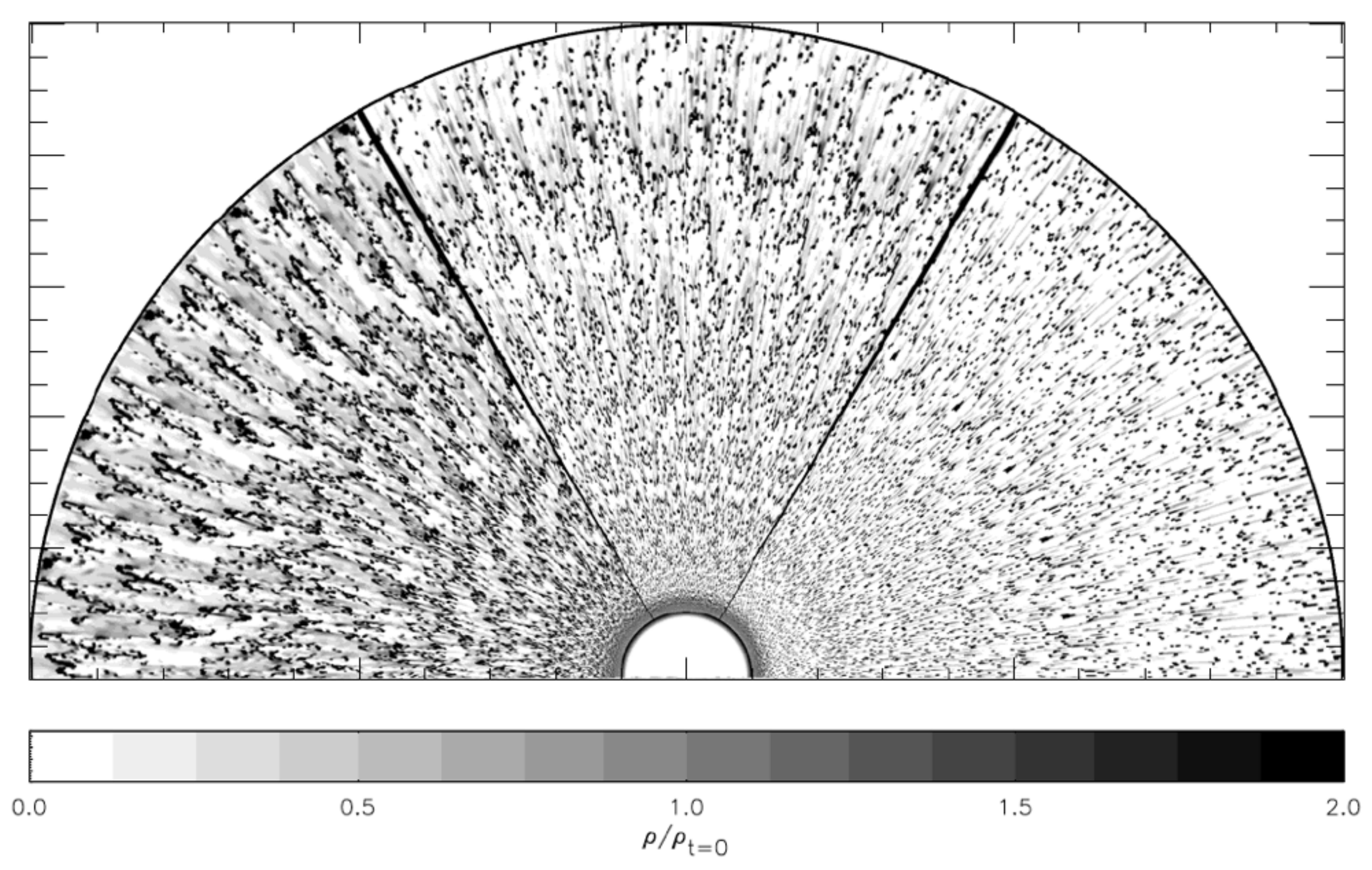

Dessart & Owocki 2003

HD 93129A (O2 If*)

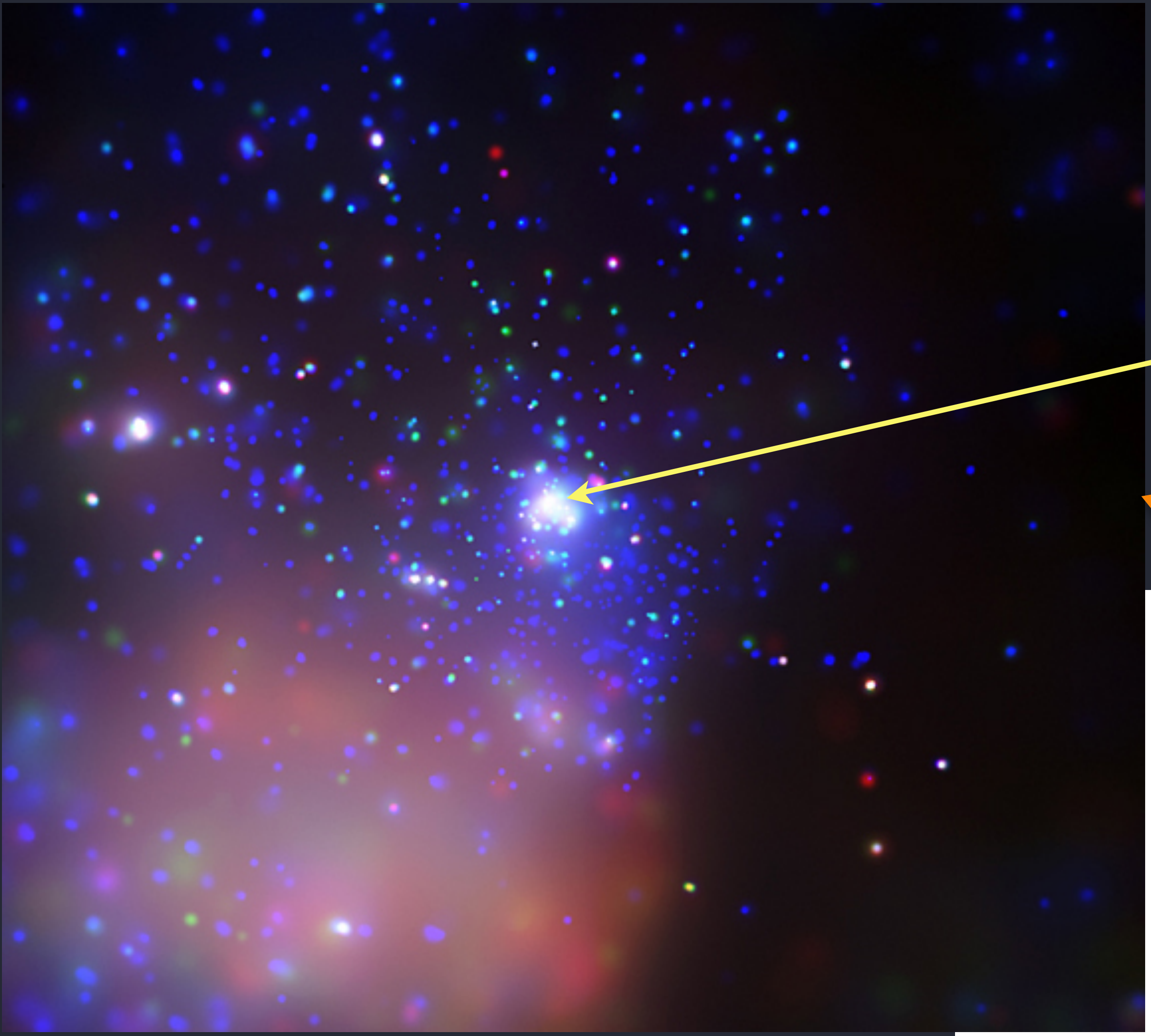

Tr 14: *Chandra*

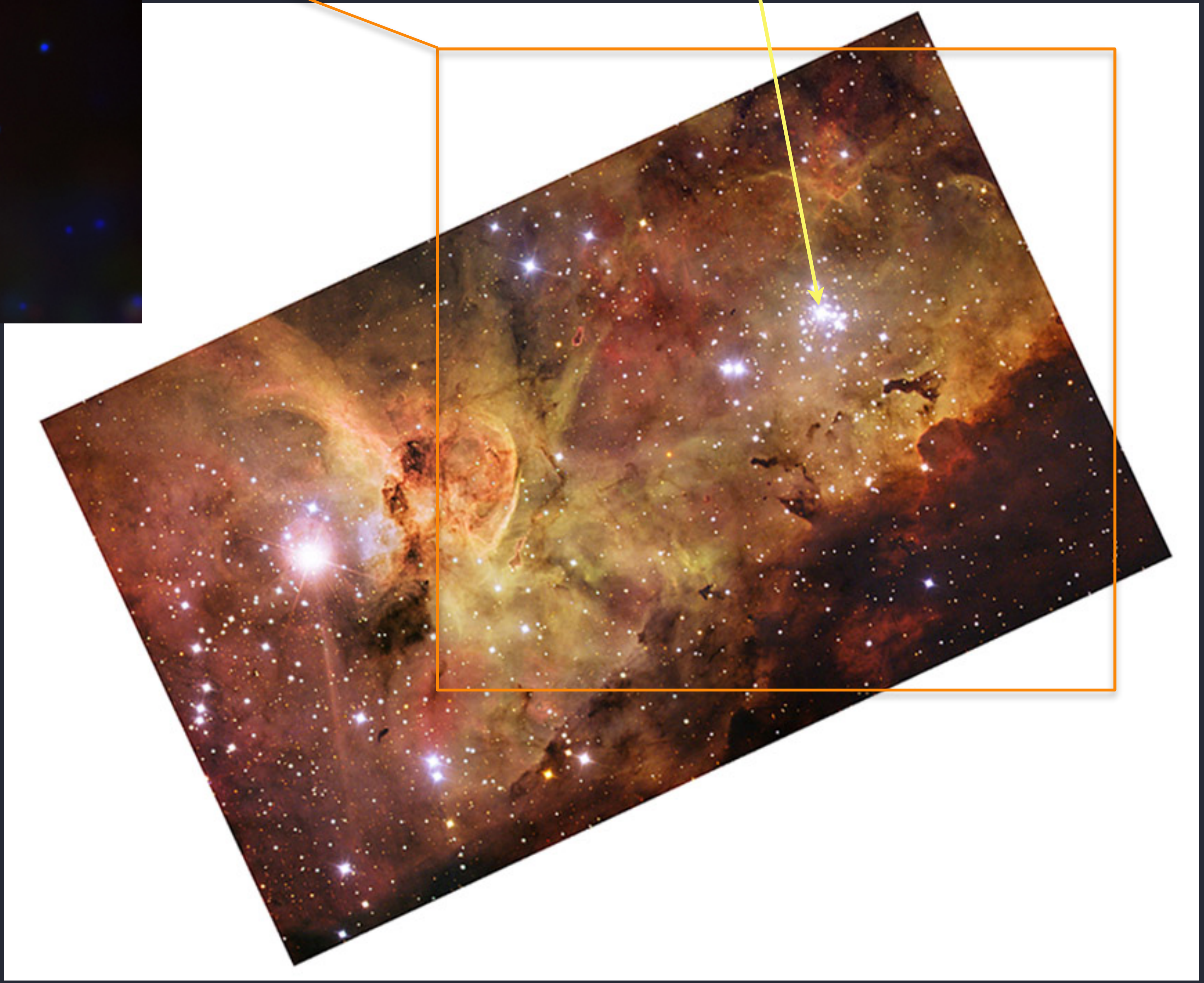

Carina: ESO

Strong stellar wind: traditional diagnostics

UV

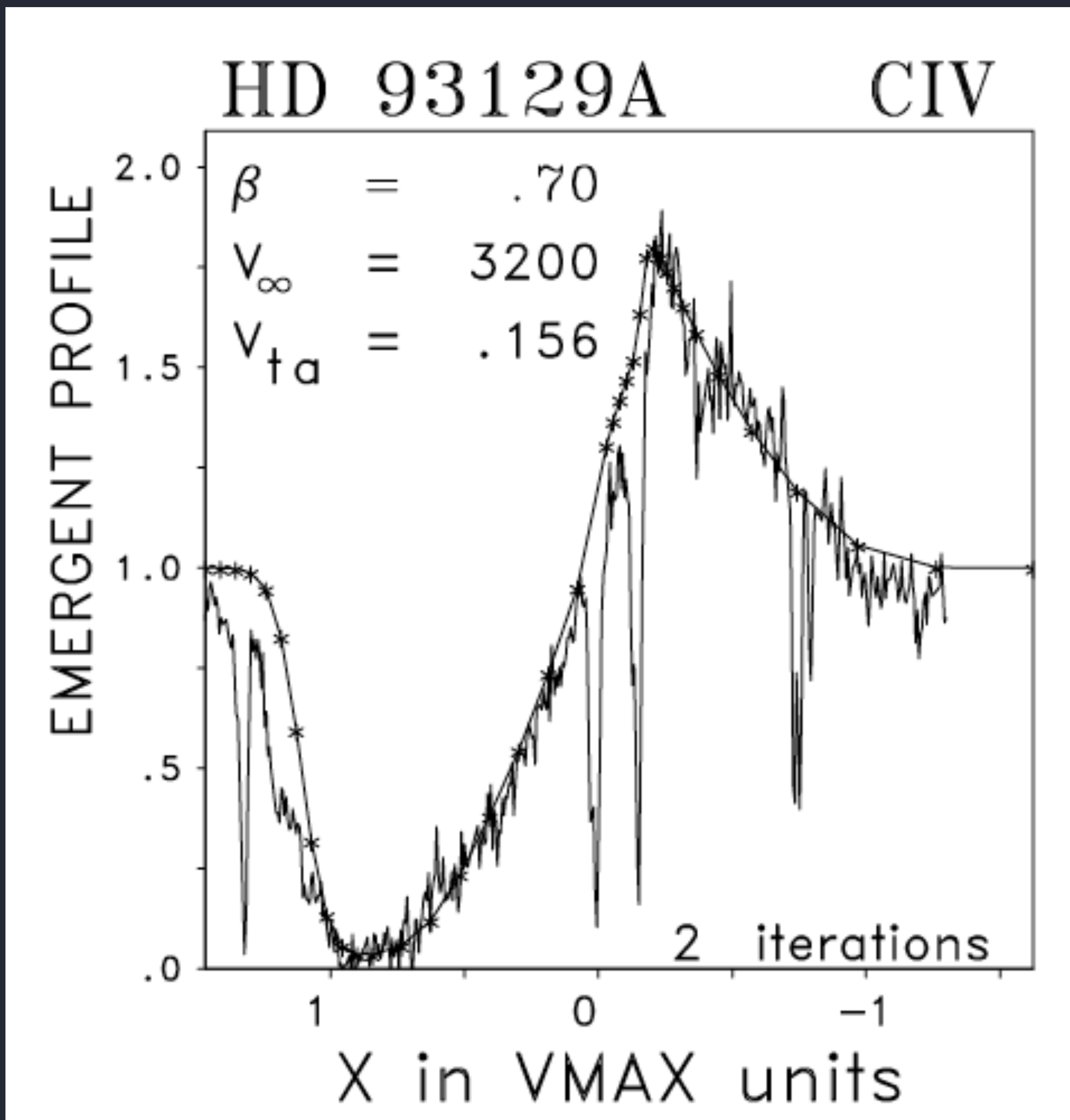

Taresch et al. (1997)

no clumping assumed

$\dot{M} = 2 \times 10^{-5}\ M_{sun}/yr$

$v_\infty = 3200$ km/s

Hα

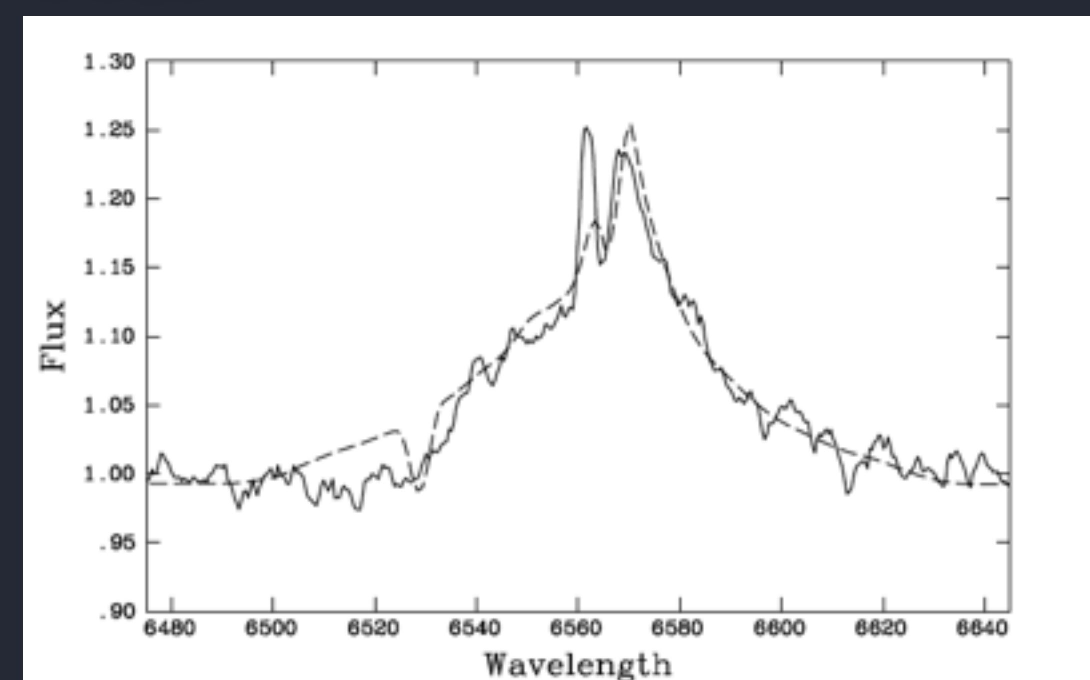

Fig. 13. Observed Hα profile (**solid**) compared with the calculation assuming a mass loss of $18 \times 10^{-6}\ M_\odot$/yr (dashed). Note that the blue narrow emission peak originates from the H II-region emission.

Chandra MEG spectrum of HD 93129A

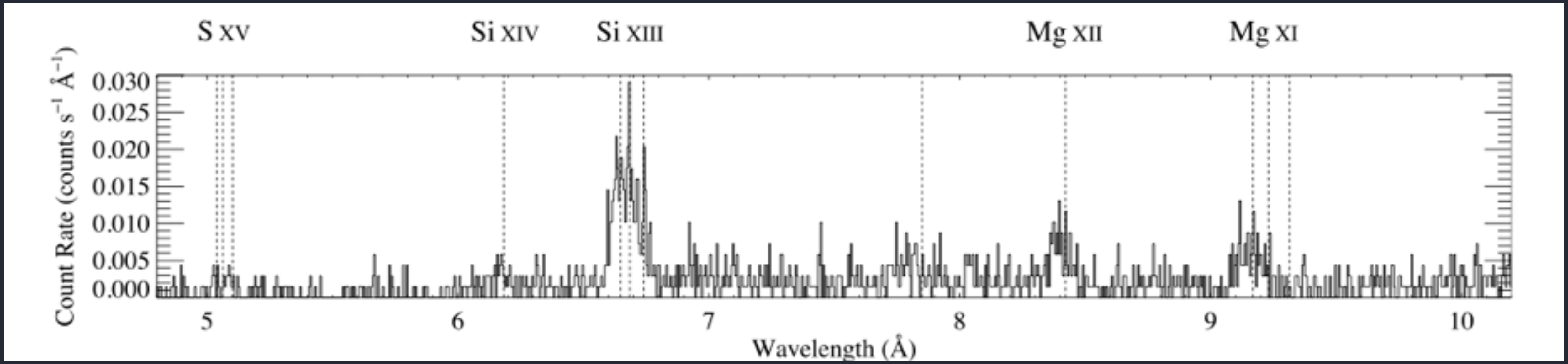

Cohen et al., 2011, *MNRAS*, 415, 3354

d = 2.2 kpc vs. 0.4 kpc for ζ Pup

HD 93129A — Mg XII Lyman-alpha

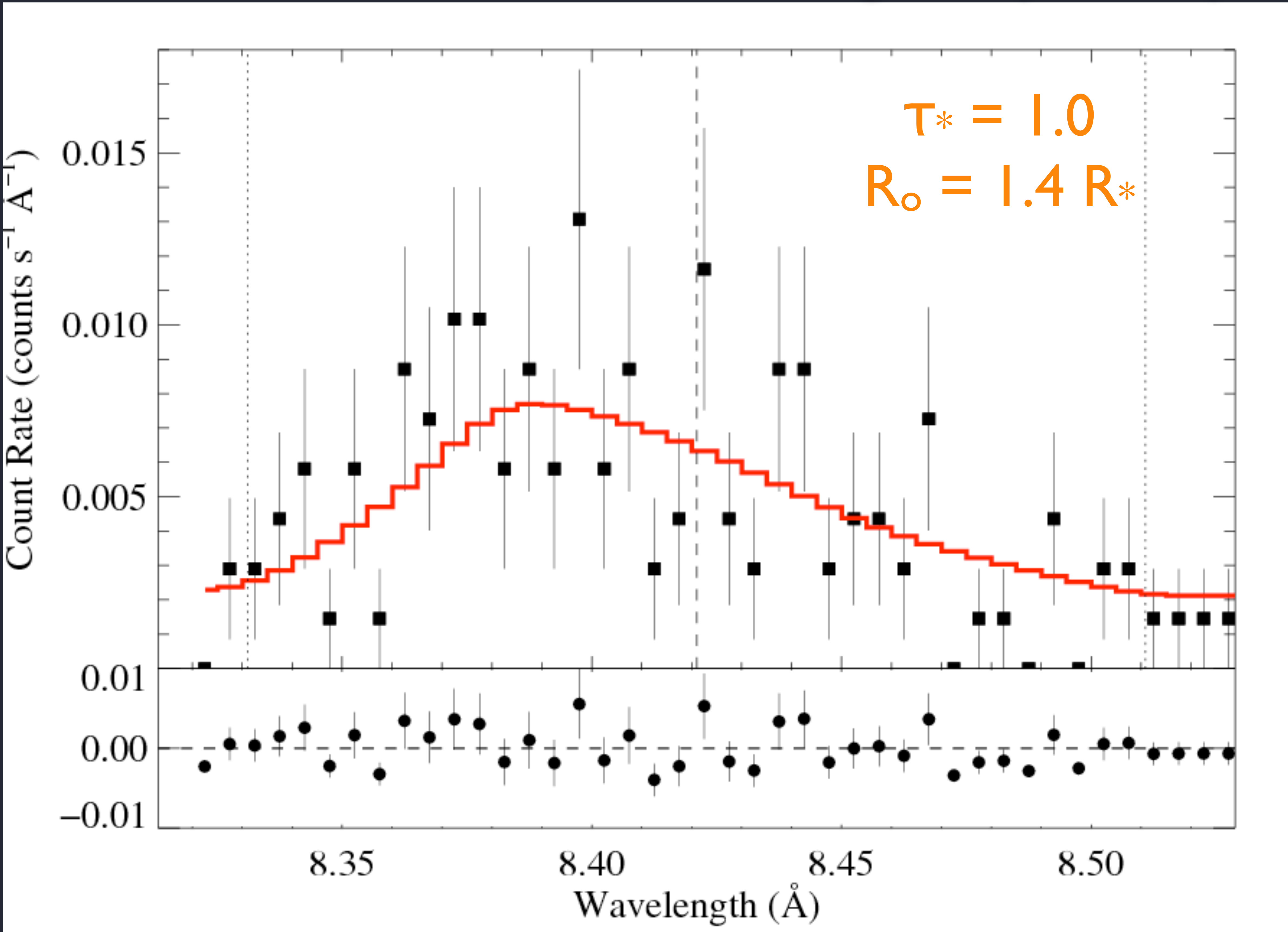

R_o = onset radius of X-ray emission

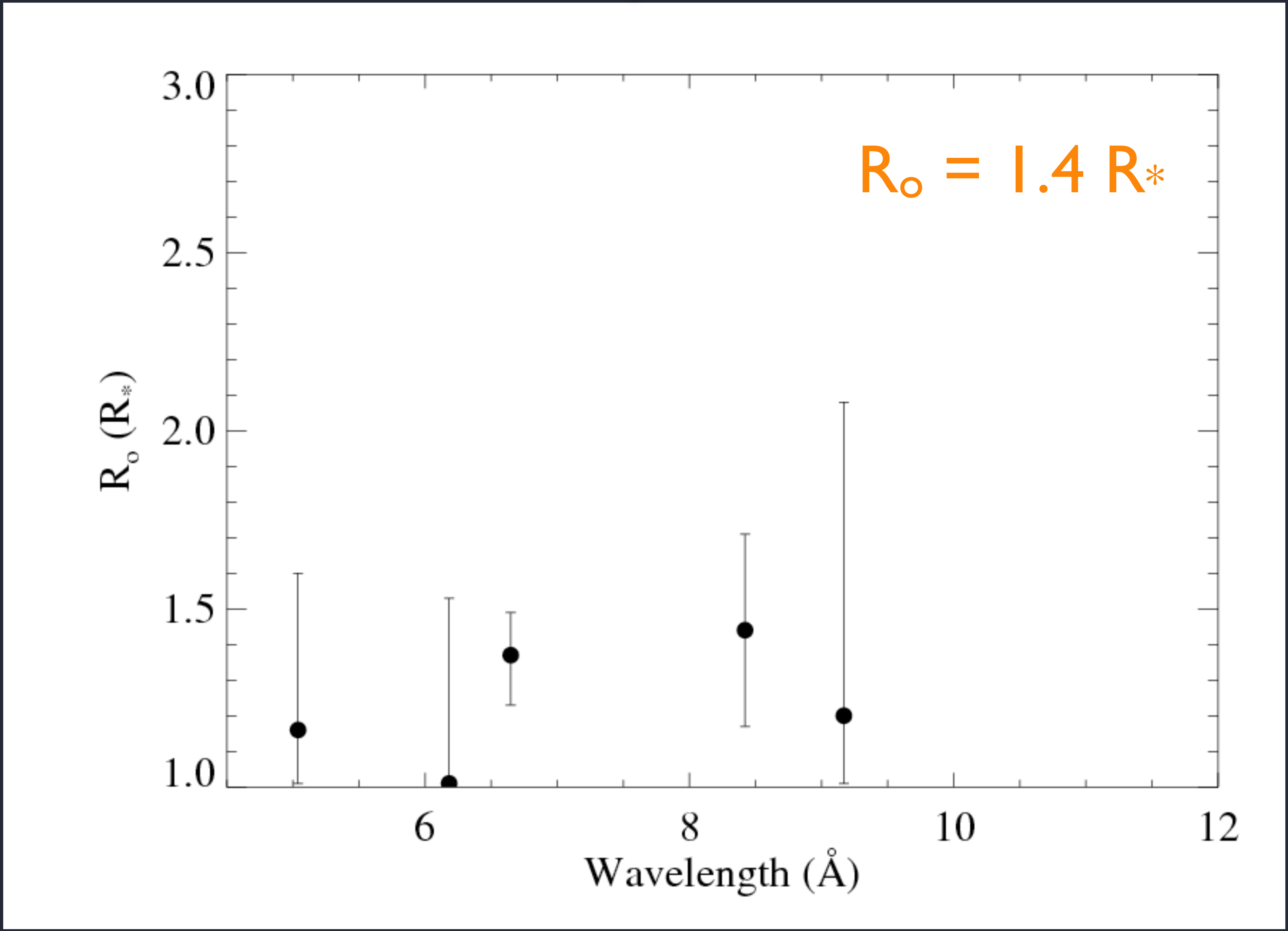

HD 93129A

τ_* from five emission lines

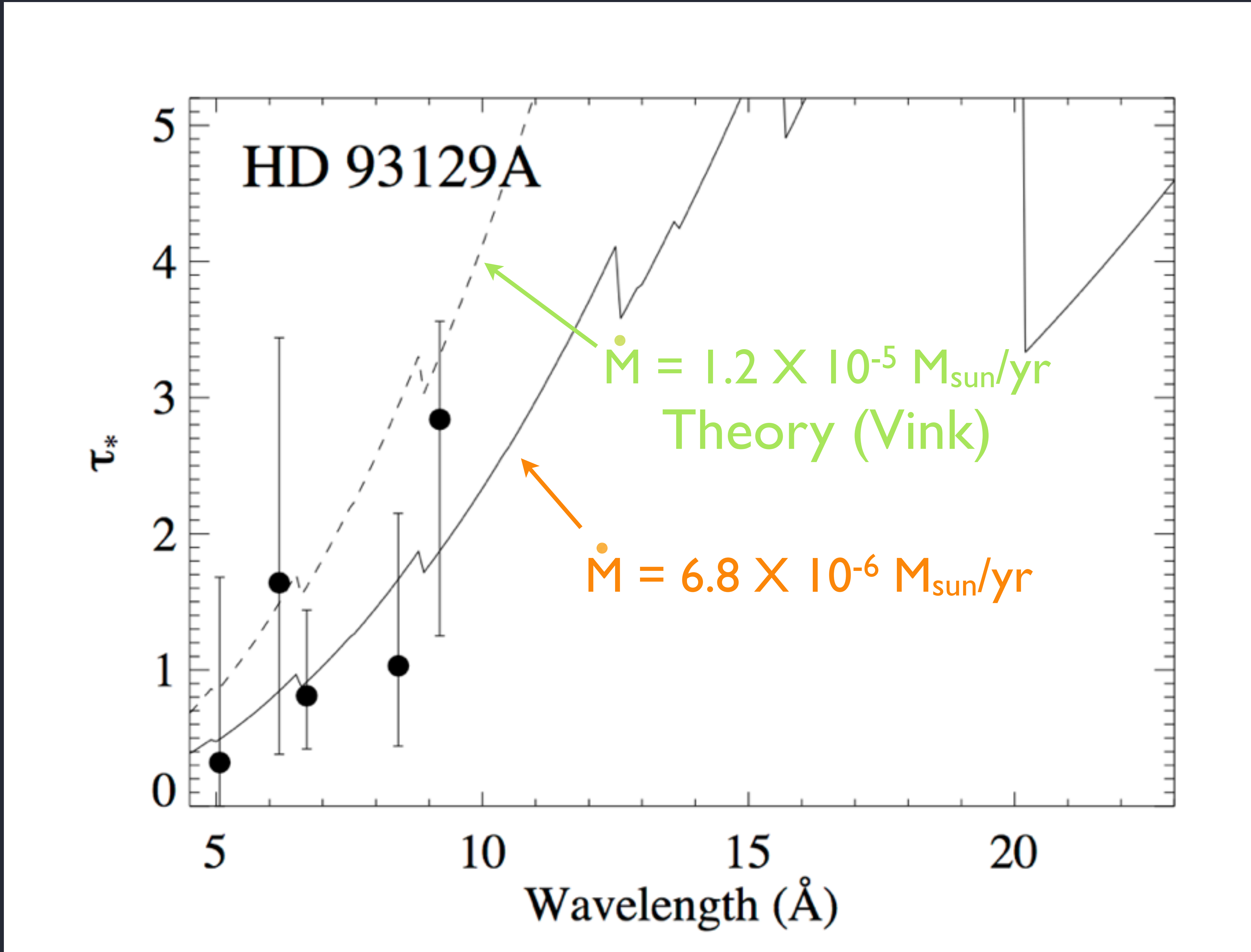

$\dot{M} = 7 \times 10^{-6}\ M_{sun}/yr$

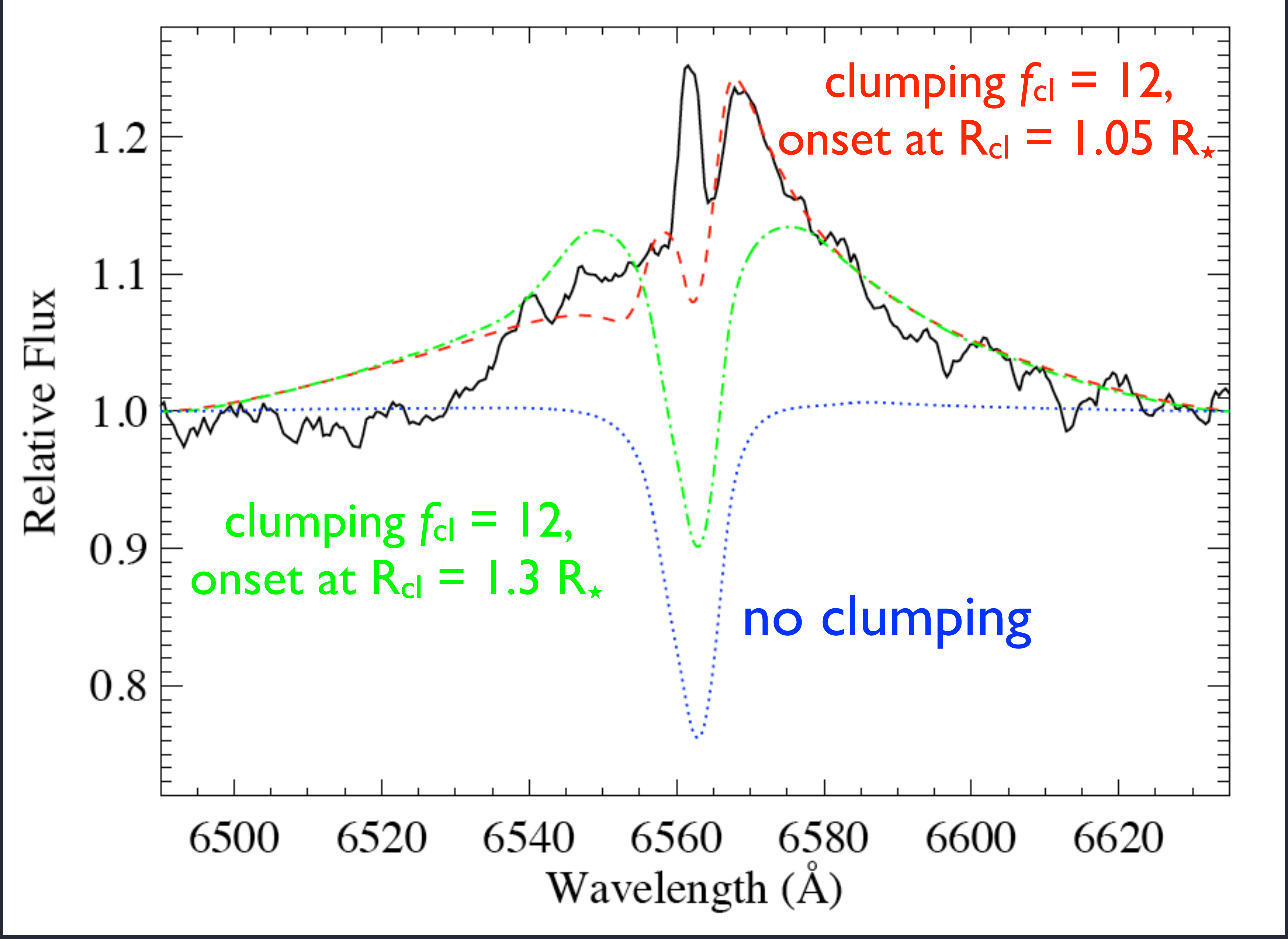

Extension of X-ray profile mass-loss rate diagnostic to other stars

lower mass-loss rates than theory predicts with clumping factors typically of ~ 20

Cohen et al., 2014, *MNRAS*, 439, 908

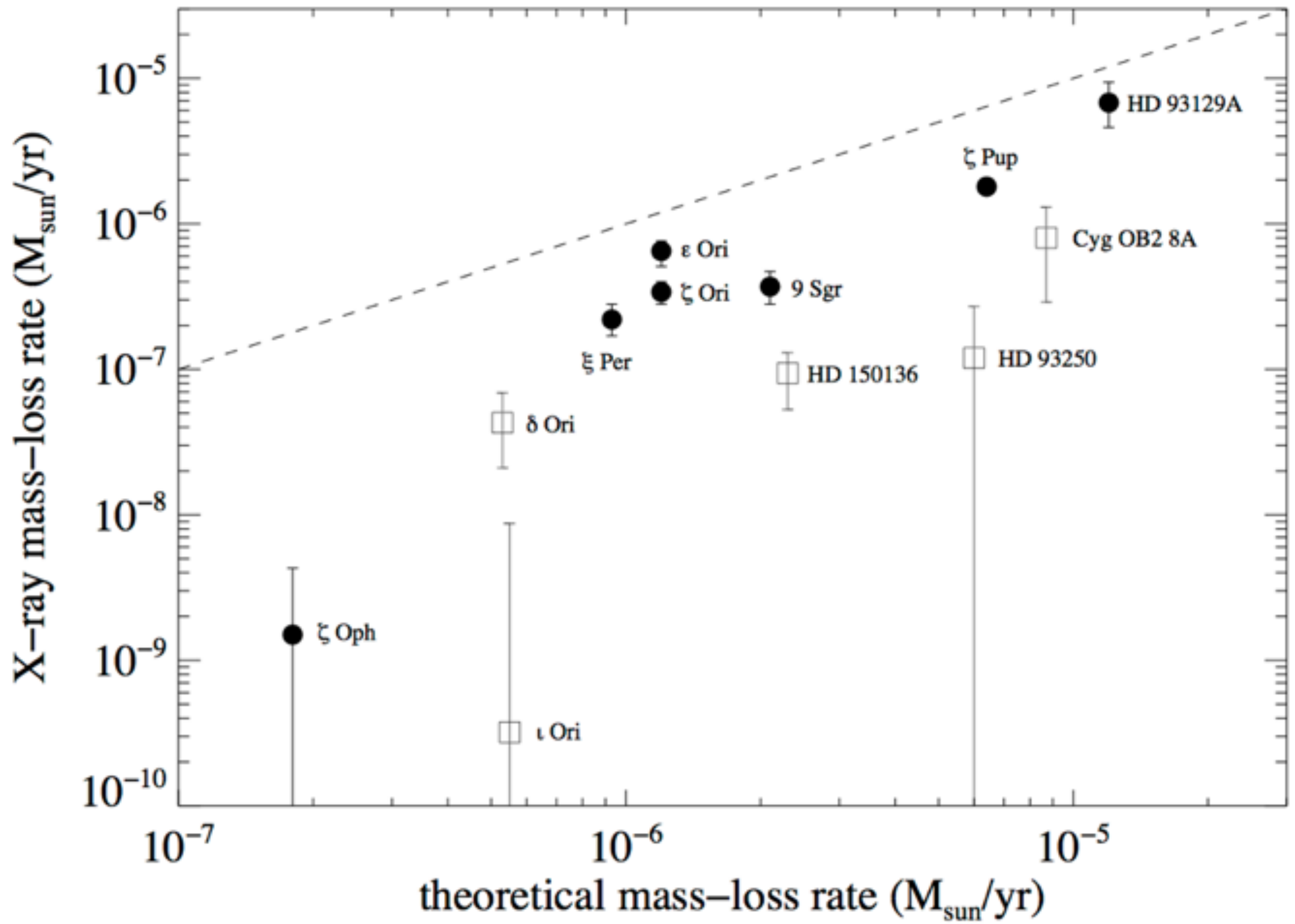

X-ray mass-loss rates: a few times less than theoretical predictions

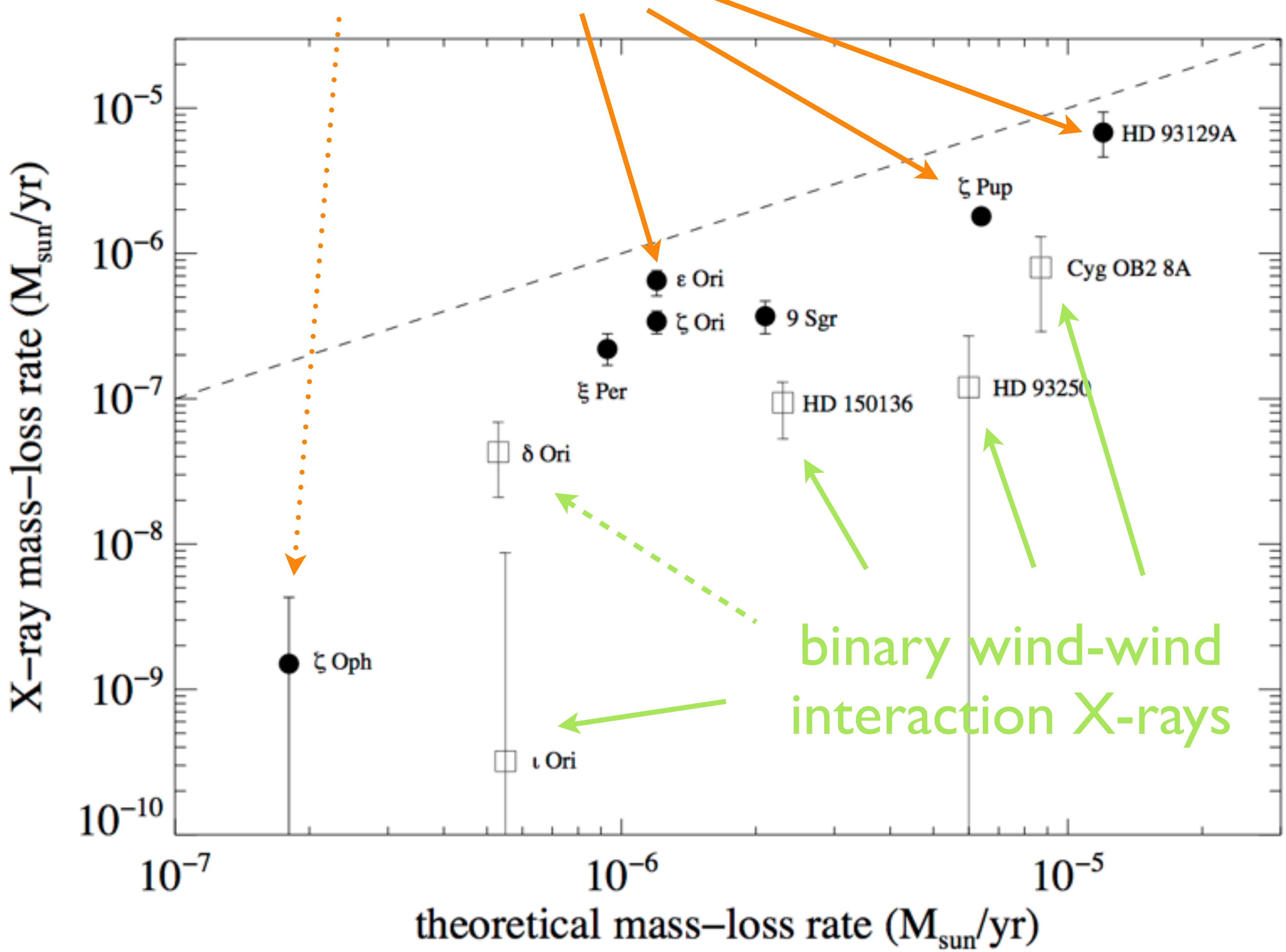

Conclusions

0. HRXS provides useful diagnostic information about hot plasma physics and also can probe surrounding material via absorption

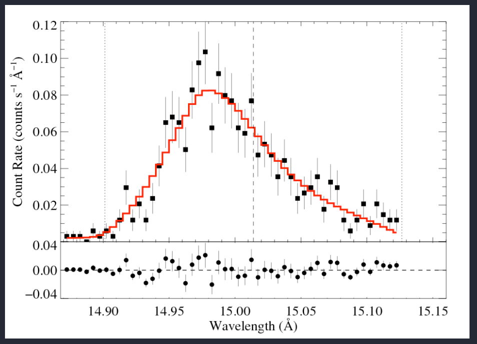

1. X-ray onset at $R_o \sim 1.5\ R_\star$

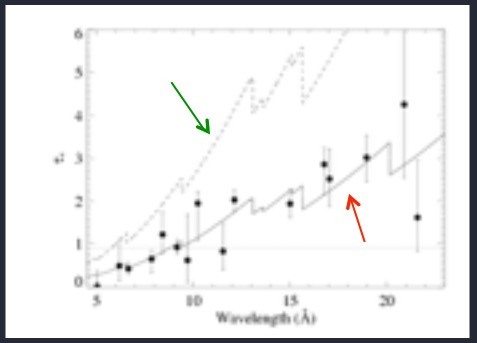

2. Mass-loss rates are lowered by roughly a factor of three

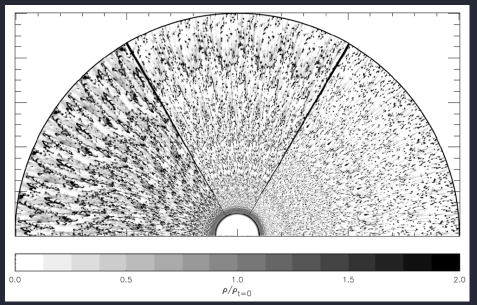

3. Clumping factors of order 10 are consistent with optical and X-ray diagnostics

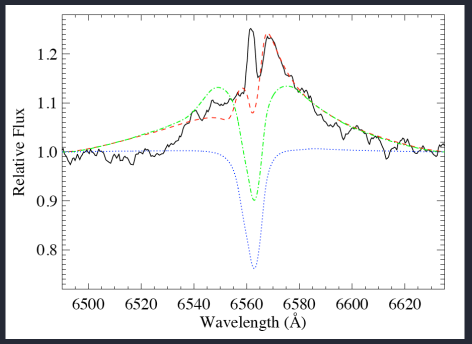

4. Clumping starts at the base of the wind, lower than the onset of X-ray emission